Use of nanostructures as oxygen carriers in chemical looping combustion

Kaisa Aho

University of Jyväskylä
Department of Physics

Master's thesis
Supervisors: Karoliina Honkala
and Hannu Häkkinen
October 1, 2013

Abstract

The usage of fossils fuels has increased carbon dioxide emissions, and the carbon dioxide is responsible for global warming and sea level rising. One of the most promising ways of carbon capturing from the power plants is chemical looping combustion (CLC). CLC is based on the alternating oxidation and reduction reactions on the air and fuel reactors. Oxygen and energy needed for combustion between the reactors is transferred by an oxygen carrier. Oxygen carrier is usually made of metal or metal oxide. One big hindrance towards commercial use of CLC is slow reaction kinetics of oxygen carriers. One possible solution for the problem is to replace the conventional carriers by nanoscale oxygen carriers. Use of nanostructures as oxygen carriers has been investigated in this master's thesis both theoretically and numerically.

There are little research about nanocarriers available in the literature, but the results are very promising. In particular very few numerical studies has been published. Based on the literature nanostructures improve reaction kinetics thus solving one major obstacle towards commercialization. A clear disadvantage of the nanostructures is a low temperature resistance, which can be enhanced by using suitable support materials. On the whole nanostructures are seen as a promising alternative to the oxygen carriers for the CLC on the basis of the current literature .

In the numerical part of the study diffusion and formation energies of vacancies on the bulk and on the surface of a metal oxide are investigated using the GPAW software, which is based on density functional theory. As the nanosturctures have more surface, comparison of these results reveals whether the nanostructures are suitable oxygen carriers or not. Finally temperature and pressure effects are investigated applying atomistic thermodynamics, because temperatures at CLC are very high. Investigated oxygen carriers are copper (CuO and Cu_2O) and manganese based (Mn_3O_4 ja Mn_2O_3) metal oxides.

Results from the calculations are very promising: both vacancy formation and diffusion are easier on the surface than on the bulk. Thus the nanosturctures can solve the problem of slow reaction kinetics. Mn_3O_4 makes an exception for the results, vacancy formation is easier on the Mn_3O_4 bulk than on the surface. Although the results are very promising, further research is needed in order to for example, explain the different behaviour of vacancy formation in Mn_3O_4. In addition it should be find out how the location of the vacancy and the number of vacancies affect the vacancy formation energies and diffusion.

Tiivistelmä

Fossiilisten polttoaineiden polttamisen seurauksena hiilidioksidipäästöt ovat kasvaneet. Hiilidioksidi taas on vastuussa ilmaston lämpenemisestä ja merenpinnan noususta. Yksi lupaavimmista teknologioista hiilidioksidin talteenottoon voimalaitoksista on kemikaalikiertopolttoprosessi (CLC). CLC perustuu vuorotteleviin hapetus- ja pelkistysreaktioihin ilma- ja polttoainereaktoreissa. Palamiseen tarvittavaa happea ja energiaa reaktorien välillä kuljettaa hapenkantaja, joka on yleensä metalli tai metallioksidi. Ennen CLC-prosessin kaupallistamista on selvitettävä miten hapenkantajien reaktiokinetiikkaa voidaan parantaa. Yksi mahdollinen ratkaisu hitaaseen reaktiokinetiikkaan on korvata hapenkantajat nanokokoluokan hapenkantajilla. Nanorakenteiden käyttöä hapenkantajina CLC-prosessissa on tutkittu tässä opinnäytetyössä sekä kirjallisuuden perusteella että numeerisesti.
Tutkimus nanorakenteiden käytöstä CLC-prosessissa on vähäistä, mutta tulokset ovat hyvin lupaavia. Erityisesti laskennallista tutkimusta on saatavilla hyvin vähän. Kirjallisuuden perusteella nanorakenteita käyttämällä reaktiokinetiikka parantuu ratkaisten näin yhden suuren esteen kaupallistumisen tiellä. Nanorakenteiden selkeänä haittapuolena on niiden heikko lämpötilakestävyys, jota voidaan kuitenkin parantaa erilaisilla tukimateriaaleilla. Kokonaisuutena nanorakenteet nähdään kirjallisuuden perusteella hyvin lupaavina vaihtoehtoina hapenkantajiksi CLC-prosessiin.
Työn numeerisessa osuudessa tutkitaan metallioksidien diffuusioita ja vakanssinmuodostusenergioita sekä metallioksidissa että metallioksidipinnalla tiheysfunktionaaliteoriaan (DFT) pohjautuvan GPAW-ohjelmiston avulla. Koska nanorakenteissa on enemmän pintaa, näitä tuloksia vertaamalla voidaan päätellä ovatko nanorakenteet toimivia hapenkantajia. Koska CLC-prosessissa lämpötilat ovat hyvin korkeita, lopuksi tutkitaan myös lämpötilan ja paineen vaikutusta vakanssinmuodostukseen ja pintojen stabiilisuuteen atomistisen termodynamiikan avulla. Tutkitut hapenkantajat ovat kupari- (CuO ja Cu_2O) ja mangaanipohjaisia (Mn_3O_4 ja Mn_2O_3)metallioksideja.
Laskujen perusteella saadut tulokset ovat hyvin lupaavia, sekä vakanssinmuodostus että diffuusio on helpompaa pinnalla ja pinnan alla kuin bulkissa. Nanorakenteiden käyttö voisi siis ratkaista hitaan reaktiokinetiikan. Poikkeuksen tähän tulokseen tekee Mn_3O_4, jossa vakanssinmuodostus on helpompaa bulkissa. Vaikka tulokset ovat hyvin lupaavia myös laskennallista tutkimusta tarvitaan lisää, jotta voidaan esimerkiksi selittää Mn_3O_4-oksidin erilainen käytös vakanssinmuodostuksessa. Lisätutkimuksissa tulisi myös selvittää vakanssin paikan ja vakanssien määrän vaikutusta vakanssin muodostumisenergiaan ja diffuusioon.

Preface

This thesis is done in collaboration with the Technical Research Center of Finland VTT between December 2012 and September 2013. I would like to thank VTT for financial support and opportunity to collaborate.
I would like to thank my supervisor Karoliina Honkala for generous and skilled help and discussions, which made this thesis possible to complete. Thank you for your patient and supporting attitude which made this process even more pleasant. It was very nice to collaborate with you!
I wish to thank professor Hannu Häkkinen and Teemu Parviainen for conversations, which gave me new aspects. I also want to express my gratitude to Soili Leskinen and other department staff.
I would like to thank Matti Tähtinen and Antti Tourunen from VTT. Thank you for inspiring discussions. You brought the technical viewpoint to this work and helped me to understand that more carefully. Thank you for collaboration.
Finally but not the least I would like to thank my family for the support, encouragement and love during my life. Especially I would like to thank my dad who gave me enthusiasm for the physic and energy technology. Heikki, I would like to thank you for your endless love, support and our conversations.
I wish to thank my friends and fellow students, you have made my life much funnier and easier.

Tampere, September 13th. 2013

Contents

List of abbreviations

AR	Air reactor
ASE	Atomic Simulation Environment
ASU	Air separation unit
BHA	Barium hexa aluminate
CCS	Carbon capture and storage
CG	Conjugate gradient method
CLC	Chemical looping combustion
CLOU	Chemical looping combustion with oxygen uncoupling
DFT	Density functional theory
FR	Fuel reactor
GGA	Generalize gradient approximation
GHG	Greenhouse gases
GPAW	Grid-based projector-augmented wave method
ig-CLC	Integrated gasification chemical looping combustion
LDA	Local density approximation
LDH	Layered double hydroxide
LDSA	Local density spin approximation
$\mathbf{Me_xO_y}$	Metal oxide
NEB	Nudged elastic band
PBE	Perdev-Burke-Emzerhof functional

1 Introduction

1.1 Background

Because of using fossil fuels, which are still important part of world's energy resources, CO_2 emissions have been increasing. The global atmospheric concentration of CO_2 increased from pre-industrial level of 280 ppm to 390 ppm in 2010 and it is predicted to rise to 570 ppm by the year 2100 [1, 2]. Counts of CO_2 emissions between years 1900 and 2008 are illustrated in figure 1. In these days it is known that CO_2 and other greenhouse gases (GHG) are mainly responsible of global warming and sea level rise. So the use and investigate of renewable energy is increased. Renewable energy is very attractive owing to its environmental-friendly and regenerating nature. But since fossil fuels can not entirely be replaced by renewable energy sources in the near future, one strategy to decrease CO_2 emissions is to separate CO_2 from the fuel gas and storage it. Nowadays a number of carbon capture and storage (CCS) technologies are developed and one of the most promising ways of CCS is chemical-looping combustion (CLC).

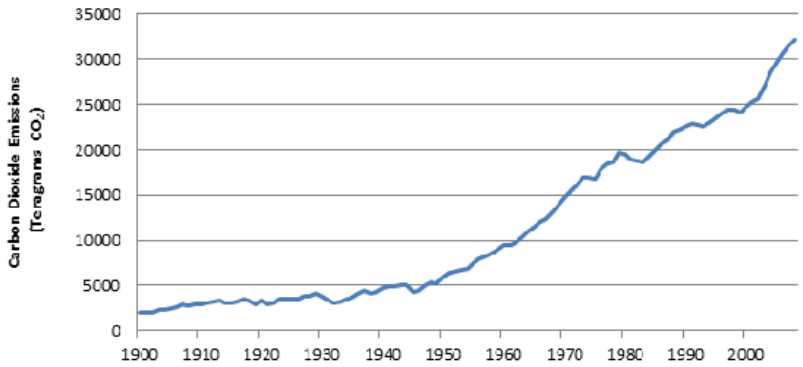

Figure 1: *Global carbon dioxide emissions from fossil fuels between years 1900-2008. It can be seen that emissions have increased considerably and between years 1990-2008 emission have risen by about 1.5 times. The figure is taken from ref [3].*

Theory of CLC was first introduced by the German scientists Richter and Knoche in 1983. But the roots of the theory are in the 1900s, when engineer Howard Lane presented his idea of using chemical-looping process for hydrogen production. In 1954 Lewis and Gillian presented idea to produce pure CO_2 using solid oxygen carrier and any oxidizable carbonaeous fuel in two interconnected fluidized beds. [4, 5]. To these days energy and environment has been researched separately, but CLC is a technique which combine both energy and environment. CLC is not yet in commercial use, but the research around CLC is widely going, because CLC appears to have potential for the most efficient and low cost technology for carbon capture and storage. [6]. Comparing to other methods CLC does not need of any extra energy for the separation of CO_2. Other advantages of CLC are that the combustion is flame-less, it operates at temperatures low enough to avoid formation of harmful NO_x oxides. In ideal situation CO_2 can be separated at high purity without direct contact to the air.

CLC process is based on two spatially separated, periodic steps: oxidation of an oxygen carrier (usually metal or metal oxide) and the following reduction of the same oxygen carrier with air and fuel, respectively. The study of CLC process is mainly focused on the selection and characterization of oxygen carriers, designing and optimization of CLC reactor and the CLC-system coupled with other techniques. [1] Identification of suitable oxygen carrier is a critical step on the way towards commercial realization of CLC. The

purpose of this thesis is to find out if the nanoparticles are suitable for oxygen carriers and what are the advantages of using nanoparticles as oxygen carriers.

CO_2 which is captured in CLC process can be either utilized or disposed. Most important and popular utilization of CO_2 is enhanced oil recovery from depleted reservoirs, in which CO_2 enhances the mobility of crude and so helps its removal. [6] CO_2 is also used in food production industry as a coolant, in chemical industry as a raw material, in fire fighting, in fish farm, agricultural greenhouses, and plastic processing. CO_2 is also used as a supercritical solvent. [6, 7]

Although CO_2 is used in industry, the use of CO_2 is very small compared to the annual production of CO_2. So most of the annual CO_2 emissions have to be disposed and stored to the suitable locations where the captured CO_2 can not be emitted to the atmosphere. Because oceans have great potential to submerge anthropogenic CO_2, one option is to dispose CO_2 in to the oceans, but in that method there are potential risks to the marine life and environmental.[6, 8] Today this is also prohibited by a law. CO_2 can also be sequestrate to the non-minable coal beds and geological rock formations [6, 7]. If CO_2 is injected to the coal beds carbon dioxide is substituted with methane in relation 2:1. So the coal beds act both CO_2 reservoirs and a source for CH_4 production.[6, 7, 21] Because CO_2 can react with the igneous rock which is composed of magnesium oxide which is bound silica and alumino-forming alumino-silicates and so form a stable, long-live solid material, this reaction is one option to dispose CO_2. Disadvantage of this process is the slowness of the reaction. [6, 7]

That CLC, or any other process, can be taken to the commercial use, the process must be economical feasible. It is foreseen that different CCS technologies will be economical feasible enough to be in commercial use in 2020 onwards.[7] The cost due to CLC process can be categorized into capital and operating costs. Capital cost are mostly derived from design and construction of the reactor as well as finding suitable oxygen carrier which is also cheap to synthesize.[9, 6] Energy cost effectiveness for the power plant with CCS is always lower than power plant without CCS.[9, 6] So there is need for the additional fuel. According to Markewitz et al additional fuel is needed 21% more even with favorable reduction effectiveness and cost of generating electricity will be increased by 37-81 % varying with the fuel used in reactor.[7] But there is also political framework which includes costs to avoid CO_2 emissions and other environmental aspects and made CLC worth of studying and investigating.[9, 6] When calculating total cost for CO_2 capture, also the costs derived from transportation and storing must take into account.

1.2 Structure of thesis

This thesis consist of the two parts: a literature review and a numerical part. In the sections 2 to 5 oxygen carriers are treated on the basis of the literature and earlier studies. Sections 6 to 7 consist of numerical methods and results of the calculations done in this thesis. Section 8 combines these results.

In section 2 commonly used carbon capture technologies are introduced. In section 3 conventional CLC and CLOU are presented in more detail. Furthermore some reactions which are unwanted in CLC are discussed more carefully.

In section 4 some properties which are required for the oxygen carrier both in CLC and CLOU are discussed. Furthermore some preparation methods are briefly considered. Copper and manganese based carriers are studied in more detail. In section 5 different results for the nano sized oxygen carriers are presented. There are also some comparisons between the nano size oxygen carriers and conventional carriers.

In section 6 different software, and theories where they are based on, are discussed. In addition it is also demonstrated how the different quantities (for example lattice constants) are going to be calculated. In section 7 results and some analysis of these calculations are presented.

2 Carbon capture technologies

There are a number of available commercial technologies to capture CO_2 from gases. Three of them are currently intensively discussed: Post-combustion in which CO_2 is separated from flue gas right after combustion, oxyfuel in which nearly pure oxygen is used in combustion instead of air in combustion to get higher concentration of CO_2 of the fuel gas and pre-combustion in which the fuel is decarbonized before combustion. All of these techniques are energy consuming so the efficiency of the power plant will decrease when these techniques are employed. But because power plants produces over third of the world's carbon dioxide emissions, they are good candidates to the carbon capture [8].

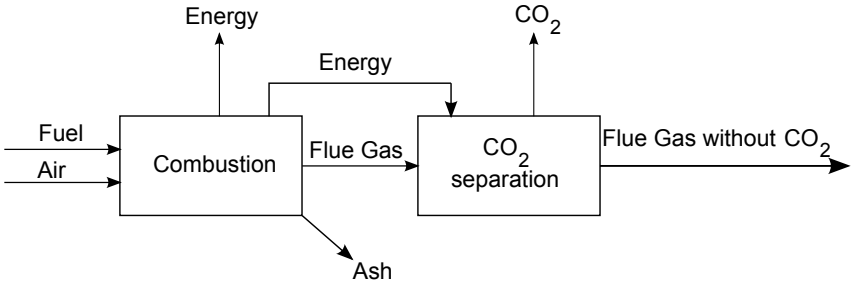

Figure 2: *Principle of post-combustion.Post-combustion is a carbon capture method where CO_2 is separated from flue gas after combustion. The figure is taken from [10].*

Principle of post-combustion is presented in figure 2. In the post-combustion process carbon dioxide is separated from flue gas after combustion, where the name post-combustion is coming from. The most promising method for carbon capture using post-combustion is chemical absorption which can be done by using for examples amines as solvents. Although there is some energy released from the combustion, also the extra energy is needed. Markewitz et al. and Johansson have listed advantages and disadvantages of post-combustion.[7, 10, 21]

Advantages of post-combustion [7, 10]:

- Chemical absorption process is well known
- Addition of the equipment for CO_2 removal may be added to a power plant
- Highest purity of CO_2 ($> 99,99\%$) of all technology routes
- High optimization potential to reduce energy losses

Disadvantages of post-combustion [7, 10]:

- High costs
- High energy penalties
- Quite a large environmental impact

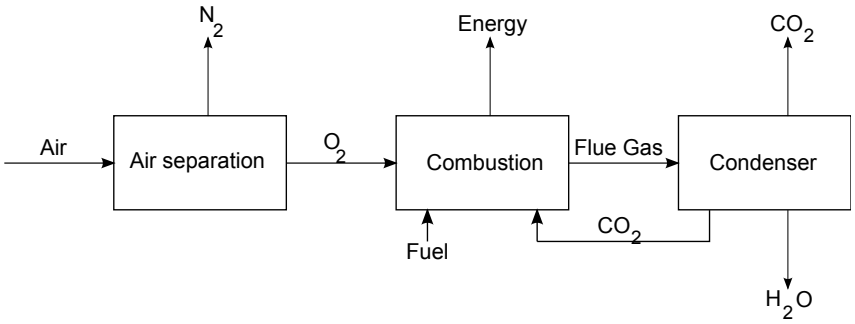

Figure 3: *Principle of oxyfuel. Oxyfuel is a carbon capture method where combustion occurs with pure oxygen instead of air. In this technique carbon capture efficiency is very high and the environmental impacts are low. The figure is taken from [10].*

Principle of oxyfuel is presented in figure 3. At the first step nitrogen is separated from the air at the air separation unit. After the separation fuel is combusted with air. Then CO_2 and H_2O are formed as products.[7, 10] Water can be easily condensed from carbon dioxide and the efficiency of the carbon capture in this method is almost 100 % [7]. Markewitz et al. and Johansson have listed advantages and disadvantages of oxyfuel.

Advantages of oxyfuel[7, 10]:

- Environmental impacts are low and no NO_x are formed
- Technique is well known
- There are high potential to reduce energy losses

Disadvantages of oxyfuel[7, 10]:

- Boiler is more sensitive to corrosion (because of the higher CO_2 contents) so there is need to modification of burners and boiler design.
- High costs

[7], [10]

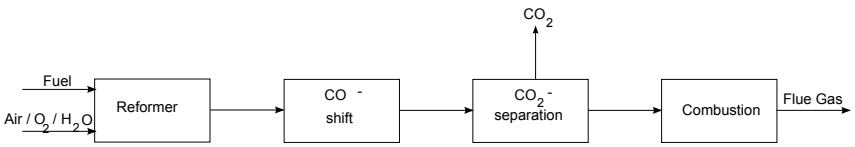

Figure 4: *Principle of pre-combustion.Pre-combustion is a carbon capture method where fuel is decarbonized before combustion. If the combustion step is removed, pre-combustion is a method to manufacture hydrogen. The figure is taken from [10].*

Principles of pre-combustion is presented in figure 4. As the name suggests CO_2 is separated from fuel before combustion in pre-combustion. At the first air or O_2 and/ H_2O and fuel is mixed and as a result mixture of CO_2, CO, H_2O and H_2 is formed. At the next, energy consumed step components of mixture are reacted at a shift reactor to form CO_2 and H_2. [7, 10] After the CO_2 separation there are hydrogen-rich flue gas which can be combusted and mainly steam has formed as a combustion product. [21] If the combustion is passed, pre-combustion offers a way to produce hydrogen from fossil fuels. With these hydrogen power plants can produce power with a minimal carbon emissions. [7, 10] Johansson has listed some advantages and disadvantages of pre-combustion in

his doctoral thesis. Also Markevitz et al. have examined pre-combustion from different aspects.

Advantages of pre-combustion[7, 10]:

- High efficiency potential
- Poly-generation of electricity and hydrogen gives flexibility

Disadvantages of pre-combustion[7, 10]:

- Investment costs are high and one reason for that is that the technology is very hard and complex to fit into existing systems.
- Availability and reliability are low
- There are less technology experience compared to other conventional power plants.

All of the three previously discussed carbon capture technologies have huge energy losses in producing pure carbon dioxide. An alternative option to carbon capture and storage is the chemical-looping combustion (CLC) which acts like oxyfuel but without need of extra energy because the fuel and nitrogen from air don't mix with each other. So the formed CO_2 is cleaner and high cost CO_2 separation step is avoided. It can also be categorized as a pre-combustion because carbon in the fuel is separated prior to combustion. In CLC oxygen needed to the combustion is transferred to the fuel reactor by oxygen carrier and so the direct contact between air and fuel is prevented.

3 Conventional CLC-process

Chemical looping combustion (CLC) is based on two cyclic reactions: oxidation and reduction. Reactions take places on two separated reactors so that metal oxide is reduced in the fuel reactor (FR) and oxidized in the air reactor (AR). Oxygen and heat is transferred between reactors by oxygen carriers. So the direct contact between air and fuel is prevented and separate air separation unit (ASU) isn't needed to separate CO_2 and N_2 from each other. Principle of CLC-process is presented in figure 5.

Primary oxygen carriers M_yO_x are usually made of metal or metal oxide. Their function is circulate between two reactors carrying oxygen and heat with. In the first step fuel is oxidized to CO_2 and metal oxide M_yO_x is reduced to M_yO_{x-1} or metal form M_y according to reaction 3.1. This reaction is either exothermic or endothermic depending on oxygen carrier and fuel used in process

$$(2n+m)M_yO_x + C_nH_{2m} \rightarrow (2n+m)M_yO_{x-1} + mH_2O + nCO_2 \qquad \Delta H_r, \tag{3.1}$$

where C_nH_{2m} and M_yO_x represent the fuel and oxygen carrier, respectively.

Gaseous H_2O and CO_2 which are released from reaction 3.1 are mixed each others. In the condensation unit they can be separated to liquid H_2O and gaseous CO_2 which can be compressed and cooled to the liquid form CO_2 (l) and then utilized or disposed. [1, 2, 5, 6, 10, 12]

In the second step oxygen carrier reacts with air's oxygen according to reaction

$$(2n+m)M_yO_{x-1} + (n+\frac{m}{2})O_2 \rightarrow (2n+m)M_yO_x \qquad \Delta H_o < 0 \tag{3.2}$$

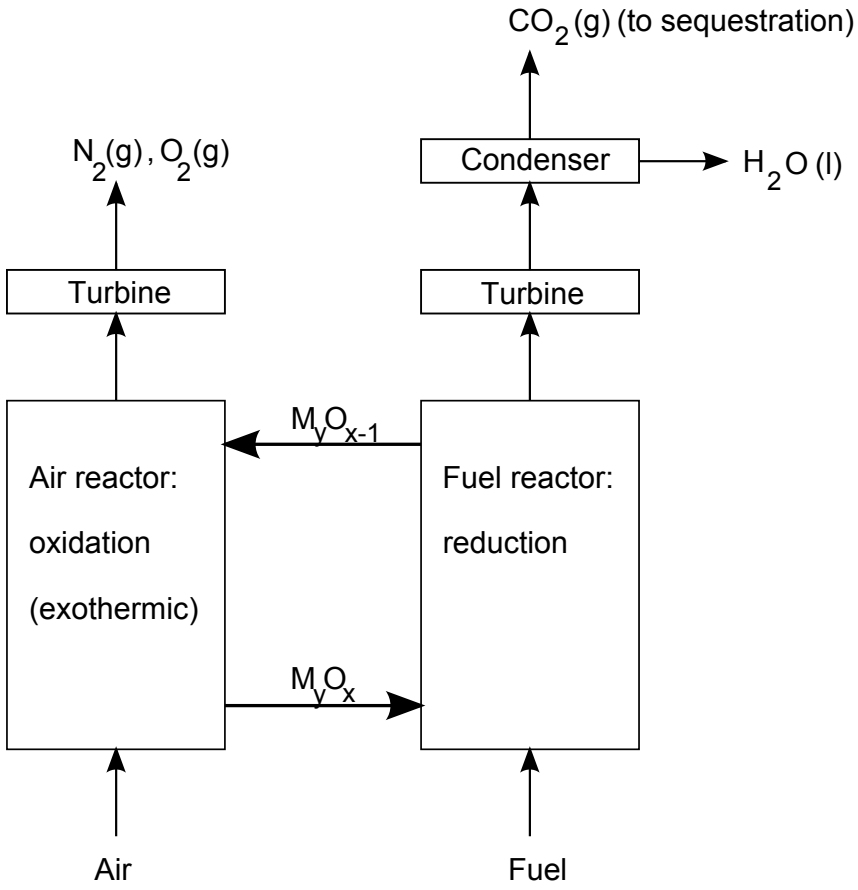

Figure 5: *The main principle of CLC-process. The concept of CLC is based on the use of oxygen carrier which transfers oxygen from the air reactor to the fuel reactor and prevent direct contact between air and fuel. In the fuel reactor oxygen carrier is reducted and oxidation of oxygen carrier takes place in air reactor. The figure is adapted from [2].*

Reaction 3.2 is always exothermic and after the this reaction oxygen carrier can transfer to the fuel reactor and begin a new loop.[6, 10] Full conversion from M_yO_x to M_yO_{x-1} and back M_yO_x isn't necessarily obtained in a real system.[1, 5, 11] And in some cases complete reduction must be avoided, because some metals can act as catalyst in unwanted reactions.[21] For example if iron oxide is reduced to the metal form Fe, it can act as a catalyst in a harmful Boudard reaction discussed later on chapter 3.3. [13] All metal oxides aren't even capable for complete reduction and in some cases the complete reduction can be prevented by covering the oxygen carrier with passivated films. [48, 15] Reduction reactions are always faster than oxidation reactions. [14] This can be result from the fact that reduction is controlled by chemical reaction resistance, while oxidation is controlled by chemical reaction resistance and product layer diffusion. [48] Tian et al. have experimentally shown that reduction reactions are nearly two times faster in the same fractional converse[20]. It is possible that oxidation can be accelerated by using smaller particles, because according to Hossain et al. smaller particle size minimize resistance of gas layer diffusion. [6] Oxygen used in reaction 3.2 is coming from air . So at the air reactors outlet there are mainly harmless N_2 and unreacted O_2 and they can be released right to the atmosphere. [2, 12] Net reaction of the process can be written as

$$C_nH_{2m} + \left(n + \frac{m}{2}\right) O_2 \rightarrow nCO_2 + mH_2O \qquad \Delta H_c. \tag{3.3}$$

The heat released at the process depends on the employed oxygen carrier and fuel and can be calculated with the help of classical thermodynamics. [1, 6, 5] Total heat of the

process is the same as the heat released from normal combustion where the air and fuel are in the direct contact. [2, 21] So the CLC does not bring any enthalpy gains. While the reduction reaction is endothermic and because the process doesn't need any extra energy the oxidation reaction has a higher heat of reaction so that equation

$$\Delta H_c = \Delta H_o + \Delta H_r < 0 \tag{3.4}$$

is satisfied.[1, 2, 5, 6, 21] Temperature range of CLC-process is between 800-1200°C and reaction could be at atmospheric pressure or pressurized.[10] Temperature is low enough that the harmful NO_x is not formed. Due to the exothermic nature of oxidation, temperature at the air reactor is higher than temperature at the fuel reactor and hot particles from air reactor supply heat to the fuel reactor. [2, 6, 5] Heat transfer is important duty along oxygen transfer. If the reaction at the fuel reactor is exothermic, oxygen carrier's temperature rises and there are risk that the carrier melts. If the reaction again is endothermic, temperature of the oxygen carrier decreases and reaction rates can lower. In both situations it is important that oxygen carrier is capable of transfer heat from one reactor to the other. [1, 6, 11, 12, 21]

Oxygen transport capability or oxygen ratio R_O defines the amount of oxygen which can be transferred from one reactor to the other in one redox-cycle and it is defined by equation

$$R_O = \frac{m_o - m_r}{m_o}, \tag{3.5}$$

where m_o is a mass of fully oxidized oxygen carrier and m_r is a mass of fully reduced oxygen carrier. Bigger R_O more oxygen carrier can carry with per mass unit. [1, 48, 9] It must be noticed that if oxygen carrier has multiple oxidation states R_O varies with the function of a extents of reaction.[21]. If oxygen carrier has some kind of a support material and it is wanted to take into account, used quantity is oxygen transport capacity R_{OC} which depends on R_O and a fraction of the active compound for the oxygen transport x_{OC} and can be defined by equation [1, 9]

$$R_{OC} = x_{OC} R_O. \tag{3.6}$$

3.1 CLC of solid fuels

CLC would be much more attractive if there was an opportunity to apply solid fuels which are notably cheaper than gaseous fuels. During the recent years investigation around the solid fuels in CLC has increased. Coal is and will be the main energy source in the near future and also the biomass as a fuel in CLC has risen to a subject of interesting.[21, 17] CLC with solid fuels is dated back to 1954 when Lewis and Gilliland patented their idea of produce pure CO_2 applying solid fuels. [5] Although the idea is so old, investigation around the solid fuels with CLC is small compared to conventional CLC. While using solid fuels reduction reaction at the fuel reactor is exothermic, so oxygen carrier must be capable of carry on heat to get the process operate. [1, 5]

There are three different ways to employ solid fuels in CLC:

- Syngas fuelled chemical-looping combustion (Syngas-CLC) in which the used fuel is first gasified and after that it is fed to the fuel reactor.
- Integrated gasification chemical-looping combustion (iG-CLC) in which solid fuel is fed right to the reactor where it forms char and volatiles which can react with oxygen carrier to product mainly gaseous H_2O and CO_2.

- Chemical-looping combustion with oxygen uncoupling (CLOU) in which solid fuel is burned by oxygen which oxygen carrier is released in the gas-phase.

These processes are more carefully discussed in the three following sections.

3.1.1 Syngas-CLC

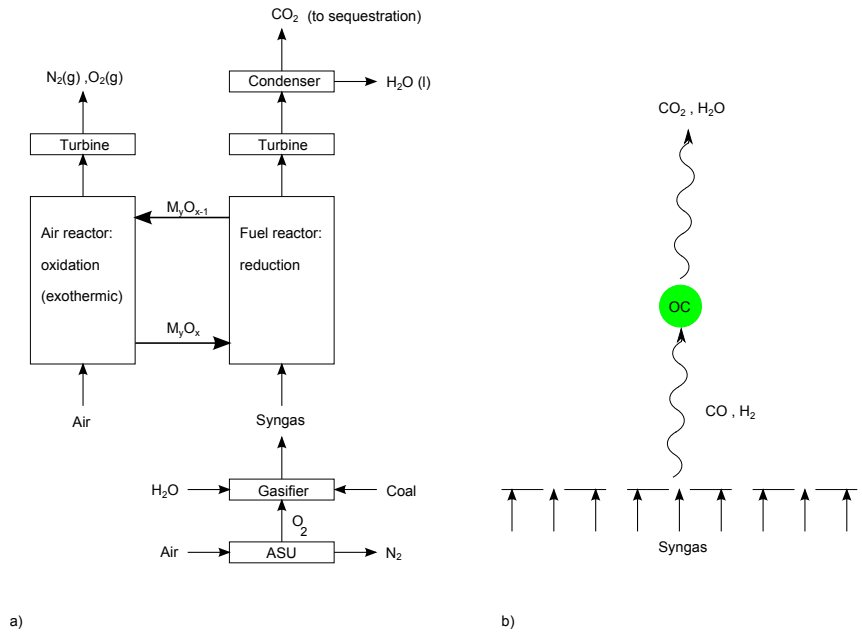

Figure 6: *Principle of syngas-CLC is presented in figure (**a**) and process happened in fuel reactor in iG-CLC is presented in (**b**). In syngas-CLC solid fuel is first gasified and after that formed syngas is fed to the fuel reactor and the it is just like conventional CLC with gaseous fuels. The figure is adapted from [1].*

Principle of syngas-CLC is presented in figure 6 (**a**). Reaction between coal and oxygen carrier is too slow to be suitable for CLC and furthermore there is a risk that coal and ash would cover oxygen carrier, so the coal must be gasified first.[18, 19, 21] Syngas, formed in gasification, is fed to the fuel reactor where it reacts directly with oxygen carrier and become oxidized. [1, 17]Processes which happened during oxidation are presented in figure 6 (**b**). Reaction with syngas and oxygen carrier is exothermic and formed CO_2 and H_2O effluents are transferred to the turbine to generate power. [1, 17, 21]

Advantage in syngas-CLC is that syngas allows high concentration of CO_2 and H_2O and hence the separation of carbon dioxide is easier. Disadvantage of this process is the energy penalty derived from air separation unit which is needed to get pure oxygen to the gasification instead of air.[1, 18, 19] Energy needed in gasification can be realized in two ways either put the gasified right to the air reactor or O_2 can operated as gasifying agent to prevent mixing of N_2 and CO_2[21].

3.1.2 IG-CLC

Principle of iG-CLC is presented in figure 7 (a). In iG-CLC solid fuel and oxygen carrier is physically mixed at the fuel reactor so there is no need to separate gasifier.[1, 23, 22] As such the reaction would be slow, so fluidized mixture of oxygen carrier- particles and fuel with CO_2 and H_2O is made. [22, 23] The process which is presented in figure 7 (b) could be thought to consist of three steps. First coal begins to devolatilizate and gaseous

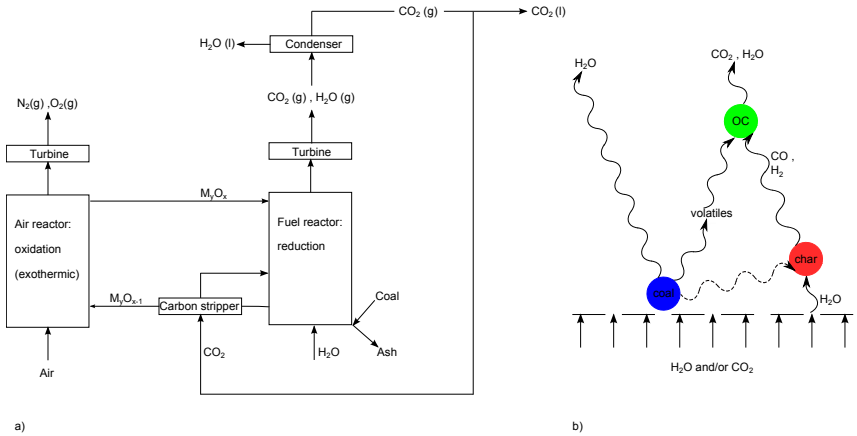

Figure 7: *Principle of iG-CLC is presented in figure (**a**) and process happened in fuel reactor in iG-CLC is presented in (**b**). Coal/other solid fuel and oxygen carrier are physically mixed in fuel reactor. Devolatilization of coal forms volatiles and char. These volatiles and H_2 and CO from char are oxidized at the surface of the oxygen carrier and after reaction gaseous mixture of CO_2 and H_2O is formed. After reduction oxygen carrier is transferred to the air reactor where it goes under reoxidation.The figure is adapted from [1].*

volatile matter and solid char (mainly C) are formed. Then char reacts with H_2O steam and/or CO_2 according to reactions [5, 22, 23]

$$C(s) + CO_2(g) \rightarrow 2CO(g) \tag{3.7}$$

$$C(s) + H_2O(g) \rightarrow CO(g) + H_2(g). \tag{3.8}$$

In second step syngas react with oxygen carrier and syngas become oxidized at the surface of the oxygen carrier according to reaction [5, 22, 23]

$$H_2(g) + CO(g) + \mathrm{n}M_yO_x(s) \rightarrow CO_2(g) + H_2O(g) + \mathrm{n}M_yO_x \tag{3.9}$$

.

In the end oxygen carrier is oxidized in air reactor according to reaction 3.2. Although volatiles are not written in the equation 3.8, they also react with oxygen carrier.[22, 23] Water gas shift reaction, discussed in chapter 3.3, can also effect on gas composition. [1] And like in conventional CLC-process the net reaction and total heat released from combustion are the same as in conventional combustion. Characteristic of used oxygen carriers are same as in conventional CLC and they are discussed later on chapter 4.1. Most promising candidates of oxygen carriers in iG-CLC are copper- and iron-based materials[1, 5].

There are both advantages and disadvantages in iG-CLC and total efficiency is mostly derived from char conversion which is usually low and reactivity of oxygen carriers with volatiles and gasification gases[1, 5]. When char particles in air reactor are exposed to oxygen from air, formation of carbon dioxide is possible.[22, 23] So the outlet of air reactor in iG-CLC can contain small amounts of CO_2. In iG-CLC ash which is accumulated to the reactors with oxygen carrier must be noticed, so that the properties of oxygen carrier does not become weaker. IG-CLC can be carried out of two different ways either using two interconnected fluidized bed reactor or appropriate oxygen carrier in a single fluidized bed with three stages. The first one is commonly investigated but the latter ones offers some advantages over the first one. Because oxygen carriers don't circulate in fluidized bed reactor, mechanical stress is minimized and so the lifetime of oxygen carrier become longer. In this concept separation of unreacted carbon can be avoided.[5, 22, 23]

3.1.3 CLOU

Lewis and Gilliland instituted principle of CLOU-process in 1954 when they patented their idea of produce pure CO_2 from carboneous solid fuels. [1] Mattisson and Lyngfelt patented their idea of alternative method for CLC in 2005 known as chemical-looping combustion with oxygen uncoupling.[25] CLOU-process skips the slow gasification step in iG-CLC and substitutes it with faster solid conversion when char/other solid fuel reacts directly with gas-phase oxygen. So CLOU has more potential to carbon capture from solid fuel. Although CLOU is designed especially for solid fuels it is also capable of combust liquid and gaseous fuels. [1, 25, 27]

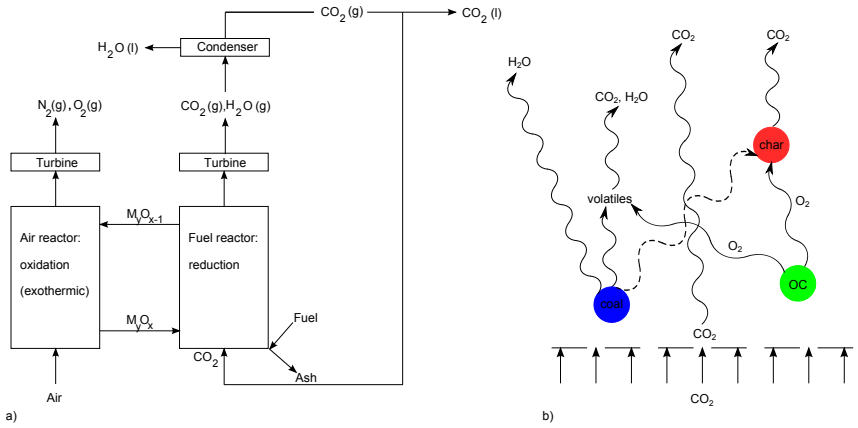

Figure 8: *Principle of CLOU is presented in figure (**a**) and process happened in fuel reactor in CLOU is presented in (**b**). In fuel reactor oxygen carrier is decomposed to the molecular gas-phase oxygen and volatiles and char released from coal's devolatilization are reacted with this oxygen to form gaseous CO_2 and H_2O which can be easily condensate from each other. There are also some H_2O released from coal's devolatilization. After reduction oxygen carrier is transferred to the air reactor where it reacts with oxygen from air and after oxidation oxygen carrier is ready to the new loop. The figure is adapted from [1]*

Principle and main processes happened in CLOU are presented in figure 8. In conventional CLC-process oxygen carrier releases oxygen during reduction reaction while in CLOU-process oxygen carrier is decomposed to the molecular, gaseous oxygen (uncoupling) which can oxidize solid fuels in a fuel reactor according to reactions [1, 5, 24, 27, 28]

$$M_yO_x \rightarrow M_yO_z + \frac{\mathrm{x-z}}{2}O_2 \tag{3.10}$$

and

$$C_\mathrm{n}H_{2\mathrm{m}} + \left(\mathrm{n} + \frac{\mathrm{m}}{2}\right)\mathrm{O}_2 \rightarrow \mathrm{n}CO_2 + \mathrm{m}H_2O \tag{3.11}$$

where $x > z$.

Gaseous CO_2 and H_2O formed in reaction with oxygen released in reduction reaction are transferred to the turbine to produce power. [21, 25] Gaseous H_2O can be easily separated with condensation and pure carbon dioxide is formed. It can then be compressed and cooled to the liquid form for the easier storage. [5, 25] If gaseous fuel is applied it reacts according to reaction 3.11 or with oxygen carrier 3.1 [24].

From fuel reactor reduced oxygen carrier is transferred to the air reactor where it is reoxidize according to reaction

$$M_yO_z + \frac{\mathrm{x-z}}{2}O_2 \rightarrow M_yO_x. \tag{3.12}$$

At the outlet of the air reactor there are only harmfulness nitrogen and unreacted oxygen from the air. [1, 5, 24, 27, 28]

Technically coal, or other solid fuel, descripting in reaction 3.11 is first devolatilizated to form volatiles, char and H_2O. After devolatilization both volatiles and char are reacted with oxygen released from decomposition of oxygen carrier to form CO_2 and H_2O just like in usual combustion.[24, 26] This process is presented in figure 8 (**b**). Reaction 3.11 however demonstrates process good enough. [1]

As can be seen reactions 3.10 and 3.12 cancel each other and CLOU is just like a normal combustion with the same enthalpy as in conventional combustion. [5] If the reaction rate in reaction 3.10 is much faster than the reaction rate in 3.11, oxygen concentration on the fuel reaction is near equilibrium and kinetics of the char combustion is determined by prevailing operation conditions in the fuel reactor. On the other hand if the reaction rate in the reaction 3.10 is much slower than the reaction rate of the reaction 3.11, concentration of oxygen is nearly zero and operating conditions in the fuel reactor are maximized to release carbon dioxide. [24, 27, 28] As a conclusion there has to be enough both oxygen carriers and solid fuel but in suitable relations.

That reactions 3.10 and 3.11 in fuel reactor can happen partial pressure of oxygen must be high enough [5, 25, 26]. This demand set certain demands to the oxygen carriers. If reactions in fuel reactor are exothermic they might cause temperature rise in fuel reactor which again lead to the rise of the oxygen's partial pressure[5, 25, 26]. This must be taken into account of the selection of the suitable oxygen carriers. On the other hand low partial pressure of oxygen produce higher purity of CO_2 stream. [24]

Oxidation at the air reactor is always exothermic reaction and temperature rise at the air reactor is possible [1, 24]. But at the air reactor oxygen's partial pressure must be high enough so that reduced metal oxide can react with oxygen to form oxidized form of metal oxide. [5, 25, 26] This phenomenon is illustrated in figure 9 [24]. Operational conditions must be limited to prevent the rising of oxygen's partial pressure.[21]

In syngas-CLC and iG-CLC solid fuel must gasificated before reacting with oxygen carrier. The problem is that this gasification step is very slow. In CLOU oxygen carrier releases gaseous oxygen which can react with solid fuel just like in normal combustion and slow gasification step is replaced with faster solid conversion. Due to this replacement fuel conversion rates are higher and also much more complete fuel conversion is reached. [25, 28] Other advantages of CLOU process are long lifetime of oxygen carrier, high and stable reactivity and resistance against ash formation. Compared to conventional CLC less oxygen carrier materials are needed. [1, 24] And as like a normal CLC there is no need for separate ASU.[21]

Disadvantages of CLOU is greatly derived from selection of oxygen carrier. Partial pressure of oxygen must be suitable in quite a high temperatures in the operational range T=600-1200 °C. [5] High cost of CLOU materials is also a con but combined with a long lifetime of oxygen carrier and small amounts of oxygen carrier materials, CLOU is also a economical feasible alternative to carbon capture.[1, 5, 24]

3.2 Oxidation and reduction

For a deeper understanding of a reaction mechanism and the redox-process, kinetics parts and thermodynamics play important role, because both are needed for describing redox-reactions. Kinetics parts and thermodynamics parts of the redox-process are illustrated in the figure 10.

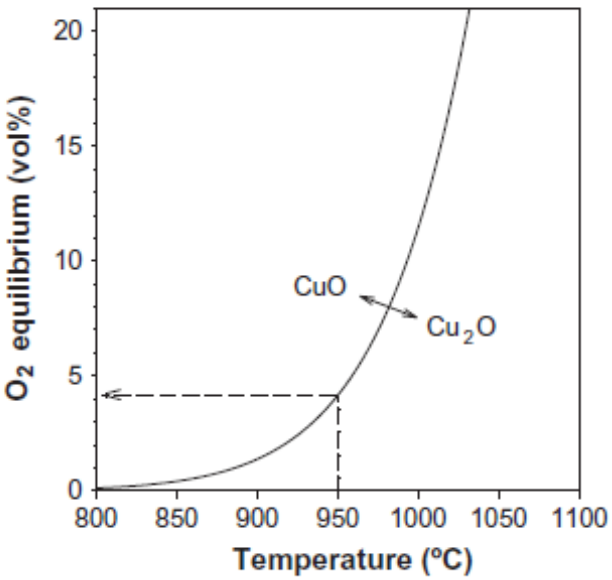

Figure 9: *Figure shows great depedence of partial pressure of oxygen on the temperature in CLOU conditions for copperoxide. It can be seen that for example in temperature 900 °C is only 1.5 vol % O_2 for this oxygen carrier while in 1000 °it is already 12.4 vol % O_2 for CuO/Cu_2O system. And this must be taken into account when choosing suitable carrier for CLOU system. The figure is from [24]*

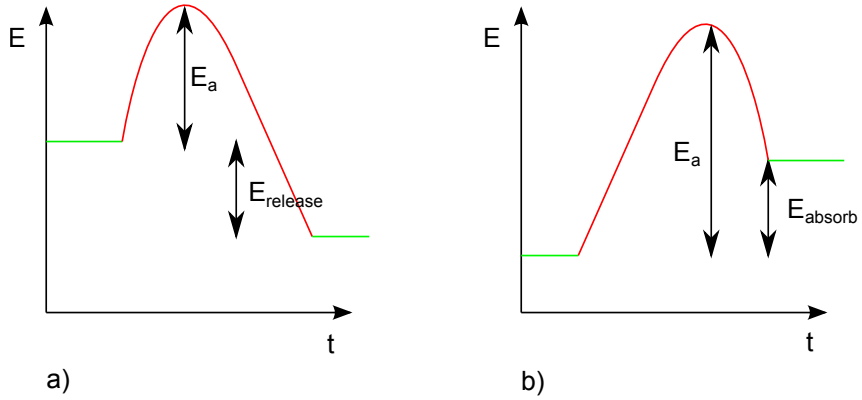

Figure 10: *Exothermic reaction is presented in (**a**) and endothermic reaction in (**b**). Thermodynamically relevant parts are presented green and kinetically relevant parts are red. E_a is activation energy needed in reactions and $E_{release}$ is energy released in exothermic reaction and E_{absorb} is energy absorbed in endothermic reaction.*

3.2.1 Kinetics

Reaction mechanism and kinetics are very important parts of a reactor designing. [6] When thinking about particle kinetics, important quantities are: mass conversion rate ($\frac{d\omega}{dt}$), extent of mass conversion $\Delta\omega$ and extent of fuel conversion γ_{red}. In the case of design data, important parameters are bed mass m_{bed}, solid circulation rate m_{sol} and fuel conversion. [9] Mass-based conversion can be determined by equation

$$\omega = \frac{m}{m_o} = 1 + R_o(X - 1) \tag{3.13}$$

and mass based redox-rates by equation

$$\frac{\mathrm{d}\omega}{\mathrm{d}t} = R_o \frac{\mathrm{d}X}{\mathrm{d}t} = -\frac{R_O}{m}\frac{\mathrm{d}m}{\mathrm{d}t}. \tag{3.14}$$

[10, 11, 51] Conversion is dependent on the fuel used and it can be determined with the help of a partial pressure [10]

$$\begin{aligned} \gamma_{CH_4} &= \frac{p_{CO_2}}{(p_{CH_4} + p_{CO_2} + p_{CO})} \\ \gamma_{CO} &= \frac{p_{CO_2}}{(p_{CO_2} + p_{CO})} \\ \gamma_{H_2} &= \frac{p_{H_2O}}{(p_{H_2} + p_{H_2O})} \end{aligned} \tag{3.15}$$

When conversion is on the intermediate range i.e. oxygen carrier isn't fully oxidized/reduced, conversion rates get improved. [9]

Oxidation and reduction kinetics can be presented with the help of three models which all are based on the physicochemical characteristics

- nucleation and nuclei growth model
- unreacted shrinking core model
- changing grain model.

[6, 11]

Regardless reaction all gas-solid processes follow same steps

1. gaseous reactants diffuse from bulk to the surface of solid particle
2. diffusion of gaseous reactants trough pores
3. adsorption of the gaseous reactants on the solid surface
4. chemical reaction between gas and solid.

First step is so called film-diffusion. If gaseous products are formed, steps one to three are repeated in the opposite direction. [1]

Nucleation model is a model for mechanism and kinetics of gas-solid reactions where solid products are formed. [1, 6] Nucleation is dynamic process which begin with the formation of the nuclei. Then the nuclei grow and overlap with each other. The nucleation sites are ingested and nuclei growth is continued. [6] Although nucleation doesn't observe morphology changes, nucleation is a significant process at the reduction of oxygen carriers. [1, 6] Nucleation is strengthened when the temperature is risen. [1]

Avrami et al. developed Avrami-Erofeev model (A-E)for the kinetics of phase transformations of steel. Latter this model is employed to describe redox kinetics of bulk and metal oxides. This model portrays reduction and oxidation of metal oxide trough nucleation and conversion function can be presented as

$$f(X_S) = n(1 - X_S)[-\ln(1 - X_s)]^{\frac{(n-1)}{n}}, \tag{3.16}$$

where X_s is conversion, n is so called Avrami exponent indicative of the reaction mechanism and crystal growth dimension. When examining certain values for Avrami exponent,

it is noticed that values $n = 2$ or $n = 3$ correspond to two or three dimensional nuclei growth, respectively. [1, 6] With the help of same A-E model conversion versus time curves can be presented as

$$\frac{\mathrm{d}X_s(t)}{\mathrm{d}t} = nk_0 \mathrm{e}^{\frac{-E_{\mathrm{app}}}{R}\left(\frac{1}{T}-\frac{1}{T_0}\right)}(1-X_S)[-\ln(1-X_s)]^{\frac{(n-1)}{n}}, \tag{3.17}$$

where k_o (mol/s) is a specific rate of the overall reaction, E_{app} is apparent activation energy for oxidation/reduction (kJ/mol), R is Boltzmann constant, T is temperature (K) and T_0 is centring temperature. [1, 6] Rate of reaction per unit volume r_g can be expressed as

$$r_g = -k'_s C_g^n C_s^m, \tag{3.18}$$

where k'_s is a kinetic constant, C_g is gas concentration and C_s is solid concentration. By integrating equation 3.17 and using 3.18 and assumed that $n = 1$ (when there is no induction period), time required to the certain conversion can be represented as [1, 6]

$$t = -\frac{1}{k'_s C_g^n}\ln(1-X_s). \tag{3.19}$$

Unreacted shrinking core model combines dependence between size and pore structure to the rate of reaction. [6] In this model metal/metal oxide interface moves to the center of the grain and leaves over metal/metal oxide layer where gaseous reactants and products can diffuse. [6, 11] When the resistance of diffuse is high the unreacted shrinking core model is a good tool for the handling of the kinetics. [1]This diffusion resistance can be reduced by using smaller particles. [6] Heterogeneous reaction can be thought to be consisting of the three parts: external mass transfer, internal mass transfer and chemical reaction. The thickness of the ash layer at the top of the carrier increases within the time leading to the apply of this model. [1, 6]

When assumed that solid-gas reaction proceeds via reaction

$$a\mathrm{A(g)} + \mathrm{b}B\mathrm{(s)} \Rightarrow \mathrm{c}C\mathrm{(g)} + \mathrm{d}D\mathrm{(s)} \tag{3.20}$$

and derivative of the core radius r_c can be expressed as

$$-\frac{\mathrm{d}r_c}{\mathrm{d}t} = \frac{bC_{\mathrm{A}}}{r_c^2/R_p^2 k_g + (R_p - r_c)r_c/R_p D_e + 1/k_s}, \tag{3.21}$$

where R_p is particle radius (cm), C_A is concentration of A and D_e is effective diffusivity ($\frac{\mathrm{cm}^2}{\mathrm{s}}$) and solid conversion can be written

$$1 - X_s = (\frac{r_c}{R_p}). \tag{3.22}$$

[1, 6] Then the time required to reach a certain conversion (assumed that particles are spherical) is

$$\begin{aligned} t &= t_{\mathrm{film}} + t_{\mathrm{pl}} + t_{\mathrm{react}} \\ &= \frac{C_{\mathrm{BO}}R}{3bkC_{\mathrm{AO}}}X_S + \frac{C_{\mathrm{BO}}R}{bkC_{\mathrm{AO}}}(1-(1-X_S)^{\frac{1}{3}}) + \frac{C_{\mathrm{BO}}R^2}{6bkD_{\mathrm{e}}C_{\mathrm{AO}}}[1-3(1-X_S)^{\frac{2}{3}}+2(1-X_S)], \end{aligned} \tag{3.23}$$

where the first term is external diffusion contribution, the second is chemical reaction contribution and the third is internal diffusion layer contribution. [1, 6] When assumed

first order reaction kinetics and Arrhennius expression, conversion versus time curves can be presented as

$$\frac{\mathrm{d}X_s(t)}{\mathrm{d}t} = k_0 \mathrm{e}^{\frac{-E}{R}\left(\frac{1}{T}-\frac{1}{T_0}\right)}(1-X_s)^{\frac{2}{3}}(1-aX_s). \tag{3.24}$$

[6]

Changing grain size model was first developed by Georgagis et al. in 1979. [12] There are some assumptions at the model. In the first place particles are consist of a number of uniform non-porous grains of uniform length r_0 and secondly redox-reactions which happen inside of the oxygen carrier can be described with the help of the reaction

$$\mathrm{a}A(\mathrm{g}) + R(\mathrm{s}) \Rightarrow \mathrm{b}P(\mathrm{s}) + \mathrm{c}CO_2(\mathrm{g}) + \mathrm{d}H_2O(\mathrm{g}). \tag{3.25}$$

[1, 12] During the oxidation step, constants c and d are zeros. Because of the different molar volumes of the product with respect to the reactant, grain size of the reduced metal or the oxidized metal oxide changes from r_1 to r_2. [12] Reduction decreases the grain size and otherwise oxidation increases grain size. [1]

Reaction rates can be determined by solving mass balance equations discussed in chapter 4.3. Just like in the case of the nucleation and nuclei growth model time to reach certain conversion is received by summing different reaction models

$$\begin{aligned} t =& t_{\mathrm{film}} + t_{\mathrm{pl,p}} + t_{\mathrm{pl,g}} + t_{\mathrm{react}} \\ =& \frac{C_{\mathrm{BO}}R}{3bkC_{\mathrm{AO}}}X_S + \frac{C_{\mathrm{BO}}R}{bkC_{\mathrm{AO}}}(1-(1-X_S)^{\frac{1}{3}}) + \frac{C_{\mathrm{BO}}R^2}{6bkD_{\mathrm{e}}C_{\mathrm{AO}}}[1-3(1-X_S)^{\frac{2}{3}}+2(1-X_S)] \\ &+ \frac{C_{\mathrm{BO}}R^2}{6bkD_{\mathrm{s}}C_{\mathrm{AO}}}[1-3(1-X_S)^{\frac{2}{3}}+2(1-X_S)], \end{aligned} \tag{3.26}$$

where the first term is external diffusion contribution, the second term is chemical reaction contribution, the third term is internal diffusion contribution and the last one is product layer around a grain diffusion contribution. [1]. Readman et al. have investigated nickel based oxygen carrier and they have noticed that at the $NiO/NiAl_2O_4$ oxygen coverage at the surface is approximately constant. And as a consequence they concluded that oxygen diffuses from bulk to the surface where the reaction occurs and that it isn't the rate-limiting step. [52]

3.2.2 Thermodynamics

Also thermodynamic is an important part of understanding reaction mechanisms and reactor design. Nucleation discussed in previous section happens when thermodynamically non-stabilize supersaturated solution is favoured. [71] Gibb's free energy is quantity used to describe favourably of thermodynamics processes. For spherical particles Gibb's free energy can be expressed as

$$\Delta G = -\frac{4\pi}{3V}r^3 k_B T \ln S + 4\pi r^2 \gamma, \tag{3.27}$$

where V is the volume of the particle, r is the radius of the nuclei, k_B is Boltzmann constant, S is supersaturation and γ is surface free energy per unit surface area. The first term in equation 3.27 is a free energy of formation of a new volume and the second term is a free energy of a new surface created. [71] Using Gibb's energy, equilibrium constant K can be presented as

$$R\ln K = -\frac{\Delta H_T^{\Theta}}{T} + \Delta S_T^{\Theta}, \tag{3.28}$$

where ΔH_T^Θ and ΔS_T^Θ are standard heat and entropy, respectively. With increasing temperature also the equilibrium constant increases.[11]

If the supersaturated solution in equation 3.27 is $S > 1$ Gibb's energy has a positive maximum which is equal to the activation energy of the nucleation. Critical nuclei size r^* can be found by minimizing Gibbs free energy and then calculating zero point of the derivative. Result is

$$r^* = \frac{2V\gamma}{k_B T \ln S}. \tag{3.29}$$

If this critical size is bigger than the radius of the nuclei, free energy decreases while size increases. Otherwise particle dissolves. When thinking of little nano particles they grow faster than bigger particles. So the nano structures aren't thermodynamically stabilized, but this kind of behaviour can be prevented by adding surface protecting reagents to the surface of the particle or nano particles can be embedded to an inert environment. [71]

Reduction of the oxygen carrier can be described with the help of the oxygen potential

$$\Delta G^\Theta = RTlnP_{O_2}, \tag{3.30}$$

where equilibrium partial pressure is determined from the equation 3.2. Reduction is harder when partial pressure is small. [11]

3.3 Hindrance reactions

There are some unwanted reactions that can be happened in CLC. Coke, which is fuel mainly consist of carbon, is not wanted product in CLC. At the low temperatures the combustion is incomplete. Carbon deposition to the surface of the oxygen carrier can prevent normal action of the carrier while carbon at the carrier's surface is oxidized to the carbon dioxide. This also reduce efficiency of total carbon capture.[6, 29] Two main ways to the coke formation in CLC are pyrolysis (R3.8) while using methane as fuel and the Boudouard reaction (R3.9) while employing syngas as fuel

$$CH_4(\mathrm{g}) \rightarrow C(\mathrm{s}) + 2H_2(\mathrm{g}) \qquad \Delta H = 88\frac{kJ}{mol} \tag{R3.8}$$

$$2CO(\mathrm{g}) \rightarrow C(\mathrm{s}) + CO_2(\mathrm{g}) \qquad \Delta H = -167,7\frac{kJ}{mol}, \tag{R3.9}$$

when temperature is 1 000 °C. [1, 6, 11, 48]. Pyrolysis is favourable in high temperatures and Boudouard, which is exothermic reaction, is favourable in low temperatures although due to kinetic limitations rates of reaction lower. In both reactions metals act as a catalyst rather than a reactant. [1, 6, 11, 21] According to Johansson and Fan nickel, copper and iron act as catalyst while manganese does not [10, 21]. Only the metal forms can catalyst reaction so the avoidance of full reduction of Ni, Cu and Fe oxides to metal helps minimize carbon deposition [46]. Catalyst can be reduced by adjustable temperature, pressure, gas-flow in the reactor and designing criteria for CLC. Pyrolysis can also be adjustable by the addition of steam. While temperature is increased or pressure decreased coke formation is reduced and methane conversion is enhanced.[4, 11, 46] Indeed too high temperature can cause sintering and melting of the carrier. Conditions where coke formation is even possible depend also on the amount of oxygen added with metal oxide[1, 10, 46]

Another unwanted reaction is a water-gas shift reaction in which carbon monoxide is reacted with water vapour to produce gaseous carbon dioxide and hydrogen according to reaction

$$CO(\mathrm{g}) + H_2O(\mathrm{g}) \rightarrow CO_2(\mathrm{g}) + H_2(\mathrm{g}). \tag{R3.10}$$

This reaction is catalysed by transition metals and their oxides. [6, 11] Also the methanation R3.11 reaction is unwanted reaction catalysed by metal

$$CO(\mathrm{g}) + 3H_2(\mathrm{g}) \rightarrow CH_4(\mathrm{g}) + H_2O(\mathrm{g}). \tag{R3.11}$$

[6, 11]

Most of the fuels contain sulphur compounds (mainly HS and COS) and this presence of sulphur species or heavy metals affects negatively to the recyclability of the oxygen carrier[1, 9, 21]. Effect of sulphur depends on concentration of sulphur and metal used. It is notable that sulphur can react also with support material and reduce its features.[1, 6, 29] If the concentration is low, sulphur binds with the surface by absorption and if the concentration is high sulphur and metal form metal sulphide via chemical bonds. In both situations reactivity of the carrier is decreased and if the metal sulphide is formed it is notable that melting points of these metal sulphides are lower than corresponding metal oxides.[9, 21, 29] Particularly reactivity of nickel based carriers is decreased due to sulphur impurities. Instead of it on copper based carriers sulphur in the fuel affects mostly to the quality of the carbon dioxide which purification is easier than in the air reactor. [1, 9, 21] Hossain et al. have examined effects on sulphur species in the fuel for different oxygen carriers and they noticed that CuO, FeO and MnO based carriers are capable to convert H_2S completely to SO_2 in the temperature range 600-1200 °C [6]. In any case when carrier is poisoned with sulphur, activity for fuel combustion might drop significantly. [29]

One option to avoid sulphur effects is remove to sulphur compound before looping unit, but this is a quite expensive alternative. Or oxygen carriers can be designed in the way they can handle of sulphur impurities or that they can avoid deactivation in the presence of sulphur. This could be carrier out so that if carriers form metal sulphides they have ability to form back to metal oxides at the oxidation step according to reaction [21]

$$MS + \frac{3}{2}O_2 \rightarrow MO + SO_2. \tag{R3.12}$$

In this reaction hazardous sulphur compounds are formed. Based on this idea Solunke et al. have present an idea on which CLC can be easily integrated with sulphur capture. [40] At the fuel reactor metal oxide captures sulphur of the fuel as metal sulphide. In the air reactor this metal sulphide is oxidized by the influence of the air's oxygen to the metal oxide according to reaction R3.12 and sulphur captured from fuel is released as SO_2 from air reactor [21, 29]. Challenges of this technique are the conservation of simultaneous thermal stabilization and fast redox kinetics while reached deep desulfurization of the fuel reactor effluent. [40]

4 Oxygen carriers

4.1 Physical and chemical properties of oxygen carriers and support materials

One of the most important aspects for CLC is a selection of a suitable oxygen carrier. By the year 2012 over 700 oxygen carriers were prepared and tested [1]. Oxygen carrier consists of an active metal oxide which is supported on different inert materials. Examined oxygen carriers are mainly transition metals: Cu, Fe, Mn, Co and Ni and their oxides supported with different inert materials.

Hossain et al. [6] and Adanez et al. [1] have listed some features which oxygen carriers should display:

1. be reactive both oxidation and reduction reactions.
2. be able to completely combustion of fuel to maximize fuel combustion efficiency.
3. have sufficient oxygen transport capacity
4. be stable under repeated oxidation/reduction cycles at high temperature
5. be fluidizable to prevent agglomeration
6. be resistant to agglomeration and attrition to minimize losses of elutriated solids
7. be mechanical resistant to the friction stress associated with high circulation of particles
8. have negligible carbon deposition that would release CO_2 in the air reactor reducing CO_2 capture efficiency
9. be economical feasible
10. be environmental friendly

The first two are the most important parameters according to Hossain et al.[6]. There isn't any direct primary order to the features but the last two are not always mentioned in other articles, so they might be less important features.

The first one is a requirement for the whole CLC-process and the second one is also important because if the fuel isn't completely combusted unreacted fuel can exit from fuel reactor with exhaust gases. [6, 29] Degree of fuel conversion to CO_2 can be calculated by minimization of Gibb's free energy. [29] Owing to their ability to convert fuel almost completely to the carbon dioxide Mn_2O_3/Mn_3O_4, CuO/Cu_2O, Fe_2O_3/Fe_3O_4 and NiO/Ni could be good candidates for the oxygen carriers according to Hossain et al.[6]. Fuel conversion is dependent on the redox system and interactions between metal oxide and inert support material can have either positive or negative effect to the fuel conversion. [9, 29]

Agglomeration is an unwanted phenomenon so the particle must be fluidizable. Fluidizability of the particle greatly affects to the controllability of the particle and mass and heat balance [9]. Fludizability is mostly derived from particle's density and size. Increase in size also affects negatively to the reaction rate by decreasing the surface-to-volume ratio.[6, 33] Other important physical property is crushing strength which ought to be in range 3.7-5.2 N. This crushing strength is depending on the active metal and inert material and sintering temperature. [1, 6, 9, 21, 33] High sintering temperature affects positively to the crushing strength by increasing it. [21, 33] Although the resistance increases with sintering, reactivity decreases.[1, 6, 21] Also the particle-particle and particle-walls collisions and continuously reduction and oxidation of carrier decrease mechanical strength by changing the morphology of the oxygen carrier.[9] Porosity which can be greatly affected by preparation method has effects to the mechanical strength. Crushing strength is much higher with less porous oxygen carrier than more porous carrier. On the other hand porosity has positive effect to the reactivity for the both oxidation and reduction reactions because the pores allow gaseous species to diffuse in and out of the particle. [1, 6, 21, 33]

Due to high temperature, the melting point of the oxygen carrier is very important feature in the designing of the CLC process.[1, 6] As mentioned, high temperatures might cause sintering and agglomeration and thereby lower the reaction rates. [1, 6, 29] For example copper have a quite a low melting point for the CLC, only 1085 °C, so the copper isn't suitable for CLC above 900 °C. [12, 48] This sintering and agglomeration can be prevented by using different preparation methods, using support material or in the case of copper substituted copper with copper oxide in which melting point is in the range 1236-1326 °C depending on the particular oxide.[6, 12, 29] Garcia-Labiano et al. have got good results for prevent agglomeration by using impregnation method for preparation of copper based oxygen carrier. [12] Agglomeration may also cause defluidization of fluidized bed and so channelling of the gas stream to make CLC system not to work. [1, 48]

Point eight is dependent on the metal oxide, inert material and H_2O/fuel ratio.[1, 6] Carbon deposition usually happens with Bourdouard reaction which is dependent on the availability of the oxygen. Carbon deposition affects to the carbon dioxide capture efficiency and reactivity if carbon generation is faster than the carbon gasification rate. Carbon deposition may be controlled by temperature control, preventing the excessive reduction of the oxygen carrier or by adding of suitable doping agents onto the particles. [1, 6, 21]

Economical cost of the oxygen carrier is the sum of the material costs of the metal oxide and a support and manufacturing which is a minor cost compared to the raw material. [1, 6, 21] When used nanoscale carriers manufacturing large amounts of carrier is more expensive than in conventional carriers. [47] Also the lifetime of the carrier have impact to the total costs. [21] Manganese and iron based oxygen carriers are the cheapest materials. Nickel and cobalt based are the most expensive materials which are studied and found to be otherwise suitable for the CLC-process.[6] Apart from price another disadvantage of using nickel and cobalt based oxygen carriers are their toxicity. [1, 21] Used and worn carriers needs to be disposed or recycled and thus materials which have low health and environmental impacts are preferred. According to Solunke manufacturing of the oxygen carrier to the CLC-process is not more expensive than absorption techniques employed in post-combustion.[29] If manufacturing is cheap, attrition isn't such an important feature. When oxygen carrier is worn and is no longer working as designed, it can be replaced by a new one.

Oxygen carrying capacity is a good measurement for the quality of the oxygen carrier although it isn't the whole truth. [6, 48] Hossain et al. have listed oxygen carrying capacities for the different metal/metal oxide pairs (without support) and the values varies from 0.083 to 0.67 moles of oxygen per mole of metal depending on the employed carrier. Co_3O_4/Co has the best oxygen carrying capacity 0.67 moles of oxygen per mole of metal and Fe_2O_3/Fe_3O_4 has the weakest ability to carry oxygen 0.083 moles of oxygen per mole of metal. However this oxygen carrying capacity drops while using inert material as a support and it is greatly dependent on the metal loading and stability of the carrier in redox cycles. Hossain et al. have also listed some oxygen carrying capacities of various oxygen carriers and capacities varies between 0.0096-0.13 moles of oxygen per mole of metal depending on the metal oxide, support material and metal loading used. NiO/$NiAl_2O_4$, NiO/$MgAl_2O_4$ and NiO/TiO_2 have the best oxygen carrying capacity 0.09-0.13 moles of oxygen per mole of metal with metal loadings 40-60%, 37-60% and 40-60%, respectively. [6, 48]

Although support material decreases oxygen carrier capacity, using suitable support material which temperature resistance is great, has a positive effect to the CLC-process as a whole. It increases reaction rate by increasing reaction surface and improves thermal stability and intensity of the oxygen carrier. It also improves mechanical resistance and

Table 1: Investigated oxygen carriers and their redox, thermodynamic and diffusivity features
+ feature has a positive effect for the process
- feature has a negative effect for the process

Feature	Cu	Mn	Fe	Ni	Co
Reactivity	+	-		+	
Redox capability	+	-	-	+	-
Temperature stability	-	-		+	
Agglomeration	-	+	+	+	+
Oxygen carrying capacity	+	+	-		+
Porosity			-	-	
Property of physical heat	-	-	-	+	+
Property of chemical heat		-	+	-	

thereby prolongs lifetime of the oxygen carrier. [9, 11, 30, 48] According to Chuang et al. reactivity of the unsupported CuO fell 90 % in three cycles while supported with SiO_2 it was maintained its reactivity over many cycles.[32] Support-inert combination works also as an ion conductor to enhance ion permeability of the oxygen carrier. [30]

In addition to the oxygen transport, another important feature of the oxygen carrier is heat transferring. So the heat capacity of the carrier must be suitable for the process. However heat capacity is quite easy to modify with a suitable support. Currently reaction rates are critical steps on the way towards commercial CLC-process. Reaction rates can be modified by increasing reaction area by using support materials or by decreasing size of the oxygen carrier even to the nanoscale. Reaction rates can also be modified by external factors. CLC-process can be either atmospheric pressure or pressurized. Increasing the pressure also the reaction rates of the oxygen carriers increase. [9]

In summary different features for most widely investigated oxygen carriers are listed. Table 1 presents differences between carriers when redox, thermodynamic and diffusivity features are taken into account. Table 2 presents economical and usability aspects for the choosing of a suitable oxygen carrier. In the table 3 there are some parameters which effect to the design process.

There are some additional requirements for the oxygen carriers in CLOU process. Oxygen carrier must be able to react reversible with gas-phase oxygen at the air reactor at high temperatures and after that it must be capable to release this oxygen through decomposition at the fuel reactor. [5] So the partial pressure of oxygen must be suitable at the temperature range 800-1200°C. Most of the suitable candidates for the CLC aren't suitable for CLOU because they aren't capable of donate and release oxygen at relevant conditions. Otherwise required features from oxygen carrier do not differ from the requirements of CLC. [31] Copper, manganese and cobalt are good candidates for CLOU. [5] Also perovskites are promising candidates for the oxygen carriers in CLOU. [50]

In the air reactor reduced metal oxide must be capable of react with air to form oxidized form of the metal oxide and hence lower the concentration of oxygen to the reasonable level. When the oxygen carrier is transferred to the fuel reactor where the partial pressure of oxygen is lower it decomposes and releases gaseous oxygen. And if the reactions at the fuel reactor are exothermic, partial pressure will be increased and so on the conversion rate of solid fuel also increases. [5, 19, 27, 28]So that any unburned compounds are not

Table 2: Investigated oxygen carriers and their usability and economical features
+ feature has a positive effect for the process
- feature has a negative effect for the process
* [1]

Feature	Cu	Mn	Fe	Ni	Co
CLOU	+	+	-	-	+
Economical feasibility	-	+	+	-	-
Toxicity	+	+	+	-	-
Lifetime	+			+	
Recyclable	-		-		
Minor coke formation	-		-		
User experience (h)*	391	70	97	2114	25
Considerations	exothermic reactions		Full reduction decreases purity of CO_2	Impurities in the FR effluents	Interaction with support

Table 3: Investigated oxygen carriers and properties which effects on the design process of the reactor
+ feature has a positive effect for the process
- feature has a negative effect for the process

Feature	Cu	Mn	Fe	Ni	Co
Fuel conversion	+	+	-	-	+
Fluidization properties	-				
Stability	+		+		
Attrition					-

formed, partial pressure of oxygen must be near to the thermodynamic equilibrium. So it would be useful if temperature at the fuel reactor is lower than sintering temperature and if the reactivity of oxygen carrier is high enough for full combustion.[26] Some features of the oxygen carriers capable for CLOU are listed in the table 4

4.2 Preparation methods

Preparation method of oxygen carrier affects greatly on its features. It affects to the reactivity, stability of the carrier in repeated redox cycles and physical properties like mechanical strength, size, shape, porosity and density. Currently there are various ways of produce carriers which are based on some of three basic methods:

- Mixing of support and powders of metal oxides (mechanical mixing, freeze-granulation, spray drying and dispersion method)
- Generating solid compounds by precipitation (co-precipitation and sol-gel method)

Table 4: Investigated oxygen carriers for CLOU-process
+ feature has a positive effect for the process
- feature has a negative effect for the process

Feature	Cu	Mn	Co
Reactivity		+	
Thermal stability	-	Work poorly at the low temperatures	
Oxygen carrying capacity	-	-	
Fuel conversion	+	+	-
Attrition	+		
Mechanical stability	-	-	
Effect of sulphur species		-	
Lifetime	-		
Economical feasibility		+	-
Environmental friendly	+	+	-
Disadvantages	formation of Cu_2O		Endothermic reaction in the fuel reactor

- Solution containing active metal oxide is deposited on the resistant and porous solid support (impregnation method)

All of these methods are just applied in laboratory scale production but spray drying and impregnation method seem to have potential also for the commercial, large scale production.

4.2.1 Mechanical mixing method

In the first step metal oxide and inert are mixed and crushed in specified ration. Then water is added to the mixture and pasty mass with suitable viscosity is formed. After that mass is slowly dried and shaped to the wanted shape. After shaping oxygen carrier is calcined at the high temperature $950 - 1300°C$. In some references this step is called for sintering. After sintering sample is sieved and oxygen carrier is ready to use. [1, 11] If it is wanted to increase mechanical strength, sintering step can be repeated, but as mentioned in chapter 4.1 this decreases reactivity. The higher sintering temperature the higher density and smaller porosity which enhance mechanical strength. [19] At the begining of the preparation process a small amount of graphite can be added to enhance reactivity and porosity of the inert or the mixture of oxygen carriers.[30, 32] The disadvantage is that regular shape oxygen carriers can't be made by this preparation method [1, 11].

4.2.2 Freeze granulation method

Freeze granulation method produces spherical and highly porous nano and micrometer scale granules with homogeneous composition and micro structure. [10, 34] In the first step active metal, inert material and certain dispersant are mixed and water is added to get pasty mass which can pulverize. Then slurry and pressurized air are placed to the

nozzle where they combine and form uniform spray mist which can be freezing with liquid nitrogen. At the end sample is calcined. [1, 10, 11] Advantages of this process are that it operates easily,uniform porosity, specific surface and density and size can be controlled. Porosity can be controlled by adjusting the water content in the spray slurry and size is adjusted through process parameters in the spraying step. [1, 10, 11, 33, 34]

4.2.3 Dispersion method

Dispersion method differs from mechanical mixing only at the beginning of the production. In first step nitrate of metal oxide and inert material is dissolved to the solution and after mixing they form homogeneous solution which can be dried at different temperature gradient. Then the oxygen carriers can be produces in the same way as mechanical mixing. [1, 11]

4.2.4 Spray drying process

Spray-drying reminds of dispersion method and pasty mass has been manufactured at the same way as mass in dispersion method. When mass is ready it is dried with spraying dried and calcined. [1, 11] Spray drying has better performance and it is easier to industrialize to the production. It has many similarities to the freeze-granulation, so it is believed to to produce similar oxygen carriers by both methods. [1, 10]

4.2.5 Co-precipitation method

Co-precipitation is based on precipitate. First two nitrate solutions are mixed slowly and they form precipitate which is covered with liquid which can be decanted away. When liquid is removed, precipitate can be washed with distilled water and filtered. [1, 19] After sieving sample is roasted at the oven. [11]

4.2.6 Sol-Gel method

Sol-gel method is for production of inorganic materials at surrounding temperature. Process begins with a formation of a colloidal suspensions which can be coagulated to get wet gel. After drying it forms dry gel called xerogel. Advantages of this method are finer and well distributed particles. But process has difficulties to operate and it costs much. [1, 11]

4.2.7 Wet Impregnation method

Impregnation method is a promising method because it operates easily. Inert support is first crushed and sieved, then it is impregnated with saturated aqueous solution of metal nitrate. Then the sample is dried and calcined at high temperature where metal nitrate decomposes to metal oxide and support generates active phase. This step can be repeated to produce particles with several loadings of metal oxides. In this method better porosity and specific surface is achieved. [11, 32] Garcia-Labiano et al. stated that impregnation method is the only method to get reaction rates high enough for Cu-based oxygen carriers. Carriers made by this method nor agglomerate. [12] On the other hand Adanez-Rubio et al. have examined copper based Al_2O_3 supported oxygen carriers and noticed that carriers made by this method can't be employed in CLOU because they can form $CuAl_2O_4$ and so lose their ability to donate oxygen. In CLC these kind of carriers operate and if they are made by spray-drying they operate well also in CLOU [19].

4.3 Mass and heat balance

Purpose of the oxygen carriers for the CLC-process is to carry oxygen (mass) and heat. Circulation rate must be convenient that carrier can transfer enough oxygen to the fuel reactor and when needed transfer heat away from the fuel reactor to avoid temperature rise in the fuel reactor and maintaining heat balance of the process. Mass and heat balances discussed below give good tools for a selection of a suitable oxygen carrier.

Although heat released from the process is depending on the oxygen carrier and used fuel, heat is same as in normal combustion. So it offers a way to calculate if the reactions in fuel reactor are exothermic or endothermic.[48] Oxidation step is always exothermic while reduction is exothermic when applied H_2 or CO as fuels. When methane is employed as fuel reduction reactions are exothermic except for in the case of copper based carriers. [1, 48].

Oxygen carrier can transfer heat by convection and radiation around the particle and just by radiation inside the particle. When consider spherical particle, the unsteady-state heat transfer equation for whole system can be written

$$\frac{1}{R^2}\frac{\partial}{\partial R}(\lambda_{\mathrm{ef}} R^2 \frac{\partial T}{\partial R}) = \overline{\rho_{\mathrm{r}} c_{\mathrm{p}}} \frac{\partial T}{\partial t} + (-r_{\mathrm{R}})\Delta H_{\mathrm{r,R}}, \tag{4.1}$$

where R is a radial coordinate within the particle, λ_{ef} is the effective thermal conductivity of the particle, $\overline{\rho_{\mathrm{r}}}$ is average true density of the particle,$\overline{c_{\mathrm{p}}}$ is a heat capacity at the constant pressure , r_{R} is a local reaction rate of the gas reactant A and $\Delta H_{\mathrm{r,R}}$ is heat of the reaction per mol of solid R. [12]

When used steady state assumption, equation 4.1 can be expressed as

$$q_{\mathrm{m,air}} c_{\mathrm{p,air}} T_{\mathrm{air}} (T_{\mathrm{air}} - T_0) + q_{\mathrm{m,fuel}} (c_{\mathrm{p,air}} T_{\mathrm{fuel}} (T_{\mathrm{fuel}} - T_0) + q_{\mathrm{m,air}}) = \tag{4.2}$$

$$q_{\mathrm{m,N_2,oxd,out}} c_{\mathrm{p,N_2}} T_{\mathrm{oxd}} (T_{\mathrm{oxd}} - T_0) + q_{\mathrm{m,O_2,oxd,out}} c_{\mathrm{p,O_2}} T_{\mathrm{oxd}} (T_{\mathrm{oxd}} - T_0) + \tag{4.3}$$

$$q_{\mathrm{m,CO_2,red,out}} c_{\mathrm{p,CO_2}} T_{\mathrm{red}} (T_{\mathrm{red}} - T_0) + q_{\mathrm{m,H_2O,red,out}} c_{\mathrm{p,H_2O}} T_{\mathrm{red}} (T_{\mathrm{red}} - T_0) + \Delta H, \tag{4.4}$$

when assumed that $T_{\mathrm{CO_2,red,out}} = T_{\mathrm{H_2O,red,out}} = T_{\mathrm{red}}$ and $T_{\mathrm{N_2,oxd,out}} = T_{\mathrm{O_2,red,out}} = T_{\mathrm{oxd}}$ and T_0 is standard temperature (289.15K). [53, 54] As mentioned in chapter 3 endothermic reaction dropped temperature at the fuel reactor. Temperature at the air reactor is about 50°C higher so the carrier can transfer heat from the air reactor to the fuel reactor to satisfy the heat balance. [48, 49]

Temperature variations depend on the mass conversion $\Delta\omega$

$$\Delta\omega = \frac{m}{m_o}, \tag{4.5}$$

where m and m_o are masses of initial and fully oxidized oxygen carriers, respectively. [48] To get small temperature change ΔT, mass conversion must be low. [1] This temperature change can be calculated with the help of a mass and heat balance while stating that enthalpy of the products is same as the enthalpy of the reactants according to equation

$$H_{react} = \sum x_i h_i = H_{prod} = \sum y_i h_i, \tag{4.6}$$

where h_i is the enthalpy of a component i and x_i and y_i are moles of reactants and products, respectively. Enthalpy at the constant pressure can be calculated with the help of molar heat capacity c_p

$$h_i = h_{0i} + \int_{T=298}^{T} c_{p,i}(T)\mathrm{d}T, \tag{4.7}$$

where H_{0i} is heat of the formation at T=289 K. With the help of equations 4.6 and 4.7 ΔT can be calculated. [48]

Mass balance is determined by the circulation rates between two reactors and it is dependent on the oxygen carrier and fuel used. Mass flow consists of transfer of oxidized and un-oxidized oxygen carrier and inert support. In the mass balance point of view the most important parameter which describes oxygen carrier is oxygen transport capability R_O.[1, 49, 53] It is defined by equation 3.5. Solid conversion X_s can be defined by the same way

$$X_s = \frac{m - m_r}{m_o - m_r} = \frac{m - m_r}{R_{OC} m_o}, \tag{4.8}$$

where m is the initial mass and m_r and m_o are the masses of fully reduced and oxidized carriers, respectively. [1].

Mass transfer between reactors is governed by an un-steady state mass balance equation

$$\frac{1}{R^2}\frac{\partial}{\partial R}(D_{\mathrm{e,A}} R^2 \frac{\partial C_{\mathrm{A}}}{\partial R}) - (-r_{\mathrm{A}}) = \frac{\partial C_{\mathrm{A}}}{\partial t} \tag{4.9}$$

with initial- and boundary conditions

$$C_{\mathrm{A}}(R,t) = C_{\mathrm{A,b}} \qquad t = 0 \tag{4.10}$$

$$\frac{\partial C_{\mathrm{A}}}{\partial R}|_{\mathrm{R=R_0}} = 0 \qquad t \gg 0 \tag{4.11}$$

$$-D_{\mathrm{e,A}}\frac{\partial C_{\mathrm{A}}}{\partial R}|_{\mathrm{R=R_0}} = k_{\mathrm{g}}(C_{\mathrm{A,s}} - C_{\mathrm{A,b}}) \qquad t \gg 0, \tag{4.12}$$

where R is a radial coordinate within the particle, $D_{\mathrm{e,A}}$ is effective diffusivity of gas A within the particle, $C_{\mathrm{A,s}}$ is gas concentration at the external surface of the particle, $C_{\mathrm{A,b}}$ is gas concentration at the bulk phase and r_{A} is the local reaction rate of the gas reactant A. [12] This equation describes gas concentration profile trough the particle. [49] When used steady state approximation and looked transporting from air reactor to fuel reactor, equation 4.9 can be simplified to the form

$$q_{\mathrm{m,solid,oxd,out}} = q_{\mathrm{m,M_yO_x,oxd,out}} + q_{\mathrm{m,M_yO_{x-1},oxd,out}} + q_{\mathrm{m,support,oxd,out}}, \tag{4.13}$$

where

$$\begin{aligned}
q_{\mathrm{m,M_yO_x,oxd,out}} &= q_{\mathrm{m,M_yO_x,red,in}} = (2n+m) q_{\mathrm{m,fuel}} \frac{M_{\mathrm{M_yO_x}}}{M_{\mathrm{fuel}} X_{\mathrm{red}}} \\
q_{\mathrm{m,M_yO_{x-1},oxd,out}} &= q_{\mathrm{m,M_yO_{x-1},red,in}} = q_{\mathrm{m,M_yO_x,oxd,out}} \frac{1 - X_{\mathrm{oxd}}}{X_{\mathrm{oxd}}} \\
q_{\mathrm{m,support,oxd,out}} &= q_{\mathrm{m,support,red,in}} \\
&= q_{\mathrm{m,M_yO_x,oxd,out}} \frac{w_{\mathrm{support}}}{w_{\mathrm{M_yO_x}}} + q_{\mathrm{m,M_yO_{x-1},oxd,out}} \frac{w_{\mathrm{support}}}{w_{\mathrm{M_yO_x}}} \frac{M_{\mathrm{M_yO_x}}}{M_{\mathrm{M_y}}}.
\end{aligned}$$

Here $q_{\mathrm{m,i}}$ is a mass flow of species i, M_{i} is a molar mass of species i, w_{i} is a weight fraction and $X_{\mathrm{oxd/red}}$ is a degree of oxidation/reduction. [53] Constants n and m are the reaction coefficients from the equations 3.2 and 3.1.

Most of the oxygen carrier is reduced in fuel reactor, but minor part does not react. So the mass flow from the fuel reactor to the air reactor can be thought in a same way as mass flow from opposite direction

$$q_{\mathrm{m,solid,red,out}} = q_{\mathrm{m,solid,oxd,in}} = q_{\mathrm{m,M_yO_x,red,out}} + q_{\mathrm{m,M_yO_{x-1},red,out}} + q_{\mathrm{m,support,red,out}}, \tag{4.14}$$

where

$$q_{\mathrm{m,M}_y\mathrm{O}_x,\mathrm{red,out}} = q_{\mathrm{m,M}_y\mathrm{O}_x,\mathrm{oxd,in}} = q_{\mathrm{m,M}_y\mathrm{O}_x,\mathrm{red,in}} - (2n+m)q_{\mathrm{m,fuel}}\frac{M_{\mathrm{M}_y\mathrm{O}_x}}{M_{\mathrm{fuel}}}$$
$$q_{\mathrm{m,M}_y\mathrm{O}_{x-1},\mathrm{red,out}} = q_{\mathrm{m,M}_y\mathrm{O}_{x-1},\mathrm{oxd,in}} = q_{\mathrm{m,M}_y\mathrm{O}_{x-1},\mathrm{red,in}} + (2n+m)q_{\mathrm{m,fuel}}\frac{M_{\mathrm{M}_y\mathrm{O}_x}}{M_{\mathrm{fuel}}}$$
$$q_{\mathrm{m,support,red,out}} = q_{\mathrm{m,support,oxd,in}} = q_{\mathrm{m,support,red,in}}. \tag{4.15}$$

Because there are CO_2 and H_2O at the outlet of the fuel reactor also they have to be taken account when calculated total heat balance of the fuel reactor

$$q_{\mathrm{m,CO_2,red,out}} = nq_{\mathrm{m,fuel}}\frac{M_{\mathrm{CO_2}}}{M_{\mathrm{fuel}}} \tag{4.16}$$
$$q_{\mathrm{m,H_2O,red,out}} = mq_{\mathrm{m,fuel}}\frac{M_{\mathrm{H_2O}}}{M_{\mathrm{fuel}}}. \tag{4.17}$$

Air needed for the combustion is a sum of incoming O_2 and N_2

$$q_{\mathrm{m,air}} = q_{\mathrm{m,O_2,oxd,in}} + q_{\mathrm{m,N_2,oxd,in}}. \tag{4.18}$$

Furthermore it must be noticed that all incoming nitrogen is leaving from the air reactor without reacting and that can be written

$$q_{\mathrm{m,N_2,oxd,in}} = q_{\mathrm{m,N_2,oxd,out}}. \tag{4.19}$$

Amount of incoming oxygen is dependent of air fraction λ, which determines the volume fraction of the oxygen in the air reactor leaving the air reactor

$$q_{\mathrm{m,O_2,oxd,in}} = 2\lambda q_{\mathrm{m,fuel}}\frac{M_{O_2}}{M_{fuel}}. \tag{4.20}$$

[48] All oxygen does not react and remain oxygen is emitted from the air reactor

$$q_{\mathrm{m,O_2,oxd,out}} = q_{\mathrm{m,O_2,oxd,in}} - (q_{\mathrm{m,solid,O_2,oxd,out}} - q_{\mathrm{m,solid,O_2,oxd,in}}). \tag{4.21}$$

Mass flow of the oxygen carrier $\dot{m}_{OC}$ from the fuel reactor to the air reactor for oxidation can be written as

$$\dot{m}_{OC} = \frac{m_{O_2}}{\Delta X_{OC} w_{MO}}, \tag{4.22}$$

where m_{O_2} is a mass of oxygen required for the fuel gas conversion, ΔX_{OC} is a difference of the oxygen carrier metal conversion between the reactors and w_{MO} is a content of an active metal in carrier in its fully oxidised state. [49]. Oxygen to fuel ratio ϕ is determined by the equation

$$\phi = \frac{R_{OC}\dot{m}_{OC}}{\dot{m}_O M_O}, \tag{4.23}$$

where $\dot{m}_O$ is an oxidant flow rate and M_O is an atomic weight of oxygen. [1] Molar equilibrium constant $K_{x,i}$ for each oxidation reactions can be determined

$$K_{\mathrm{x,i}} = \frac{X_{\mathrm{CO_2}}}{X_{\mathrm{fuel}}} = \exp(-\frac{\Delta G_{\mathrm{f,i}}}{T_{\mathrm{FR}}}), \tag{4.24}$$

where T_{FR} is a temperature of the fuel reactor. Purity of CO_2 steam can be qualify from the molar fraction of CO_2 in water free fuel reactor exit gas flow. [49]

4.4 Cu-based oxygen carriers

High reactivity and fast redox-kinetics of copper-based carriers are proven in many studies. [1, 9, 10, 12, 19, 32, 51, 65, 66] Also the oxygen carrying capacity R_0 is better in copper compared to the other materials.[1, 19, 32, 51, 68] Rate of conversion is increased as a function of temperature and there have not any thermodynamics restrictions for the complete conversion to CO_2 and H_2O. [1, 65]

Biggest disadvantage of a copper carrier is derived from the thermal properties of copper. Because melting point is low, sintering and agglomeration is observed in many studies.[10, 30, 66] On the other hand agglomeration and thermal stability depend greatly of the support used. Gayan et al. [68] have examined different preparation methods (co-precipitation, mechanical mixing, wet impregnation) and they made conclusion that impregnation method is an optimal preparation method for the copper carrier while Chuang et al. [32] ended up to the conclusion that co-precipitation method is the only way to produce sintering-resistant copper carriers with high loading of copper. Also Garciá-Labiano et al. [12] noticed that copper carriers made by impregnation method do not agglomerate while reactivity is still high. Zeng et al. [9] again find out that impregnation method is the only way to manufacture recyclable oxygen carriers. By co-precipitation method pH is the only parameter which affects to the oxygen carrying capacity. If the porosity of the carrier is high, pH must be quite a low ($\sim$ 7.1) to get high R_0. If the material is dense, suitable pH is much higher ($\sim$ 9.7) [32] Gayan et al. again noticed that impregnation method ensures high reactivity and stability for the copper carriers. [68] In his doctoral thesis Johansson [10] made a suggestion that freeze-granulated method could be useful when prepared copper-based carriers but Cho et al. [66] again have observed that carriers made by this method are prone to agglomerate. Agglomeration could be prevent by using a suitable support. But for example Al_2O_3 supported copper can react with support material and so avoid normal action of the carrier. [34] Copper can go through two step reduction $CuO \rightarrow Cu_2O \rightarrow Cu$.[9] Intermediate Cu_2O suffers from low reaction rates slowing the whole process. [9, 67].

One important feature which makes copper an optimal oxygen carrier is that both oxidation and reduction reactions are exothermic regardless from fuel used. [9, 10] Along these properties some features which make copper feasible oxygen carrier are that copper is not toxic and it is rather cheap. [9, 10, 32]

4.5 Mn-based oxygen carriers

Manganese is an another oxygen carrier material deal with this thesis. The results from the manganese-based carriers are somewhat conflicting. Cho et al. stated that the reactivity of the manganese is too low to be suitable for CLC. [66] Shulman et al. and Zafar et al. again are of the opinion that manganese has high reactivity with high recirculation rates at least at the CLOU-process. [27, 51] On the other hand, Zeng and collaborators [9] have come to the conclusion that manganese has good redox-properties. It is clear that reactivity depends on many properties of the material, like metal oxide content, inert and sintering temperature. [30]

Manganese although suffers from poor thermal properties. When temperature is too low (T<700 °C), reaction rates are too low. [9] When temperature is too high (T>1100 °C) there are more problems. First of all there are some thermodynamic restrictions and secondly if manganese is supported with SiO_2, irreversible silicates can be formed causing reduced reactivity. [10, 51] At high temperatures Adanez et al. [1] have observed

Table 5: Investigated nano carriers

Oxygen carrier	Support	Diameter of carrier (nm)	Diameter of porous (nm)
Fe, Ni, Cu, CuO	BHA	10	5
Pt	BHA	10	
Fe_3O_4	SiO_2	12	
Fe	BHA	15-20	
Cu, Ni	BHA		20
Cu	BHA	10 (BHA), 50 (Cu-phase), 40 (Otherwise)	
Fe		100	
$LaMnO_3$		40-50	
Cu-Al	LDH	12-40	

agglomeration. Furthermore manganese has lower methane conversion compared to the copper, and there are also some fluidization problems when manganese-based oxygen carriers are employed, which is proven in the study of Mattisson et al. [65] Decomposition of manganese oxide MnO_2 is dependent of the temperature. When temperature is quite a low (T=500 °C) it is decomposed to the Mn_2O_3 while at the higher temperatures (T=950 °C) it decomposes to the Mn_3O_4. [30] Clear benefits of using manganese-based oxygen carriers are high oxygen carrying capacity and high crushing strength. Crushing strength again is one primary parameter that gives an indication of the mechanical strength of the carrier. The higher crushing strength, the higher mechanical strength and again longer lifetime of the carrier. Manganese is also cheap and non-toxic. [1, 9, 65]

5 Nanostructures as oxygen carriers

Because of their ability of faster redox kinetics, nano structures as oxygen carriers have shown great potential, although investigation around topic is little and new compared to the conventional carriers. There is not yet any computational research around this subject and researches have focused to the experimental approach.

Examination around nano carriers have widely going around iron, nickel and copper based carriers combined with barium hexa aluminate (BHA) matrix. [20, 29, 38, 39, 40, 41, 42, 44] Perovskite based nano carriers are investigated by Sarshar et al. [2]. Park et al. [43] have done studying around silica-encapsulated, iron based nano carriers. Copper based layered double hydroxide (LDH) precursor as a prototype for the chemical looping combustion with a nano carrier is analyzed by Song et al. [50]. LDH is a class of a two-dimensional nanostructured anionic clay. [50] When comparing sizes of these carriers it is notably that diameter of the smallest particle is about 10 nm while the largest nano carriers have diameter about 100 nm. Sizes and investigated nano carriers are listed in the table 5.

5.1 Synthesis and characterization

Different preparation methods are discussed in chapter 4.2. One method not discussed there is reverse microemulsion. Reverse microemulsion based on sol-gel method is applied to prepare nano oxygen carriers. Method is based on dispersion of water phase into oil phase using a surfactant and co-surfactant [35]. Reverse microemusion is more detailed

discussed Sakka S. [36] and Demchenko A.P. [37] in their books. Reverse microemulsion method for the preparation of the nanocarriers have employed Solunke et al. [29, 39, 40, 41], Najera et al. [42], Kirchhoff et al. [38], Park et al.[43] and Liu et al. [44]. Impregnation method for preparation of nano carrier is used Sarshar et al. [2], Tian et al. [20] have applied mechanical mixing method and Song et al. [50] have employed co-precipitation method for the synthesis of the nano carriers.

5.2 Oxidation and reduction of metals in nano-scale

5.2.1 Oxidation and reduction pathways: $CuO \rightarrow Cu_2O \rightarrow Cu$

When nano copper oxide is reduced, it isn't reduced from oxidized form CuO right to the reduced form Cu. Typically reduction of bulk CuO is shown direct transformation to Cu without formation of intermediate phases. Nano crystalline CuO reduced first to the Cu_2O and then to Cu as the reaction 5.1 states

$$CuO \rightarrow Cu_2O \rightarrow Cu. \tag{5.1}$$

[64] This might be seen as a disadvantage while using nano carriers because the activation energy of Cu_2O reduction to Cu is twice as large as that of CuO. It would make the reaction more difficult to happen. [9]

5.2.2 Thermodynamics and kinetics

It is experimentally proven that oxidation and reduction is easier and faster at the nano scale. Song et al. have investigated nickel nano particles and their properties in oxidation behavior with thermogravimetric analysis and scanning calorimetry under different heating rates. They found out that unlike in conventional carries activation energy of the nickel nano particle is not constant but it is dependent on the conversion ratio. After all the activation energy for the oxidation process of the nano particles was smaller than bulk one following from the decreased energy barrier for oxidation. [15]

Song et al. have also studied oxidation and oxidation kinetics at the nano scale with the same methods as previously, but under heating and isothermal modes. [15, 16] They have found out that oxidation is different at the nano scale and it could be possible to make diffusion easier by modifying the diffusion path, which again is a synergy of different factors.[16] Although they stated that oxidation is different at the nano scale, they also remind that further investigation is needed for deeper understanding. Especially further research is needed at the high temperatures where sintering is notable and diffusion is not longer only transport mechanism albeit dominant. [15] It would be important to examine these diffusion routes at the high temperatures to achieve some kind of picture on what happens at the micro scale and what are the most dominant mechanisms for the oxidation of the nanoparticles at high temperatures.

5.3 Metals for nanocarriers

When thinking of whether to use metal or metal oxide, some features must be taken into account. First, melting points of metal oxides are higher and so they are more durable against thermal stress. [29] Second, Schallow et al. have experimentally proven that initial reaction rates are low after oxidation and they have concluded from that, that CO_2 reaction probability on a nano metal oxide surface is much higher than on a metallic

surface [55]. As discussed earlier 3.3 some metals can act as a catalyst in the harmful Boudouard and pyrolysis reactions, thus the full reduction back to the metal form must be avoided. So it might be useful if the carriers were ready at the oxide form in the beginning of the redox cycle.

Copper based nanocarriers, whose sizes (diameters) vary from 10 nm to 40 nm, 5 are investigated by Solunke et al. [29, 40, 41], Tian et al. [20] and Song et al. [50]. It was noticed that redox-kinetics is improved (oxidation kinetics by a factor of five and reduction kinetics about by a factor three) and structure is thermally stable. [20, 29, 40, 41, 50] According to Tian et al. acceleration in redox-kinetics is mild but significant. [20] Furthermore copper based nanocarriers show high oxygen storage (12 wt%). [50] Compared to the nickel based carriers they have shown slower sulfur uptake and copper based nanocarriers are more prone to sulfide formation. [29, 41] Tian et al. have observed that redox kinetics is accelerated more on nickel based nanocarriers than on copper based nanocarriers. [20] On the other hand oxygen carrier capacity R_O is increased 57 % for copper based carriers and only 27 % for nickel carriers in the presence of H_2S. [41] Because on the study of Tian et al.[20] there was no sulfur, it can concluded that if there is some sulfur copper should be better carrier and if there is not sulfur, nickel should be better alternative.

Nickel based nanocarriers have experimentally investigated Liu et al. [44] and Solunke et al. [29, 41]. In these research improved redox kinetics and thermally stable structure was observed. [29, 41, 44] When compared to the conventional carriers nickel based nanocarriers show instantaneous re-oxidation ($<$ 1min) while for conventional carriers this step is much longer ($\sim$ 60 min). [44]

Iron based nanocarriers are investigated by Solunke et al. [39], Najera et al. [42] and Wen at al. [47]. They all noticed that kinetics is enhanced. [39, 42, 47] In the studies of Solunke et al. [39] and Najera et al. [42] iron based nanocarriers are shown to be thermal stable. [39, 42] Instead of it Wen at el. have observed that nanocarriers melt and sinter in the early state. Furthermore they stated that iron based nanocarriers suffer from agglomeration, poor fluidization properties and morphology changes. [47] It must be noticed that Wen et al. have not used any support material, so it is quite logic that thermal stability is not as good as on the investigations of Solunke et al. and Najera et al. There is not much investigation around manganese based nanocarriers, but Sarshar et al. have made a research about manganese based nano perovskite oxygen carrier and they got promising results from accelerated redox-kinetics.

5.4 Suitable supports for nanocarriers

Most extensively studied support material for a nano carrier is a barium hexa aluminate (BHA) [20, 29, 38, 39, 40, 41, 42, 44]. BHA makes carrier active, sintering-resistant, thermal stable and it offers high reactivity and fast redox kinetics and it is stable in multiple redox cycles. [29, 38, 41, 42] BHA also offers stable operation in CLC sulfur-free as well as sulfur-laden syngas. [40] Tian et al. have observed that particle size and distribution do not change during the CLC cycle when oxygen carrier is embedded to the BHA matrix. [20] Kirchhoff's experiments were focused to the thermal features of the BHA supported nano structures, not to the CLC process. They found out that BHA is an amorphous structure which remains its thermal stability up to 1200 °C. After that point, crystallization point of the BHA is achieved and large mass transport leads to the collapse of the textural structure of the agglomerates and surface area is reduced. [38] Thus BHA is not suitable support material on temperatures over 1200 °C.

The disadvantages of the BHA support include: It is quite a difficult to produce compared for example bentonite support (used for conventional carriers). Tian et al. have used mechanical mixing method for the preparation and they made experimental observation that during the drying phase strongly bound agglomerates were formed. [20] Furthermore, toxicity of the BHA is not known, but at least barium aluminate $3\,BaO{\cdot}Al_2O_3$ is known to be toxic. So BHA should be handled with caution until more knowledge is available. [41] In the presence of sulphur residues, BHA can react with sulphur and form $BaSO_4$. When support becomes sulfidized, its activity decreases. [29]

Silica-encapsulated iron oxide nanocarrier is applied on the study of Park et al. [43]. Carrier was built of a Fe_3O_4/Fe core of thickness 15.5 ± 2.0 nm and a mesoporous silica shell of thickness 4.5 ± 1.0 nm. They believed that porous silica shell can protect oxygen carrier against sintering. This kind of carriers can reach 100 % fuel conversion, which is experimentally proven in the study, and still retain their magnetic features. Silica shell makes carrier sintering resistant and resistant to the bulk phase transition. [43] Carrier studies on silica encapsulated nano platinum carriers indicate that they are thermally stable at high temperatures and capable for CO oxidation. [63] For CLC platinum is not suitable because of its poor oxygen storage capacity. The silica shell stabilizes the core and impedes morphology changes. It also enables that the oxygen storage capacity does not lower at the repeated cycles. Disadvantages of this carrier is that activity of the CO oxidation greatly depends on the size, shape and phase of the core material. [43]

Song et al. have investigated a layered double hydroxide (LDH) precursor as a support material. LDH is a class of two-dimensional nano structured anionic clay and it can be presented by the general formula $[(M^{2+})_n(M^{3+})_m(OH)_{2(n+m)}]^{m+}[(A^{x-})_{m/x} \cdot yH_2O]$ where M^{2+} could be the metal cations: Ca2+, Mg^{2+}, Zn^{2+}, Co^{2+}, Ni^{2+}, Cu^{2+}, Mn^{2+}, Fe^{2+} and M^{3+} could be: Fe^{3+}, Cr^{3+}, Al^{3+}, Ga^{3+}, Mn^{3+} and A^{x-} is an interlayer exchangeable anion (like OH^-, NO_3^-, CO_3^{2-}, Cl^-, SO_4^{2-}) and m is varied between 0.17-0.40. [50] Advantages of this support are stable gaseous oxygen release capacity, high oxygen storage, good thermal stability and high reaction rates. Reduction is more facile owing to the smaller crystal and more porous structure. Carriers on this support do not seem to be agglomerated. And if there are some sodium added to the support, melting point of the support increases making carrier more thermally stable and enhance oxidation simultaneously. LDH also maintains morphology which improves cycling stability in recyclables cycles in both conventional CLC and CLOU. At temperatures above 950 °C sintering and agglomeration take place reducing available surface area. [50]

5.5 Can the nanostructures be suitable for CLOU?

Studies dealing with both nano carriers and CLOU at the same article are sparse. But in the case of conventional carriers, copper and manganese based carriers are found to be suitable for CLOU. Furthermore there are some research about copper based nano carriers. Although further research is needed to ensure that nano copper carriers could be used in CLOU, it seems that it might be possible that they can be applied in CLOU process. Song et al. [50] have investigated CuO/Al_2O_4 derived from the LDH precursor and they found out that formation of $CuAl_2O_4$ reduce oxygen release capacity at typical CLOU operating temperatures. And thus make it suitable carrier for CLOU because of the suitable partial pressure of oxygen. In order to have a suitable partial pressure for CLOU, overmuch $CuAl_2O_4$ can not be formed. Formation can easily be regulated by adding small amounts of sodium to the carrier. Carriers made by same method as in reference [50] allow regulation of amount of formed $CuAl_2O_4$. In conventional CLC small amounts of $CuAl_2O_4$

enhance mechanical stability without reducing oxygen release capacity. [50] Derived from their smaller size, melting points of the nano carriers are lower. On the other hand Zeng et al. stated that surface melting and smaller size enhance properties needed for CLOU. [9] This statement supports the applicability of nanocarriers in CLOU.

5.6 Advantages and disadvantages of using nanostructures as oxygen carriers

Derived from their smaller size nano carriers have more facet, edges and terraces compared to the conventional carriers. It is proven that oxygen mobility is better at the grain boundaries than on the bulk and because in the nano scale there are more boundaries, it could be possible that diffusivity is better at the nano scale. [9] It is also proven that regeneration of copper oxide is controlled by this mobility. [2] Diffusivity again is one restrictive property when considering reactivity of the carriers. All studies dealing with nano carriers, came to same conclusion that reactivity is enhanced in nano size. And this is derived from the improved volume per area ratio. Nanocarriers have also better oxygen carrying capacity. [2, 20, 29, 38, 39, 40, 41, 43, 47, 50] Solunke et al. have made observation that oxidation rate is decreasing with increasing degree of oxidation. [29] This is not the truth with the nano carries. Nano carriers are capable for complete oxidation, while the conventional carriers do not fully oxidize. This feature is derived from the increasing diffusion layer which forms when the oxide layer on the metal particle grows. Because of their smaller size, nano carriers do not have this problem. It could be deduced that it is easier to remove oxygen from deep inside to the surface at the nano carrier than at the conventional carrier, because of the diffusion layer at the nano scale is not so wide as in the case of the conventional carriers. Although the oxidation is complete for nanocarriers, the heat released from the oxidation proses is smaller than for conventional carriers at the corresponding proses.

As discussed earlier, enhanced porosity increases reactivity but decreases mechanical stability. It is experimentally proven that porosity is distributed to the wider area at the nano carriers. [39, 41] Then diffusivity gets easier and reactivity is getting better. When the diffusion is getting better, it is easier for oxygen to move and so the mobility of oxygen enhances. Sarshar et al. have examined perovskite based nano carriers and they found out that nano perovskites have much surface oxygen and density of anion vacancies is large. [2] Both of these properties (surface oxygen and anion vacancies) enhance diffusion and thereby increases reaction rates. Mamontov et al. have shown that oxygen vacancies have larger effect on diffusion than surface oxygen. [56] They have also found that amount of vacancies decreases whit increasing temperature. This decrease can be prevented by doping oxygen carrier with another atoms. [56] Similar phenomenon is noticed when ceria based nano structures have examined. When the size of the structure is reduced, oxygen vacancies and other lattice defects improve diffusion. [57] Because these vacancies play important role for oxygen storage and diffusion, it could be possible that reactivity could be enhanced by increasing amount of oxygen defects. Reduction at the nano scale is reversible, so nanocarriers do not suffer from any morphology changes which can change diffusion or reduction properties. [56]

Li et al. have investigated nano iron oxides and their abilities for the CO oxidation and they have found out that nano structures are more effective for carbon monoxide oxidation than conventional structures which is derived from the smaller size (diameter 3 nm) of nano carriers. [58] So it could be generalized that smaller size could lead to the higher conversion effectiveness. Schalow et al. have also studied oxygen storage in

Table 6: Comparison between conventional (i.e. no-nano) and nano oxygen carriers variables affecting to the diffusion
+ feature has a positive effect for the process
- feature has a negative effect for the process

Feature	nano	conventional
Reactivity	+	-
Porosity	+	-
Mobility of oxygen	+	-
Oxygen vacancies	+	

nano particles. They have noticed that at the beginning CO_2 formation is reduced and then suddenly it remains finite for a long time. [45] There are also some disadvantages of using nano carriers. Due to their smaller size, melting points are lower and at the range of the normal CLC process where the temperatures are quite high, it is possible that they melt. Anyway if they do not melt, their thermal properties and stability are less optimal and some agglomeration can take place. On the other hand, by choosing a suitable support material thermal stability can be improved. Kirchhoff et al. have examined BHA supported nano carriers and they have noticed that BHA makes carrier even more stable structure than conventional (non supported) carrier [38] BHA supported nano carrier is also used in the experimental studies of Tian et al. and Solunke et al and also they reached out that BHA makes carrier thermal stable and suitable for the CLC process. [20, 29, 39, 40, 41]

There are several advantages to apply nanocarriers. To get same amount of captured CO_2, nano carriers need shorter run time at the reactor compared to the conventional carriers. They are also more easier to recycle although their lifetime is shorter than for the conventional carriers. Purity of the effluents is also higher for nano carriers. On the other hand less harmful coke is formed during the combustion in the case of the conventional carriers than nanocarriers. [29]

One big disadvantage of nano carriers is related to the reactor design process. Increasing reactivity by decreasing size complicates reactors design. If the particles are too small they can not be used in a moving beds reactor, because the pressure gradient between reactors increases. [9] Furthermore nano size also changes fluidization properties of the oxygen carrier and Wen et al. stated that these properties are more difficulty to model for nano particles. Fluidization behaviour of nano particles have investigated by [47] Valverde et al., Zhu et al., Hakim et al. and Seipenbusch et al. and they have found out that nano particles have bigger interparticle forces and so they stated that this led to the increment of the size of stable agglomerates and so cause a change in fluidization behaviour. [59, 60, 61, 62] Some of the reactors employed in CLC require suitable magnetic properties for the carrier. In CLC conditions these properties can change, but it is investigated that nanocarriers remain their magnetic properties. [43] Recently it was shown that nano copper oxide CuO is toxic and can cause DNA damage. [69, 70] Also the manufacturing cost are higher for the nanocarriers due to more expensive preparation method. [29] The investigation around nanocarriers are just at the beginning and this can also be seen as a con.

Table 7: Comparison between conventional (i.e. no-nano) and nano oxygen carriers variables affecting to the thermodynamics and redox properties
+ feature has a positive effect for the process
- feature has a negative effect for the process

Feature	nano	conventional
Complete oxidation	+	-
Agglomeration/sintering	-	
Heat released from oxidation	-	+
Oxygen carrying capacity	+	
Reversible reduction → no morphology changes	+	
Rate of oxidation increasing with increasing oxidation degree	+	

Table 8: Comparison between conventional (i.e. no-nano) and nano oxygen carriers variables affecting to the cost and usability
+ feature has a positive effect for the process
- feature has a negative effect for the process

Feature	nano	conventional
Shorter run time at the reactor	+	-
Recyclable	+	
Lifetime	-	+
Manufacture cost	-	+
Investigation	-	+
Purity of effluents	+	
Minor coke formation	-	
Toxicity	-	+

6 Numerical Methods

Density functional theory (DFT) is used to model and calculate atomic and electronic structure of a carrier material. Furthermore DFT is employed to calculate oxygen diffusion in the bulk and diffusion from near the surface to the surface and energy needed to release oxygen from surface. Comparing calculated properties we can conclude which step is limiting step at the oxidation process. By modification of oxide surfaces we can make indirect conclusions about properties of nano oxygen carriers. Exchange and correlation functional used in our calculations is a Perdev-Burke-Ernzerhof (PBE) which takes electron density and the gradient of density into account [97]. Furthermore we apply a mean field Hubbar-like term which describes correlation between electrons.

6.1 Density functional theory

In brief density functional theory (DFT) is based on solving equations which describe the electron motion and then find the lowest energy configuration for the examined system.

Table 9: Comparison between conventional (i.e. no-nano) and nano oxygen carriers variables affecting to the reactor design
+ feature has a positive effect for the process
- feature has a negative effect for the process

Feature	nano	conventional
Conversion ratio	+	-
Fluidization properties	-	+
Mass resistance	+	
Thermal/mechanical resistance against attrition		+
Reversible reduction → no morphology changes	+	
Mechanical stability	-	+
Magnetic properties	+	

Time independent Schrödinger equation has the form

$$H\Psi = E\Psi, \tag{6.1}$$

where H is hamiltonian operator which describes the total energy of system, Ψ is is the wavefunction of the system, which describes quantum state of the system and E is the energy of the state Ψ. When there are N electrons interacting with multiple nuclei Schrödinger equation changes many body problem and it could be written

$$\left[-\frac{\hbar^2}{2m}\sum_{i=1}^{N}\nabla_i^2 + \sum_{i}^{N}V(\overline{r}_i) + \sum_{i=1}^{N}\sum_{j<i}U(\overline{r}_i,\overline{r}_j)\right]\Psi = E\Psi. \tag{6.2}$$

The first term is kinetic energy of electron (m is mass of electron), the second term is interaction energy between an electron and a collection of the atomic nuclei. The third one is interaction energy between electrons. [72] In DFT, Hartee product is made by breaking wavefunction to the wave functions of a single electron. Probability that N electrons are located at the positions $\overline{r}_1,\ldots,\overline{r}_N$ can be written as a product of wave function and its complex conjugate $\Psi^*(\overline{r}_1,\ldots,\overline{r}_N)\Psi(\overline{r}_1,\ldots,\overline{r}_N)$. In many body problems its usually physically interesting to investigate density of electrons at a particular position in space, denoted $n(\overline{r})$ which can be calculated by summing former probability over single electron $n(\overline{r}) = 2\sum_i \Psi^*(\overline{r})\Psi(\overline{r})$, where the factor 2 is derived from the spin and Pauli exclusion principle. [72]

DFT is based on the two theorems made by Kohn and Hohenberg.

Theorem 1. *1. The Ground-state energy from Schrödinger equation is a unique functional of electron density.* [72]

So that theorem could be understood functional must be defined. Functional F takes a function f and defines a single number from the function

$$F(f) = \int_a^b f(x)\mathrm{d}x. \tag{6.3}$$

[72]

Alternative form for the theorem one is that the ground-state density $n(\overline{r})$ of a many body quantum system in external potential $V_{\text{ext}}(\overline{r})$ determines the potential uniquely. [73] All variables derivable from hamiltonian H trough the solution of time independent Schrödinger equation are determined by the ground-state density $n(\overline{r})$, for example ground-state energy $E(n(\overline{r}))$. [72, 73]

Theorem 2. *The electron density that minimizes the energy of overall functional is the true electron density corresponding to the full solution of the Schrödinger equation.* [72]

Alternative form for the theorem two states that: For any trial density $n(\overline{r})$ it holds that $E_0 \leq E(n(\overline{r}))$, where E_0 is ground-state energy. [73] In practice electron density can be changed until energy from the functional is minimized.

Energy functional can be written

$$E[\{\Psi_i\}] = E_{\text{known}}[\{\Psi_i\}] + E_{\text{XC}}[\{\Psi_i\}]. \tag{6.4}$$

$E_{\text{known}}[\{\Psi_i\}]$ involves electrons kinetic energy and Coulomb contribution for electron and nuclei, pairs of electrons and pairs of nuclei. $E_{\text{XC}}[\{\Psi_i\}]$ is so called exchange functional which contains all quantum mechanical effects that do not include in $E_{\text{known}}[\{\Psi_i\}]$. [72]

Solution to the many body problems is to put system of interacting electrons onto a non-interacting system with same density and as a result this method yields single particle equations. [74] Kohn and Sham equations use this kind of approximation

$$\left[-\frac{\hbar^2}{2m}\nabla^2 + V(\overline{r}) + V_{\text{H}}(\overline{r}) + V_{\text{XC}}(\overline{r})\right]\Psi(\overline{r}) = E\Psi(\overline{r}), \tag{6.5}$$

where the first potential term is the same as in normal Schrödinger equation, the second term is Hartee term which describes Coulomb repulsion between electrons and the third potential term is functional derivative of the exchange-correlation. [72] To use the DFT this equation is solved with some initial guess in a four-stage process presented in figure 11.

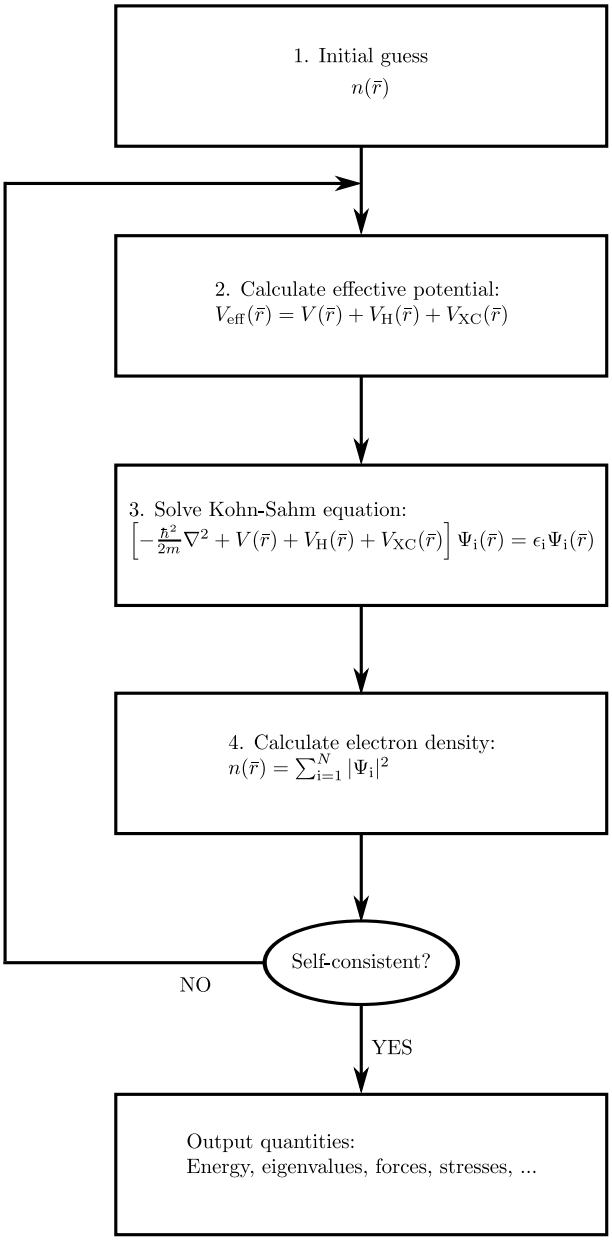

Figure 11: *Principle of DFT. In the first step program made some initial guess of the ground state density. Then the effective potential is calculated and Kohn-Sham equation is solved. After that electron density is calculated. If the result is self-consistent, output quantities are obtained. Otherwise initial guess must be done again and steps two to four must be repeated until the electron density is self-consistent. Figure is adapted from [73].*

That DFT can be employed, exchange correlation functional must be found. It can be derived accurately only for uniform electron gas where the $n(\overline{r})$ is constant. So the different approximations must be used. Most common applied exchange correlation functional is local density approximation (LDA). If system contains spin polarization local density spin approximation (LDSA), which take density of each spin into account, can be used. In LDA potential can be written as $V_{\mathrm{XC}}(\overline{r}) = X_{\mathrm{XC}}^{\text{electron gas}}[n(\overline{r})]$. [72, 73] This approximation is good if the densities only vary slowly. [73] In the real physical systems densities oscillate and because LDA does not take this account there are different methods to improve model. [74] If local gradient in electron density is also known along to electron density generalized gradient approximation (GGA) can be used. Perdev-Burke-Ernzerhof

functional (PBE) is one of the GGA functional. [72] PBE is employed in this study, because it gives reasonable bulk and surface properties.

6.2 Computational details and employed software

The numerical part was performed using GPAW (Grid-based projector-augmented wave method) software and the ASE (Atomic Simulation Environment) user interface. The VMD program was used to visualize structures. Nano structures were modelled with the slabs, one example of slab applied in this work is presented in the figure 20a. Because nano structures consist mostly of the most stable surface, the most stable surface of the metal oxide is searched from the literature. When this surface is found, it is created with a program called Materials Studio, which is a commercial software package [86]. For the copper oxide, the most stable surface is CuO(111). [83] For cuprous oxide the most stable surface is $Cu_2O(111)$ [84]. For manganese oxides the most stable surfaces are $Mn_2O_3(110)$ and $Mn_3O_4(001)$. [85] So that the slab can be modelled as a nano structure, it has to be thick enough. If the suitable slab thickness is mentioned in the literature, it is used. Otherwise some kind of a compromise between accuracy and calculation time has been done.

Energy barrier of the oxygen's diffusion can be determined using nudged elastic band method (NEB). It is based on the identification of a lowest energy path of a group of atoms from one stable configuration to another. [82] In the NEB method components are connected to each others with the springs and the program makes images i between initial and final states. In the NEB force acting on images can be written as

$$\overrightarrow{F}_i = -\overrightarrow{\nabla} V(\overrightarrow{R}_i) + k_{\mathrm{i+1}}(\overrightarrow{R}_{\mathrm{i+1}} - \overrightarrow{R}_{\mathrm{i}}) - k_{\mathrm{i}}(\overrightarrow{R}_{\mathrm{i}} - \overrightarrow{R}_{\mathrm{i\text{-}1}}), \tag{6.6}$$

where $\overrightarrow{R}_i$ is a displacement of image i and k_i is a spring constant. The choice of a suitable spring constant is quite arbitrary, because the spring force only affects on the distribution of the images. [82]

NEB method is very simply to use. In the first step energy and the gradient need to be evaluated and also the coordinates of the two adjacent atoms are required for each images. All this information is available from the earlier vacancy calculation. Then some kind of an initial guess is needed to start the path finding algorithm. [82]

After this calculation, energy barrier of a diffusion can be simply determined just a remainder of an energy of the highest point of a path and an initial state (i.e. metal oxide with vacancy) of diffusion. In order to minimize numerical errors the energy differences are obtained by fitting a polynomial to the obtained free energy values. As an example we show in figure 12 the determination of the energy barrier for diffusion between surface and subsurface on Mn_3O_4. This computation turned out to be numerically most unstable, for the other diffusions consider in this work the fit quality was siqnifiqantly better.

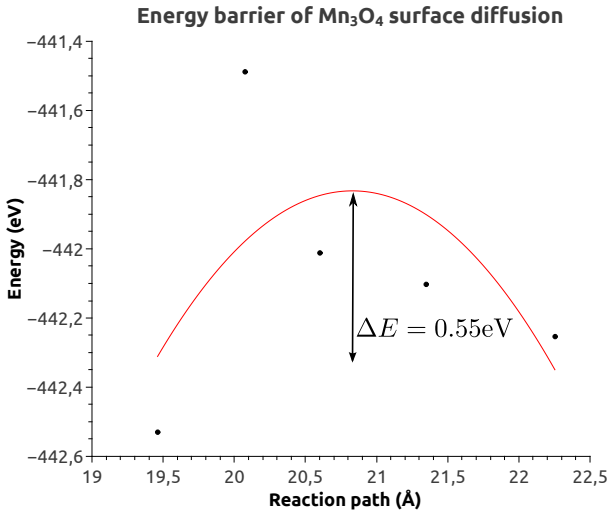

Figure 12: *Determination of the energy barrier for diffusion between surface and subsurface on Mn_3O_4.*

Another way to calculate oxygen diffusion is to use the FixedLine or the FixedPlane class in ASE. In the fixed line method a given atom is constrain to move on a given plane only. This line is defined by its direction. In fixed plane method a given atom is constrain to move on a given plane which is defined by its normal. [97]

Functional applied in all calculations was PBE and eigensolver was cg. Cg is an abbreviation form the worlds conjugate gradient method which is an iterative method for calculating huge systems of linear equations of form

$$Ax = b, \tag{6.7}$$

where x is unknown vector. It is based on the finding minimum point of a quadratic form or more commonly it is minimized whatever function f whose gradient f' can be calculated. [75] Hubbard correction was used in all calculations and Hubbard's term U was set to the 4.0 eV for all oxides, because it was showed to be the best alternative for manganese and copper oxides in the study of Wang et al. [76] Mixers and values used in mixers varied depending on the metal oxides. Due to convergence problems number of maximum iterations had to increase in some cases. Other calculation parameters are listed in the table 10. Only gamma point was used in the calculations of Mn_2O_3 and Mn_3O_4 surface. This is justified because in the both cases energy difference between gamma point calculation and calculation with (4,4,4)/(4,4,1)-kpts was small.

6.3 Atomistic thermodynamics

One big disadvantage for using DFT is that it is a zero-temperature and zero-pressure technique. However CLC, for example, is a high temperature process and also the pressure is far from zero being from 1 atm to up. When DFT calculations are combined with statistical mechanics and thermodynamics by entering DFT total energies to the calculations of G(T,p), result is ab initio thermodynamics i.e. atomistic thermodynamics [98, 99] It makes possible to apply DFT calculations to describe high temperature and high pressure process like CLC or catalysis. Method is however valid on a thermodynamic equilibrium where the chemical potential μ is same in the whole system (surface, bulk, metal, gas). [98]

Table 10: Calculation parameters used in this thesis. nbands is a number of electronic bands, h is a grid spacing, width is a width of bands and kpts is a number of k-points.

Metal oxide	nbands	h	width	kpts	spinpol
CuO bulk	-50	0.18	0.2	4*4*4	True
Cu_2O bulk	-25	0.18	0.1	4*4*4	False
Cu_2O surface	-25	0.18	0.1	4*4*1	False
Mn_2O_3 bulk	-50	0.2	0.2	Γ	True
Mn_2O_3 surface	-75	0.2	0.2	Γ	True
Mn_3O_4 bulk	-50	0.2	0.2	4*4*4	True
Mn_3O_3 surface	-50	0.2	0.2	Γ	True

The purpose of ab initio thermodynamis is to screen number of known oxygen containing surface structures and find out which is the most stable one (i.e. minimize for example the Gibbs free energy) under which (T, p_{O_2}) conditions.[98] How is the thermodynamics linked with the DFT total-energy calculations? The approach to the next analyse is from the articles [98, 99].

Consider a metal oxide Me_xO_y surface in contact with oxygen atmosphere. If the system is modelled by a slab with two equivalents surfaces, surface free energy γ is

$$\gamma(T,p) = \frac{1}{2A}(G^{\text{slab}}(T,p,N_{\text{Me}},N_{\text{O}}) - \frac{N}{x}g^{\text{bulk}}_{\text{Me}_x\text{O}_y}(T,p) + (\frac{y}{x}N_{\text{Me}} - N_{\text{O}})\mu_{\text{O}}(T,p)), \quad (6.8)$$

which depends only on μ_{O}. In equation 6.8 A is the area of the surface unit cell, N is number of atoms, G is Gibbs free energy and g is Gibbs free energy per formula unit. [99] Surface free energy can be though as a energy amount required to create one unit of surface area. Atoms are not as tightly bonded on the surface than on the bulk and when the system is reaching the equilibrium state, surface free energy is reducing.

μ_{O} can't be varied without limits. If μ_{O} becomes too low all oxygen would leave the sample, so

$$\max[\mu_{\text{Me}}(T,p)] = g^{\text{bulk}}_{\text{Me}}(T,p). \quad (6.9)$$

On the oxygen poor limits with the condition p=0 atm and T=0 K it yields

$$\min[\mu_{\text{O}}(T,p)] = \frac{1}{2}[g^{\text{bulk}}_{\text{Me}_x\text{O}_y}(0,0) - g^{\text{bulk}}_{\text{Me}}(0,0)]. \quad (6.10)$$

At oxygen rich conditions gas phase oxygen would condense on the sample and upper limits become

$$\max[\mu_{\text{O}}(T,p)] = \frac{1}{2}E^{\text{total}}_{\text{O}_2}, \quad (6.11)$$

where $E^{\text{total}}_{\text{O}_2}$ is the total energy of a free, isolated oxygen molecule at T=0K. Now the Gibbs free energy of formation of the oxide could be written

$$\Delta G_f = g^{\text{bulk}}_{\text{Me}_x\text{O}_y}(T,p) - g^{\text{bulk}}_{\text{Me}}(T,p) - g^{\text{gas}}_{\text{O}_2}(T,p). \quad (6.12)$$

When taking limits of μ_O into account, one obtains

$$\frac{1}{2}\Delta G_f(0,0) < \mu_{\text{O}_2} - \frac{1}{2}E^{\text{total}}_{\text{O}_2} < 0 \quad (6.13)$$

[99].

How to obtain the Gibbs free energy from the DFT total energies? E^{total} corresponds Helmholtz's free energy at zero temperature and neglecting zero-point vibrations. Helmholtz's free energy F can be written as

$$\begin{aligned} F(T, V, N_{\text{Me}}, N_{\text{O}}) &= E^{\text{total}}(T, V, N_{\text{Me}}, N_{\text{O}}) + F^{\text{vib}}(T, V, N_{\text{Me}}, N_{\text{O}}) \\ &= E^{\text{total}}(T, V, N_{\text{Me}}, N_{\text{O}}) + E^{\text{vib}}(T, V, N_{\text{Me}}, N_{\text{O}}) - TS^{\text{vib}}(T, V, N_{\text{Me}}, N_{\text{O}}), \end{aligned} \tag{6.14}$$

where E^{vib} and S^{vib} are the vibrational energy and entropy, respectively. [99] Helmholtz's free energy and Gibb's free energy are connected to each others with relation $G = F + pV$. When pressure is small enough (i.e. $p < 100$ atm), pV-contribution to the Gibb's free energy is negligible compared to the F. When using phonon density of states, F can be written as an integral over modes ω

$$\begin{aligned} F(T, V, N_{\text{Me}}, N_{\text{O}}) &= \int F^{\text{vib}}(T, \omega) \mathrm{d}\omega \\ &\approx \frac{\hbar\omega}{2} + kT \ln[1 - \exp(-\frac{\hbar\omega}{kT})]. \end{aligned} \tag{6.15}$$

In several systems also the vibrational contributions to the Gibb's free energy are neglected. But that must be checked separately for each system. Due to limited time, this is not done in this thesis. If this approximation applies, it says that change in the Gibb's free energy is equal to the DFT total energy and surface free energy can be written as

$$\gamma(T, p) \approx \frac{1}{2A}(E^{\text{slab}}(V, N_{\text{Me}}, N_{\text{O}}) - \frac{N_{\text{Me}}}{x} E^{\text{bulk}}_{\text{Me}_\text{x}\text{O}_\text{y}}(V) - (\frac{y}{x} N_{\text{Me}} - N_{\text{O}}) E^{\text{bulk}}_{\text{Me}}(V)). \tag{6.16}$$

[99]

For the surface with a vacancy, this energy can be determined from the equation

$$\gamma_{\text{vac}}(T, p) \approx \frac{1}{2A}(G^{\text{slab}}_{\text{vac}}(V, N_{\text{Me}}, N_{\text{O}}) - N_{\text{Me}} g^{\text{bulk}}_{\text{Me}_\text{x}\text{O}_\text{y}}(V) + (y \cdot N_{\text{Me}} - x \cdot N_{\text{O}}) \mu_{\text{O}}(T, p)), \tag{6.17}$$

where $G^{\text{slab}}_{\text{vac}}$ is energy of surface with a vacancy.

When γ is known as a function of a μ_O, it should be known how $\mu_O(T, p)$ depends on pressure and temperature. Chemical potential can be written as a function of pressure p and temperature T

$$\mu_O(T, p) = \mu_O(T, p^\circ) + \frac{1}{2} kT \ln\left(\frac{p}{p^\circ}\right), \tag{6.18}$$

where p° is a particular pressure and $\mu_O(T, p^\circ)$ can be found in literature. At the end stability range of the different phases can be plotted in (T, p_{O_2})-space. [98, 99]

6.4 Electron Structure

CuO is reduced to the Cu_2O at the nanoscale. So in the case of copper carrier, the calculations are carried out with these oxides. Mn_2O_3 and Mn_3O_4 are the only oxides of manganese with high enough melting points (940 °C and 1567 °C, respectively) and suitable partial pressure for the CLOU-process, so they are used in this thesis. However

Table 11: Calculation parameters used in electron structure and lattice parameters calculations are presented in table. Table is continued in the table 12.
[a] Antiferromagnetic
[b] Ferromagnetic
[c] Diamagnetic

Metal oxide	Space Group	Magnetic structure	lattice parameters (Å)
CuO	15 [87]	AFM^a [76]	$a = 4.55$, $b = 3.34$ $c = 4.99$, $\beta = 99.507°$[77]
Cu_2O	224 [78]	DM^c [76]	$a = 4.32$ [78]
Mn_2O_3	206 [93]	AFM^a [95]	$a = 9.4090$ [93]
Mn_3O_4	141 setting 1 [81]	FM^b [76]	$a = 5.7674$, $c = 9.457$[81]

manganese oxides need support material that partial pressure and thermic stability can be modified suitable. Reactions happened in redox-cycle can be presented as

$$4CuO \longleftrightarrow 2Cu_2O + O_2 \qquad \Delta H_{850\,^\circ C} = 263.2 \frac{kJ}{molO_2} \tag{6.19}$$

$$6Mn_2O_3 \longleftrightarrow 4Mn_3O_4 + O_2 \qquad \Delta H_{850\,^\circ C} = 193.9 \frac{kJ}{molO_2} \tag{6.20}$$

[5, 27]

Electron structures are calculated with the lattice parameters found in earlier DFT studies and with the help of a GPAW's spacegroup subpackage.

CuO is found to be a monoclinic structure and a space group of a copper oxide is 15 with a setting one. Lattice parameters, relative coordinates and magnetics structures are tabulated in the tables 11,12 and 13. Other calculation parameters are listed in the table 10. Cu_2O is a cubic structure and information needed in the calculations can be found from the same tables than for the CuO

Mn_2O_3 has three different phases, but the dominant phase under CLOU conditions in nano scale is a cubic α phase [80, 94, 95] α- form of the Mn_3O_4 is dominant in the CLOU conditions. Infromation of the lattice parameters relative coordinates and magnetics structures are collected in the tables 11, 12 and 13. Other calculation parameters are listed in the table 10.

6.5 Lattice constants

In order that calculations on the bulk and on the surface can be executed, optimized lattice parameters have to be found. Then the calculations are carried out with these parameters, not the ones found from literature.

After the primary electron structure calculations, lattice parameters can be determined on the basis of calculations. In all structures excluding CuO all the angels are rectangular. Calculations are beginning with fixing specified parameters and after that parameters are varied with one by one and then the minimum for each parameter can be found. GPAW executes calculations by the same way as in the case of electron structures.

Table 12: Calculation parameters used in electron structure and lattice parameters calculations are presented in table. The first coordinate(s) is (are) for a metal atom(s) and the last coordinate is for a oxygen atom. Table is a continuation of the table 11.

Metal oxide	fractional coordinates	U
CuO	(0.25, 0.25,0)	4.0 [76]
	(0, 0.42, 0.25)[87]	
Cu_2O	(0.25, 0.25, 0.25)	
	(0,0,0)[78]	4.0[76]
Mn_2O_3	(0,0,0),	4.0 [76]
	(0, 0.25, 0.2848),	
	(0.4162, 0.1286, 0.3555)[93]	
Mn_3O_4	(0,0,0)	4.0
	(0.5, 0.25, 0.125)	
	(0, 0.25, 0.375)	[81]

In Cu_2O there is only one lattice parameter a to optimize. Lattice parameter a corresponding to energy minimum is searching between 4.12-4.31 Å with increments of 0.01 Å.

In cubic α-Mn_2O_3 there is again only one lattice parameter to optimize. Lattice parameter a corresponding to energy minimum is searching between 8.4681-10.3499 Å in 10 different points and with the same calculate parameters used in the electron structure calculations.

In α-Mn_3O_4 there are two lattice parameters a and c. In the firs step value of a is finding with the fraction $\frac{c}{a}$ fixed and after that value of c is calculated using a determined from the earlier calculation. Value of a is searching between 5.4739 Å and 6.0501 Å in 20 points and value of c between 8.96705 Å and 6.0501 Å in 20 points.

6.6 Oxygen vacancies

In CLOU oxygen is released to the gas phase and oxygen vacancy is formed. It is interesting to know how much this vacancy formation requires energy. Oxygen vacancies are created for both reduced and oxidized form of the metal oxides just simply deleting one or more oxygen atom(s). Vacancies are created alternately in adjacent oxygen places and between them oxygen diffusion can be calculated using NEB method 6.2. Energies for vacancies are calculated with the same method and same calculation parameters than in the case of the electron structure. Formation energy of the vacancy, E_{form} is determined as follows:

$$E_{\text{form}} = E(\text{MO}_{\text{x,vac}}) - E(\text{MO}_{\text{x}}) + \frac{1}{2}E(\text{O}_2), \tag{6.21}$$

where $E(\text{MO}_{\text{x}})$ is the energy of metal oxide, $E(\text{MO}_{\text{x,vac}})$ is the energy of metal oxide with a vacancy and $E(\text{O}_2)$ is the energy of molecular oxygen.

In the case of surfaces vacancies are created on a surface and on a subsurface. Only way for a vacancy formation on the subsurface is that vacancy is first formed on the surface and then oxygen from the subsurface diffuses to the vacancy on the surface.

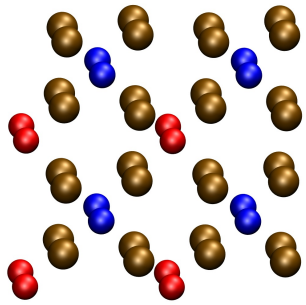

(a) Vacancy made in Cu_2O.

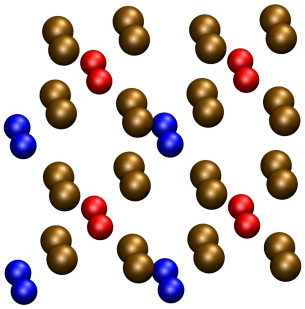

(b) Second vacancy made in Cu_2O.

Figure 13: Vacancies made in Cu_2O. Red balls present oxygen atoms,ochre balls are copper atoms and blue balls are vacancies.

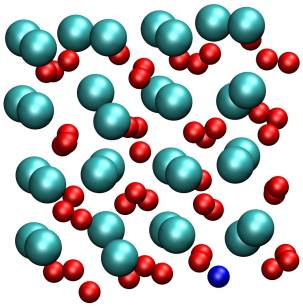

(a) Vacancy made in Mn_2O_3.

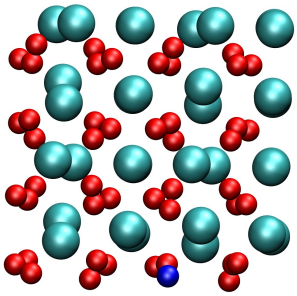

(b) Second vacancy made in Mn_2O_3.

Figure 14: Vacancies made in Mn_2O_3. Red balls present oxygen atoms,cyan balls are manganese atoms and blue balls are vacancies.

In the case of Cu_2O oxygen vacancies are created as in figures 13a and 13b. One of the two oxygen atoms from the unit cell of Cu_2O is removed one by one, so the vacancy concentration is very large 50%.

In Mn_2O_3 oxygen vacancies are created like in figures 14a and 14b. One of the 48 oxygen atoms are removed one by one. In this case the vacancy concentration is really small compared to the other metal oxides, being only 2.1 %.

In the case of Mn_3O_4 oxygen vacancies are creates like in figures 15a and 15b. One of the sixteen oxygen atom from the unit cell is removed, so the oxygen vacancy concentration is 6.25 %.

(a) Vacancy made in Mn_3O_4. **(b)** Second vacancy made in Mn_3O_4.

Figure 15: Vacancies made in Mn_3O_4. Red balls present oxygen atoms, cyan balls are manganese atoms and blue balls are vacancies.

7 Results and discussion

7.1 Electron structure and lattice parameters

Bulk structures created and calculated in GPAW are presented in figures 16, 17, 18 and 19.

Chemical potential of oxygen molecule μ_{O_2} (with some approximations) can be determined by relation

$$\mu_{O_2} = H(T, p^\circ, O_2) - H(0\text{K}, p^\circ, O_2) - T[S(T, p^\circ, O_2) - S(0\text{K}, p^\circ, O_2)] \qquad (7.1)$$

[99]. Values used in equation 7.4 are listed in thermochemical tables at standard pressure . [100]

Calculated energies, magnetic moments and lattice parameters are collected to the tables 13 and 14.

Magnetic moments of CuO 13 are in very good agreement with the experimental neutron-scattering studies[87, 88] and computational studies [76, 77]. From the results it can be seen the antiferromagnetic nature of CuO. Lattice parameters for CuO 14 are also in good agreement with the earlier calculated values: a and c differ 2 % while b differs only 0.6% and angel β only 0.2 %. They are also very close to the experimental values: a differs only 0.5, b differs 3%, c differs only 0.6 % and angel β 2 %. CuO proved to be a material with which has insurmountable technical problems. So it is not discussed more briefly in this master's thesis.

Cu_2O is a diamagnetic material. Calculated lattice parameter a 14 is slightly too big, but the result is still valid and acceptable because the energy differences between lattice parameters were very small (order 0.1 eV) while the accuracy of the calculations is in the same order. Lattice constant a differs from earlier calculated value only 0.5 % and from

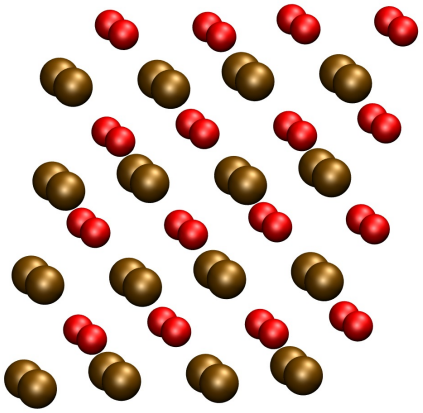

Figure 16: Atomic structure of CuO. Copper atoms have magnetic moments 0.617 μ_B Red balls present oxygen atoms and ochre balls are copper atoms.

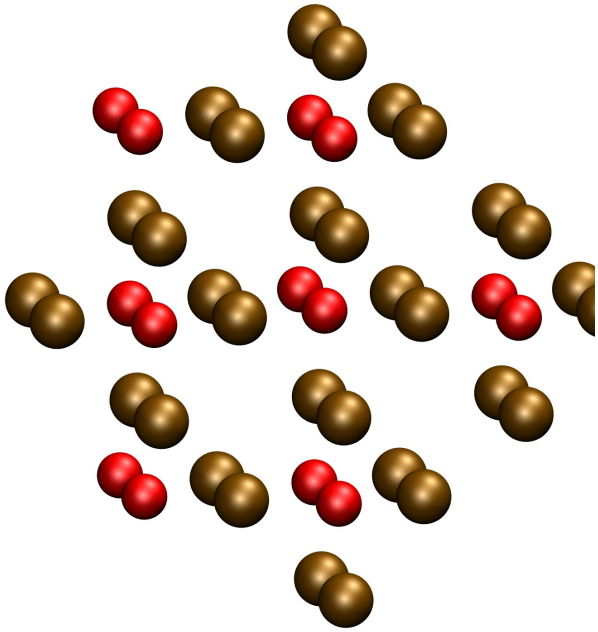

Figure 17: Atomic structure of Cu_2O. Red balls present oxygen atoms and ochre balls are copper atoms.

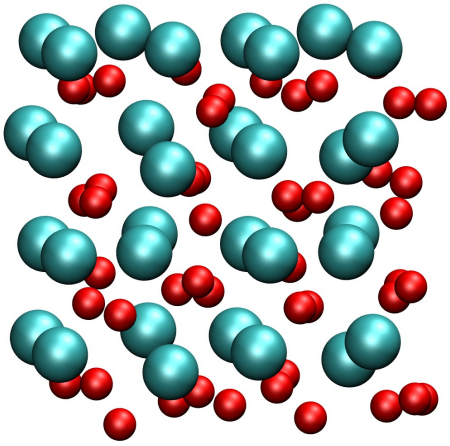

Figure 18: Atomic structure of Mn_2O_3. Manganese atoms have magnetic moments in order $\pm$ 4.6 to 4.75 μ_B. Red balls present oxygen atoms and cyan balls are manganese atoms.

experimental value 1.7 %. Result is good because also the earlier calculated value differs 1.2 % from the experimental values. There is always some deviation between numerical and experimental values. And it is noticed that use of PBE+ U method significantly overestimates the experimental lattice parameters. [103]

Srutucture of Mn_2O_3 is antiferromagnetic as it should be, but magnetics moments are big compared to experimental (difference 3-16 %) and slightly too big compared to the earlier calculated parameters (difference 5-9 %) 13. Relative error between determined lattice parameter and earlier calculated value is 1.4 %. These calculations are carried out without Hubbard term. If one takes Hubbard correction into account, value differs only 0.6 % [103]. From the experimental value the result differs 1.4 %. [94]

Magnetic moments of Mn_3O_4 are very close to earlier calculated values 13. There are two different values for the magnetic moments of manganese depending on the displacement of the atom. Other result is exactly the same as earlier calculated and the other differs 3 %. Also the lattice parameters determined in this study are in good agreement with the earlier studies 14. Value of a differs from the experimental value 1.5 % and from the calculated value only 0.04 %. Value of c differs from the experimental value 0.96 % and from the calculated value it differs 0.34 %.

Formation energies of oxides can be calculated according to the equation

$$\Delta G^f = \sum_{products} G - \sum_{reactants} G. \tag{7.2}$$

In equation 7.2 energy for oxygen molecule is obtained from chemical potential, which can be determined by equation

$$\mu = E_{\mathrm{ZPE}} + \Delta_f H - TS + k_b \ln \frac{p}{p^\circ} + E_{\mathrm{DFT}}, \tag{7.3}$$

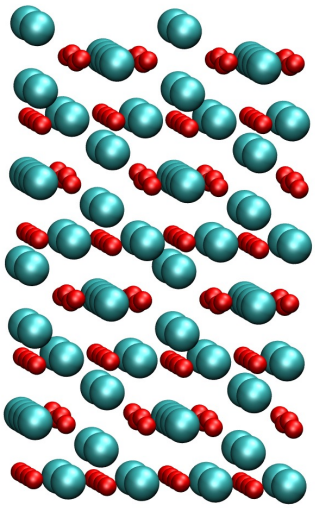

Figure 19: Atomic structure of Mn_3O_4. Manganese atoms have magnetic moments in order 4.706 μ_B and 4.123 μ_B depending on the location of the atom. Red balls present oxygen atoms and cyan balls are manganese atoms.

Table 13: Calculated energies and magnetic moments for different metal oxides are presented in the table. Also the corresponding experimental and theoretical (calculated in earlier studied) values are presented.

Metal oxide	Magnetic moment (μ_B)	Experimental (μ_B)	Theoretical (μ_B)
CuO	0.617	0.5-0.68 [87, 88]	0.5-0.6 [76, 77]
Cu_2O			
Mn_2O_3	3.7-4.3	3.0-3.6 [93]	3.92 [76]
Mn_3O_4	4.706		4.70
	4.123		4.01 [76]

where vibrational contributions E_{ZPE} is negleted, H, T and S are literature values and E_{DFT} is from DFT calculations. Formation energies for different oxides are collected in the table15 together with the experimental values from CRC [101] and earlier calculated DFT studies made by Saidi et al. [102] and Franchini et al. [103]. In the case of manganese oxides γ-Mn was used as a reference. This is justified because the energy difference between α- and γ-phase of manganese is only 0.67 meV. [104]. Formation energies are

Table 14: Calculated lattice parameters and their comparison with the experimental and the theoretical (earlier calculated parameters) is presented in figure.
* Value for a is computed by T.Parviainen.
** Values are computed by Karoliina Honkala

Metal oxide	Lattice parameters (Å)	Experimental (Å)	Theoretical (Å)
CuO	$a = 4.64^{**}$	$a = 4.662$ [87]	$a = 4.55$ [77]
	$b = 3.32^{**}$	$b = 3.417$ [87]	$b = 3.34$ [77]
	$c = 5.09^{**}$	$c = 5.118$ [87]	$c = 4.99$ [77]
	$\beta = 99.307°^{**}$	$\beta = 97.29°$[87]	$\beta = 99.507°$[77]
Cu_2O	$a = 4.34$	$a = 4.27$ [90]	$a = 4.32$ [78], $a = 4.30$ [91]
Mn_2O_3	$a = 9.54^{*}$	$a = 9.40800$ [94]	$a = 9.4090$ [93]
Mn_3O_4	$a = 5.85$	$a = 5.762$	$a = 5.844$
	$c = 9.53$	$c = 9.53$ [81]	$c = 9.498$ [92]

in good agreement with the earlier calculated values and with the experimental values although they are not exactly the same. Mn_2O_3 differs most from the results. This may be do to complicated magnetic structure, which is not exactly the same as in previous DFT studies. Furthermore relative errors are large in the case of manganese oxides, 6 % for Mn_2O_3 and 5% for Mn_3O_4. When these error limits are taken into account $\Delta_f G°$ for Mn_3O_4 is acceptable. Formation energy for Cu_2O is calculated with VASP and Huddard correction is not employed, so this can explain why the value differs from the earlier calculated.

Table 15: Calculated formation energy for each metal oxide is listed in the table. Literature values are from CRC [101], earlier calculated DFT values are from references [102, 103] and calculated values are from DFT calculations combined with atomistic thermodynamics.

Metal oxide	$\Delta_f G°$, literature (eV)	$\Delta_f G°$, DFT (eV)	$\Delta_f G°$, calculated (eV)
Cu_2O	-1.51	1.26 [102]	-1.46
Mn_2O_3	-9.13	-9.39 [103]	-11.53
Mn_3O_4	-13.3	-13.68 [103]	-13.85

7.2 Oxygen vacancies and oxygen diffusion

Vacancy formation energy for Cu_2O is 1.981 eV and vacancy concentration is 50 %. Energies are listed in the table 16. Cu_2O is a semiconductor so most of the studies are concentrated on the copper vacancies and their formation energies are available, but not the formation energies of oxygen vacancies. So there is not any relevant point of reference. In Cu_2O activation energy of diffusion is 3.235 eV, so the mobility of oxygen is not very good in this metal oxide. Furthermore the oxygen concentration is very high and when the concentration is high, activation energy of diffusion is however smaller, because its easier for oxygen to move. Thus it can be concluded that Cu_2O is probably not the best candidate for oxygen carrier in the bulk form.

Table 16: Calculated formation energy of vacancy per formula unit and activation energy of diffusion for each metal oxide system is presented in the table.

Metal oxide	Vacancy concentration (%)	Formation energy of vacancy (eV)	Activation energy of diffusion (eV)
Cu_2O	50	1.98	3.24
Mn_2O_3	2.1	2.08	2.54
Mn_3O_4	6.25	0.98	0.81

In Mn_3O_4 vacancy formation energy is 0.98 eV. Vacancy formation energy might increase, because magnetic structure differs from the pure bulk. Magnetic moments for manganese atoms are 4%-5% smaller in the bulk with vacancies than magnetic moments for the pure Mn_3O_4 bulk. Magnetic moments of oxygen are about six times larger in the structure with vacancy than without it. So the additional research is needed. Earlier calculated results for the formation energies of oxygen vacancy are not available. From the thermodynamically point of view vacancy formation is very favourable, but there is no information how is the kinetic part. For the full understanding of the vacancy formation also the kinetic part needs to be calculated and examined. In Mn_3O_4 activation energy of diffusion is very small 0.82 eV even with the small vacancy concentration 6.25 %, so the mobility of oxygen is good in this metal oxide and it can be concluded that Mn_3O_4 is a good material for the oxygen carrier even in the bulk form. If the magnetic structure of Mn_3O_4 is inaccurate, also diffusion can change and energy barrier of diffusion increases.

In Mn_2O_3 bulk vacancy formation energy is the biggest compared to the other oxides, vacancy concentration again is smallest. Earlier calculated results for the formation energies of oxygen vacancy are not available. In Mn_2O_3 activation energy of diffusion is 2.536 eV. This is a little less than for Cu_2O, but much more than for Mn_3O_4. So in the bulk form it can be said that Mn_3O_4 seems to have most potential for the oxygen carrier and Cu_2O least potential for the carrier.

Comparing different oxides, it can be seen that vacancy is formed easier for the Mn_3O_4 and then for the Cu_2O. Vacancy formation is most difficult for the Mn_2O_3. This applies only to the bulk metal oxides. In order to compare results, vacancy concentration must to take into account. Vacancy concentration is largest on the Cu_2O and smallest on the Mn_2O_3. One can imagine that vacancy formation gets easier when vacancy concentration rises, because then there are less atoms and thus bonds between atoms are weaker. When the vacancy concentration is taken into account, vacancy is anyway formed hardest to the Mn_2O_3. Vacancy formation gets easier on Cu_2O compared to the Mn_3O_4, but further research and calculations are needed to determine exactly values of vacancy formation energies with the same vacancy concentration.

When comparing activation energy of diffusion on the bulk, it is clear (on the basis of these calculations) that oxygen diffusion happens easiest in Mn_3O_4, hardest the situation is on the Cu_2O. When comparing results, different vacancy concentrations must be take into account. The larger the concentration, it is easier to oxygen to move. Biggest the concentration is on Cu_2O and smallest on Mn_2O_4. In bulk oxide it seems that manganese based carriers have more potential for oxygen carrier. In order to know if the nano carriers solve the slow reaction kinetics, comparison with these bulk oxide results and surface results (7.3) must be done.

Chemical potential of an oxygen molecule μ_{O_2} (with some approximations) can be determined by relation

$$\mu_{O_2} = H(T, p^\circ, O_2) - H(0K, p^\circ, O_2) - T[S(T, p^\circ, O_2) - S(0K, p^\circ, O_2)] + E_{DFT,\, O_2} \quad (7.4)$$

[99]. For standard pressure p°=1 atm values used in equation 7.4 are listed in thermochemical tables. [100] Inserting them into the equation 7.4 leads μ_{O_2}(T,p°), which are listed in the table 17 in temperature range 700 -1600 K.

Table 17: Calculated chemical potential μ_{O_2}(T,p°) in the temperature range of interest to CLC.

T (K)	μ_{O_2}(T,p°) (eV)	T (K)	μ_{O_2}(T,p°) (eV)
700	-1.46	1200	-2.71
800	-1.70	1300	-2.97
900	-1.95	1400	-3.24
1000	-2.20	1500	-3.50
1100	-2.45	1600	-3.77

To study vacancy formation energies temperatures relevant in CLC, atomistic thermodynamics is must. Then the energy of oxygen molecule in the equation 6.21 can be simply replaced by oxygen chemical potential presented in the table 17 according to equation

$$\Delta G_{form} = E(MO_{x,vac}) - E(MO_x) + \frac{1}{2}\mu_{O_2}. \quad (7.5)$$

As a result vacancy formation energy for different oxides as a function of temperature is achieved.

Figure 29 shows that formation of a bulk vacancy is the most favourable for the Mn_3O_4 and then for the Mn_2O_3 and hardest for the Cu_2O. CLC is a high temperature process and from the graph it can be seen that formation energy of vacancy is decreased when temperature is rising and all the reactions are exothermic. So vacancy formation is more favourable at high temperatures.

7.3 Surfaces

Most stable surface for Cu_2O is (111) and it is presented in the figure 20. Calculations are executed with the 12 atomic layers. According to Soon et al. best results for the Cu_2O surface is achieved with the slab thickness 12 atomic layers [96]. To the bottom and above the surface 5 Å of vacuum is added.

For comparison of diffusion on the bulk and from the subsurface to the surface, vacancies are also created at the surface and on the subsurface. Then the diffusion between vacancies is calculated with the same method like in the bulk one.

In Cu_2O surface vacancies are shown in figures 21a and 21b. Vacancy concentration of the surface is 12.5 %. Surface with vacancy on the subsurface is 7 eV upper in energy than the corresponding pure surface, and if the vacancy is made at the surface, it is 8 eV upper energy, thus the vacancy on the subsurface is more stable. Anyway it would be better if the vacancy was more stable on the surface than on the subsurface, because

Table 18: Most stable surface orientation (found from literature) for each metal oxide and energy of this surface is presented in the table.

Metal oxide	The most stable surface
CuO	(111) [83]
Cu_2O	(111) [84]
Mn_2O_3	(110) [85]
Mn_3O_4	(001) [85]

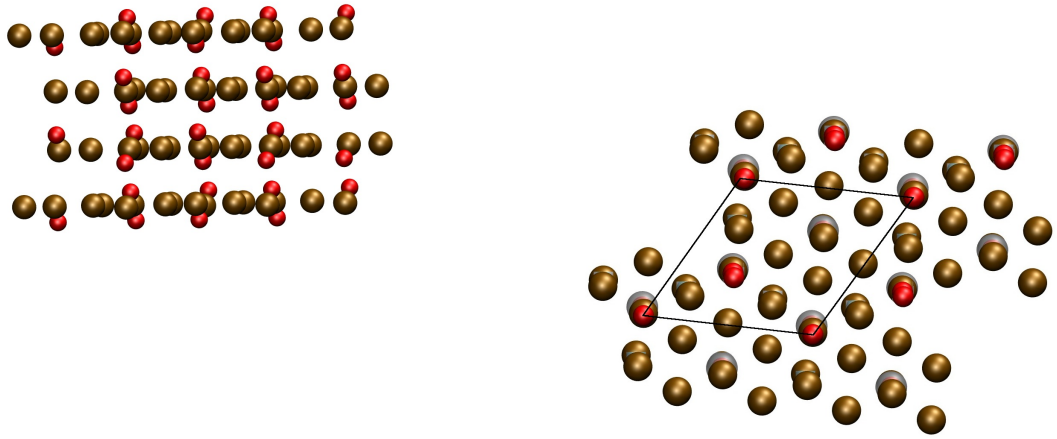

(a) Side view of the most stable surface of $Cu_2O(111)$.

(b) Unit cell of the most stable surface of $Cu_2O(111)$.

Figure 20: Side view and and unit cell of Cu_2O (111) surface. Red balls present oxygen atoms and ochre balls are copper atoms.

vacancy on the surface is easier to exploit in CLC. Formation energy of vacancy Cu_2O on the subsurface is smaller than formation energy on the surface. Formation energy of vacancy on the subsurface is smaller than on the bulk and formation energy on the surface is bigger than on the bulk. It is notable that when the vacancy is formed on the subsurface or on the bulk, there have to be earlier formed vacancies on the surface, where oxygen molecule can diffuse. When this is take into account it can be said that vacancy is formed easier on the surface than on the bulk. Vacancy formation energies and the activation energy of the diffusion from the subsurface to the surface are presented in the table 19. In order to obtain more reliable results, one should use smaller grid spacing when performing surface calculations.

At least less external energy is needed for the vacancy formation in the $Cu_2O(111)$ surface than in the bulk in the Cu_2O. More energy is needed for the vacancy formation on the subsurface than on the surface and vacancy is more stable when it is formed on

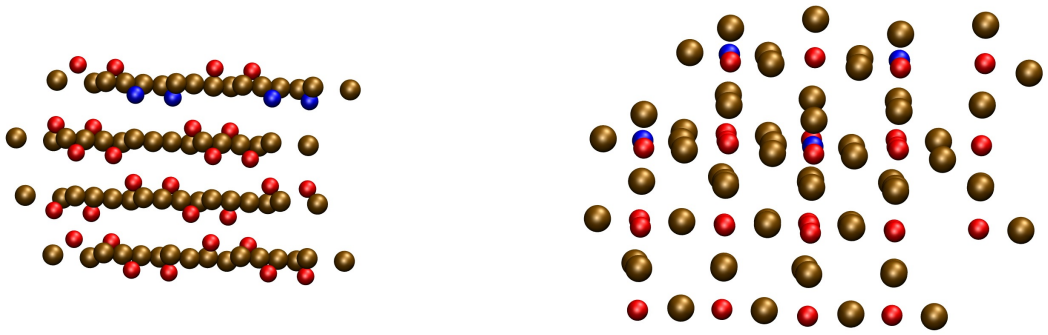

(a) Most stable surface of $Cu_2O(111)$ with vacancy on the subsurface. Pure surface is 7 eV lower in energy than this one. Vacancy formed at this place requires 2.24 eV energy per formula unit.

(b) Most stable surface of $Cu_2O(111)$ with vacancy at the surface. Pure surface is 8 eV lower in energy than this one. Vacancy formation energy is 0,24 eV per formula unit.

Figure 21: Vacancies made in Cu_2O (111) surface and on the subsurface. Red balls present oxygen atoms, ochre balls are copper atoms and blue balls are vacancies.

the subsurface than on the surface. Vacancy concentration on the bulk is much higher than that on the surface. If the concentrations are same, one can imagine that vacancies are formed even more conveniently on the surface than on the bulk. It is know that nano structures have more reactive surfaces than conventional structures, so the vacancy formation could be easier for the nano oxygen carriers than conventional carriers, because the energy difference in vacancy formation energies between the bulk and the surface is quite large. For the deeper understanding of the process, vacancy formation from the deeper subsurface needs to be examined. After these calculations more accurate conclusions can be done.

When looking at the effect of temperature for the vacancy formation energies, atomistic thermodynamics is a suitable tool. Vacancy formation energy on the bulk is presented on the figure 29 and on the surface and on the subsurface as a function of temperature is presented in figure 22. Under CLC temperatures vacancy formation is exothermic reaction. When temperature is rising, formation energy is decreasing, which is good because temperature in the CLC process is high. Vacancy formation on the surface is thermodynamically more favourable than vacancy formation on the subsurface. In the nano carriers point of view it is good that less energy is released for the vacancy formation at the bulk, because nano carriers have more surface area. More energy releasing when the vacancy is formed on the surface than on the subsurface. Vacancy on the subsurface is more stable than that on the surface. It would be interesting to know how the distance of the vacancy from the surface affects to the vacancy formation energy.

In Cu_2O oxygen diffusion from vacancy presented in figure 21b to vacancy 21a is

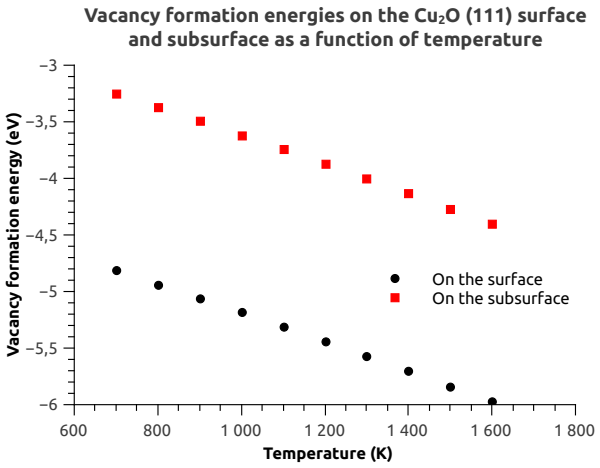

Figure 22: Vacancy formation energy on the surface and on the subsurface as a function of temperature at pressure 1 atm. Temperature dependence has been obtained using atomistic thermodynamics. Oxygen vacancy concentration is 12.5 % on the surface. Energies are calculated per formula unit.

examined with the constraint line method. On the basis of the calculations, activation energy for the diffusion at the surface is 1.69 eV. Activation energy for the diffusion at the bulk is 3.24 eV which is much higher than 1.69 eV. Vacancy concentration is much higher at the bulk and nevertheless activation energy of the diffusion is smaller from the subsurface to the surface. Because nanoparticles has higher volume per area ratio and they have more surface and diffusion at the surface is easier than on the bulk, it can be concluded from calculations that diffusion is easier at the nanoscale. Because diffusion is one big restrictive feature for the oxygen carrier, it can be seen that nano carriers have higher reactivity because of better diffusion. Due to enhanced diffusion, nano carriers have potential to be better oxygen carriers than conventional ones. And thus solve the slow reaction kinetic and make the CLC-process more attractive. Diffusion calculations are zero temperature and zero pressure calculations. If an estimate for the temperature dependence is required, one can assume that diffusion satisfies the Arhennius equation. It says that diffusivity D is $D = D_0 \exp(-E_a/RT)$, where D_0 is system-specific constant, R is gas constant, T is temperature and E_a is activation energy for the diffusion. From the equation it can be seen that diffusion gets easier when the temperature is rising. This is true for the all metal oxides examined in this thesis. From the Arhennius equation one can see that a little difference in activation energies causes bigger differences in diffusivity.

Most stable surface for Mn_2O_3 is (110) and it is presented in figure 23. Mn_2O_3 (110) surface calculations are carried out with 8 atomic layers and 5 Å vacuum at the bottom and above.

In Mn_2O_3 surface vacancies are created like in figures 24a and 24b. Vacancy concentration in these cases is quite small. If the vacancy is made on the subsurface it is 7 eV upper in energy than corresponding pure surface and if it is made at the surface it is 6 eV upper, i.e. vacancy is more stable on the subsurface than on the surface. Vacancy formation energies and the activation energy of the diffusion at the surface are presented in the table 19.

Much less external energy is needed for the vacancy formation in the Mn_2O_3(110)surface than at the bulk one in the Mn_2O_3. In Mn_2O_3 less energy is needed for vacancy formation on the surface than under the surface. In any case vacancy formation is actually lot easier

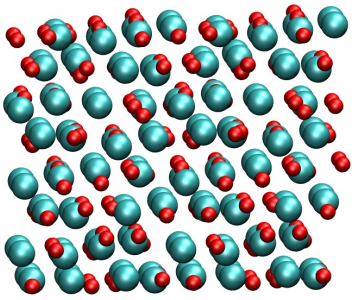

(a) Side view of the most stable surface of $Mn_2O_3(110)$.

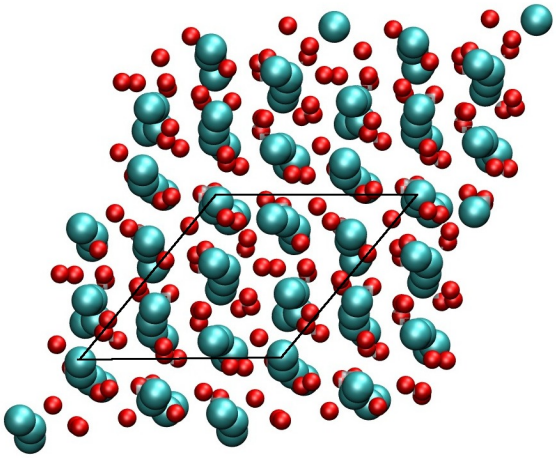

(b) Unit cell of the most stable surface of $Mn_2O_3(110)$.

Figure 23: Side view and and unit cell of Mn_2O_3 (111) surface. Red balls present oxygen atoms and cyan balls are manganese atoms.

on the surface (or near it) than on the bulk. In this case oxygen vacancy concentration is same on the bulk and on the surface. Because pure surface is lower in the energy than surface with vacancy, oxygen diffusion to the surface is driven by a thermodynamic force. This result supports of the nano carriers, because nano structures have more reactive

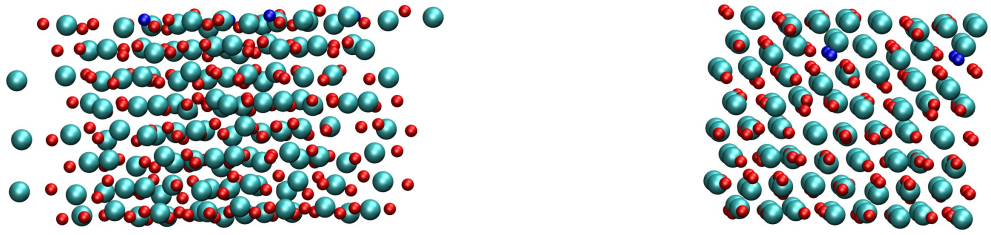

(a) Most stable surface of Mn_2O_3(110) with vacancy on the surface. Pure surface is 7 eV lower in energy than this one. Vacancy formed at this place requires 0.086 eV energy per formula unit.

(b) Most stable surface of Mn_2O_3(110) with vacancy on the surface. Pure surface is 6 eV lower in energy than this one. Vacancy formed at this place requires 0.561 eV energy per formula units.

Figure 24: Vacancies made in Mn_2O_3 (110) surface and under the surface. Red balls present oxygen atoms, cyan balls are manganese atoms and blue balls are vacancies.

surfaces than conventional structures, so the vacancy formation could be easier for the nano oxygen carriers than conventional carriers, because the energy difference between bulk and surface is so large.

Vacancy formation energy on the bulk, on the surface and on the subsurface as a function of temperature is presented in figures 29 and 25. One positive effect for CLC is that when temperature is rising, formation energy is decreasing. Furthermore in the temperature range under CLC, all vacancy formation reactions are exothermic. Less energy is released for the vacancy formation on the bulk. Vacancy formation under the surface is also much more favourable than on the bulk. Vacancy formation on the subsurface is not thermodynamically such favourable than formation on the surface, although vacancy is more stable on the subsurface. In summary vacancy formation is very easy at the surface compared to the bulk, so the nano structures can have very much potential for the oxygen carrier because of their bigger reaction surface area.

In Mn_2O_3 oxygen diffusion from vacancy presented in figure 24a to vacancy 24b is examined with the constraint plane method. On the basis of the calculations, activation energy for the diffusion from the subsurface to the surface is 0.379 eV. Activation energy for the diffusion at the bulk was 2.536 eV which is much higher than 0.379 eV. Vacancy concentration in these calculations is same, so the results are comparable. Because of nano structures higher surface area, it can be concluded that diffusion is easier at the nano scale. And because slow reaction kinetics is one big restrictive feature of the CLC-process, oxygen carrier made of Mn_2O_3 could be better at the nano size than conventional carrier and so solve the slow reaction kinetics, causing CLC working better.

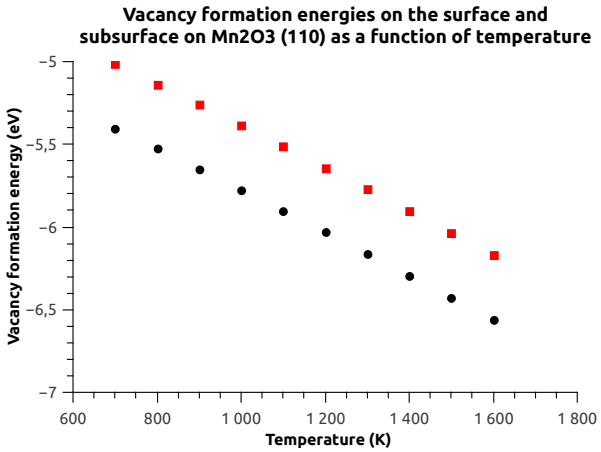

Figure 25: Vacancy formation energy on the surface and on the subsurface as a function of temperature at pressure 1 atm. Temperature dependence has been obtained using atomistic thermodynamics. Vacancy concentration on both cases is same. Energies are calculated per formula unit. Black circles represent vacancies on the surface and red squares on the subsurface.

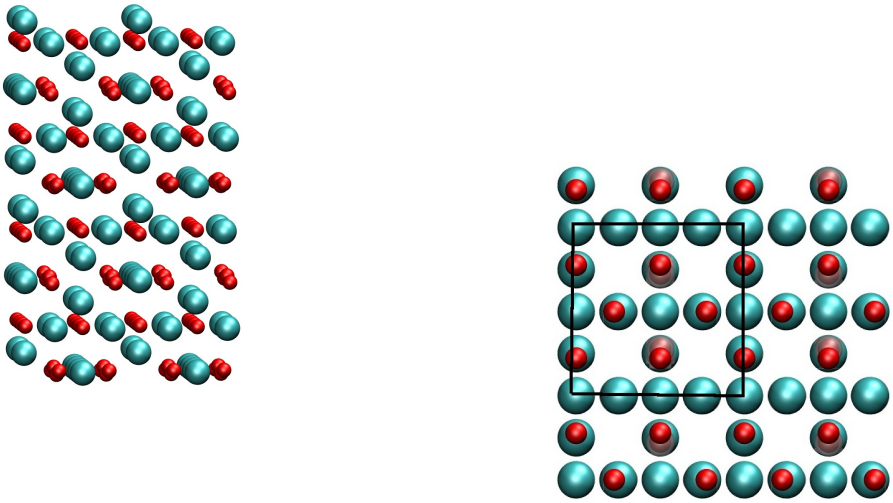

(a) Side view of the most stable surface of $Mn_3O_4(001)$.

(b) Unit cell of the most stable surface of $Mn_3O_4(001)$.

Figure 26: Side view and and unit cell of Mn_2O_3 (111) surface. Red balls present oxygen atoms and cyan balls are manganese atoms.

Most stable surface for Mn_3O_4 is (001) and it is presented in figure 26. In Mn_3O_4 (001) surface there are eight different atomic layers and calculations are carried out with 16 atomic layers and 5 Å vacuum at the bottom and above.

In Mn_3O_4 surface vacancies are created like in figures 27a and 27b. Vacancy made on the subsurface is 9 eV upper in energy than corresponding pure surface and vacancy made at the surface is 8.6 eV upper, thus vacancy on the subsurface is more stable than

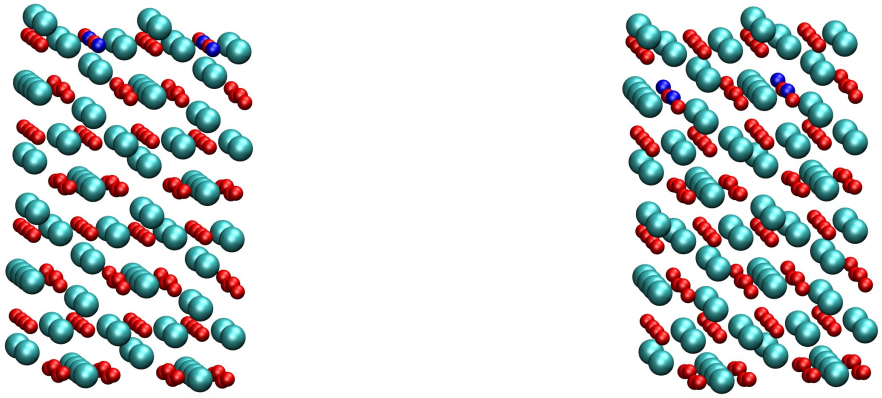

(a) Most stable surface of $Mn_3O_4(001)$ with vacancy on the surface. Vacancy formed at this place requires 0.65 eV energy.

(b) Most stable surface of $Mn_3O_4(001)$ with vacancy on the subsurface. Vacancy formed at this place requires 0.70 eV energy.

Figure 27: Vacancies made in Mn_3O_4 (001) surface and subsurface. Red balls present oxygen atoms, cyan balls are manganese atoms and blue balls are vacancies.

vacancy on the surface. Vacancy is formed easier on the surface than on the subsurface. Vacancy formation energies and the activation energy of the diffusion at the surface are presented in the table 19.

In Mn_3O_4 less energy is needed for vacancy formation on the surface than under the surface. Vacancy formation on the surface is thermodynamically more favourable than on the subsurface. For the whole truth of the vacancy formation, also some kinetic information is needed. It is somewhat unexpected that more energy is needed when vacancy is formed on the bulk than on the surface, because there are more bonds on the bulk, which should break to form vacancy, also the vacancy formation energy should be higher on the bulk than on the surface. Furthermore vacancy concentration on the bulk is higher than on the surface. If the concentrations were same, vacancy formation would be easier on the surface and harder in the bulk. Nanostructures have more surface area, so this result is speaking on behalf of the conventional structures. Or at least the vacancy is formed easier for the conventional carrier. It is notable that surface calculations should be carried out with the tighter calculations parameters, for example h value of 0.16 Å. It is also possible that there is some kind of a mistake in the calculation method. So additional research is desirable.

Vacancy formation energy on the bulk, on the surface and on the subsurface as a function of temperature is presented in figures 29, 28. When temperature is rising, vacancy formation changes more exothermic on the bulk and exothermic on the surface and on the subsurface. In Mn_3O_4 vacancy formation on the bulk is much lower in the energy than formation on the surface and on the subsurface. This is true on the whole temperature range interesting in CLC. This result implies that conventional carriers would

be more appropriate than nano carriers. This unexpected result might due to slightly different magnetic structure between bulk and bulk with vacancy. Or maybe the calculation method is not valid in this case. Vacancy formation energies are calculated per formula units in the both cases. One should check if the results change when, in the case of the surface, the energies are calculated per unit area and in the case of the bulk, per unit volume. Because reaction in the interesting temperature range is exothermic, this material seems to be a good candidate for the oxygen carrier both in the conventional and in the nano form. And however a key feature is an activation energy of diffusion, not the vacancy formation.

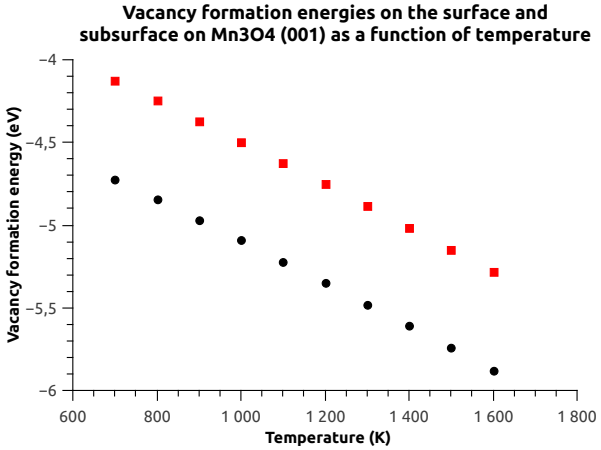

Figure 28: Vacancy formation energy on the surface and on the subsurface as a function of temperature at pressure 1 amt. Temperature dependence has been obtained using atomistic thermodynamics. Oxygen vacancy concentration on the bulk is 3.1 % on the surface. Energies are calculated per formula unit. Black circles represent vacancies on the surface and red squares on the subsurface.

In Mn_3O_4 oxygen diffusion from vacancy presented in figure 27b to vacancy 27a is examined in two pieces. The first piece is carried out with the constraint plane method and the second piece with the constraint line method. On the basis of the calculations, activation energy for the diffusion from the subsurface to the surface is 0.55 eV. Surface is very specific for the calculation parameters. Due to this property number of maximum iterations was increased to 500 steps and parameters used in mixer were (0.02,1,100). Otherwise the calculations parameters were same as for the bulk one. Free energy calculated by DFT along the diffusion path turn out to depends strongly on small displacements, which affects to the reliability of the value obtained for the energy barrier.

Activation energy for the diffusion at the bulk is 0.81 eV which is quite larger than 0.55 eV. Because nano particles have higher area per volume ratio and they have more surface and diffusion between the surface and subsurface is easier than on the bulk, it can be concluded from the calculations that diffusion is easier at the nano scale. Because diffusion is a large restrictive feature for the oxygen carrier, it can be seen that nano carriers have higher reactivity because of better diffusion. Due to enhanced diffusion, nano carriers have potential to be better oxygen carriers than the conventional ones.

As previously discussed, vacancy formation is easier on the surface or near the surface. This applies on each material excluding Mn_3O_4. Thus it can be concluded that vacancy formation is easier on the nano structures than on the conventional carriers. Also the diffusion is easier on the surfaces than on the bulk, since activation energy of diffusion is

Table 19: Calculated formation energy of vacancy, vacancy concentration and activation energy of diffusion for each metal oxide surface is presented in the table.

Metal oxide	Vacancy concentration (%)	Formation energy of vacancy (eV)	Activation energy of diffusion (eV)
Cu_2O	12.5	2.87 and 1.89	1.69
Mn_2O_3	2.1	1.37 and 1.53	0.38
Mn_3O_4	3.1	3.60 and 4.00	0.55

much less on the surface than on the bulk. Diffusion is one big restrictive feature in CLC, so this result can provide a solution to the problem, because nano structures have more surface area.

The effect of temperature can be examined with the help of atomistic thermodynamics. The results are shown in the graph 30. Vacancy formation is most difficult in the Mn_2O_3 bulk and easiest vacancy is formed in Mn_3O_4. And when the temperature rises, formation energies change exothermic. The general trend is that vacancy is formed easier to the surface or under the surface. Mn_3O_4 makes an exception in this, but the calculation method may not work correctly in this case. Or at least magnetic structure is slightly different on the pure bulk and on the bulk with vacancy. So, generally speaking, the vacancy is formed easier on the surface and second easiest on the subsurface. From this point of view, nano structures should be more suitable oxygen carriers than conventional carriers in the temperature range interesting in CLC.

If one wants to compare different oxides in temperature range interesting in CLC, it can be seen in the figure 30 that a vacancy is formed easier in the case of Mn_2O_3 surface and second easiest it is on the Mn_2O_3 subsurface. Vacancy formation is more convenient in Cu_2O nano carriers than in conventional carriers. If someone wants to use nano carriers, manganese based carriers should be better choice than copper based carriers, from the vacancy formation point of view.

7.4 Atomistic thermodynamics

When temperature and pressure effects are applied to the DFT calculations, a good way to demonstrate phenomenons is atomistic thermodynamics discussed in section 6.3. In this case surface free energies of different surfaces and surfaces with defects (for example vacancies) are examined as a function chemical potential of oxygen (or some other additional material) 6.8. Chemical potential depends on temperature and pressure according to the equation 6.18. In this thesis 1 atm is selected as a reference pressure, so the pressure term disappears. Temperature is examined in temperature range interesting (and little bit wider) in CLC, 600-1600 K.

It can be seen from the figure 31 that surface with a vacancy is more stable than pure surface. This is a good feature for CLCs point of view. Surface with a vacancy becomes also more stable when temperature rises. Instead of it pure surface is constant as a function of temperature. So the surface with a vacancy becomes more stable compared to the pure surface when temperature increases, which is a good property. Behaviour is similar also in other metal oxides, as can seen from pictures 33 and 34.

Free energies of surfaces without vacancies are constants with increasing temperature,

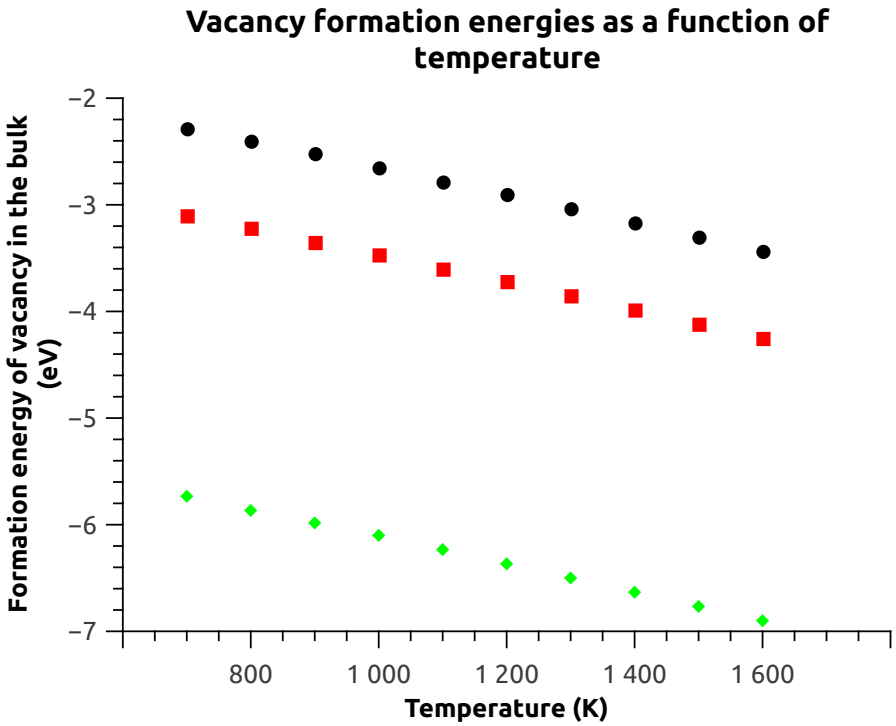

Figure 29: Vacancy formation energy on the Cu_2O, Mn_2O_3 and Mn_3O_4 bulk as a function of temperature. Temperature dependence has been obtained using atomistic thermodynamics. Energies are calculated per formula unit. Black circles are Cu_2O, red squares are Mn_2O_3 and green quadrilateral are Mn_3O_4.

while surfaces with vacancies become more stable 32. Surfaces with vacancies are lower in energy compared to the corresponding pure surfaces. This a good phenomenon, because redox-cycle (which requires vacancy formation) is essential part in the whole CLC. When comparing surfaces free energies, it is notable that Cu_2O (111) surface with vacancy is the most stable and so the best surface for the process. There is one unexpected feature in the graph. Mn_2O_3 (110) surface is more stable than Mn_3O_4(001) surface. From the CLCs point of view it would be better that reduced form of the metal oxides would be lower in energy. In follow-up studies it would be interesting to study surface free energy of pure metal (not metal oxide) surface. In this case metal surface should not be lowest in energy, because then the risk that metal acts as a catalyst increases. However there is not any investigation that manganese based oxygen carriers can act as a catalyst in harmful reactions in CLC. But some metals can act.

8 Conclusions and Outlook

Chemical looping combustion (CLC) is a promising novel method for capturing carbon from the power plants. It is based on alternating reduction and oxidation reactions in the fuel and air reactors. Between the reactors oxygen needed for oxidation is transferred by an oxygen carrier. One big hindrance towards commercial use of CLC is a slow reaction kinetics of oxygen carriers. One possible solution to the problem is to use nanostructures as oxygen carriers, and their potential to act as suitable carriers is investigated in this master's thesis. This thesis consists of a literature review and a numerical part where the

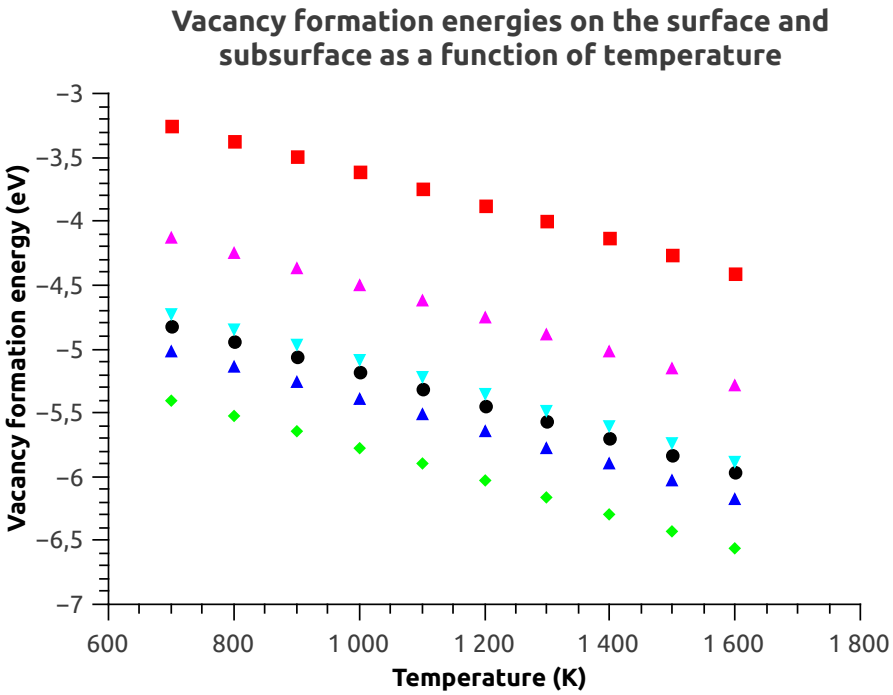

Figure 30: Vacancy formation energy on the surface and on the subsurface as a function of temperature. Temperature dependence has been obtained using atomistic thermodynamics. Energies are calculated per formula unit. Red squares, purples triangles, turquoise triangles,black circles, blue triangles and green quadrilateral are vacancies on the Cu_2O subsurface, Mn_3O_4 subsurface, Mn_3O_4 surface, Cu_2O surface, Mn_2O_3 subsurface and Mn_2O_3 surface, respectively.

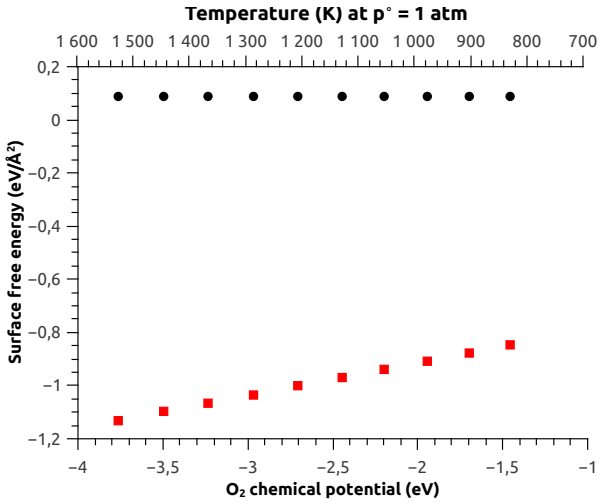

Figure 31: Surface free energy of $Cu_2O(111)$ surface and surface with vacancy as a function of O_2 chemical potential and temperature at pressure 1 atm. Temperature dependence has been obtained using atomistic thermodynamics. Black balls represent pure Cu_2O surface and red squares represent Cu_2O surface with a vacancy.

diffusion properties of copper and manganese based metal oxides are studied.

In previous literature articles the examined nano oxygen carriers are copper, nickel, iron and manganese based metals or metal oxides. Of these carriers suitable for CLOU process are copper and manganese based carriers. Although they are not investigated on

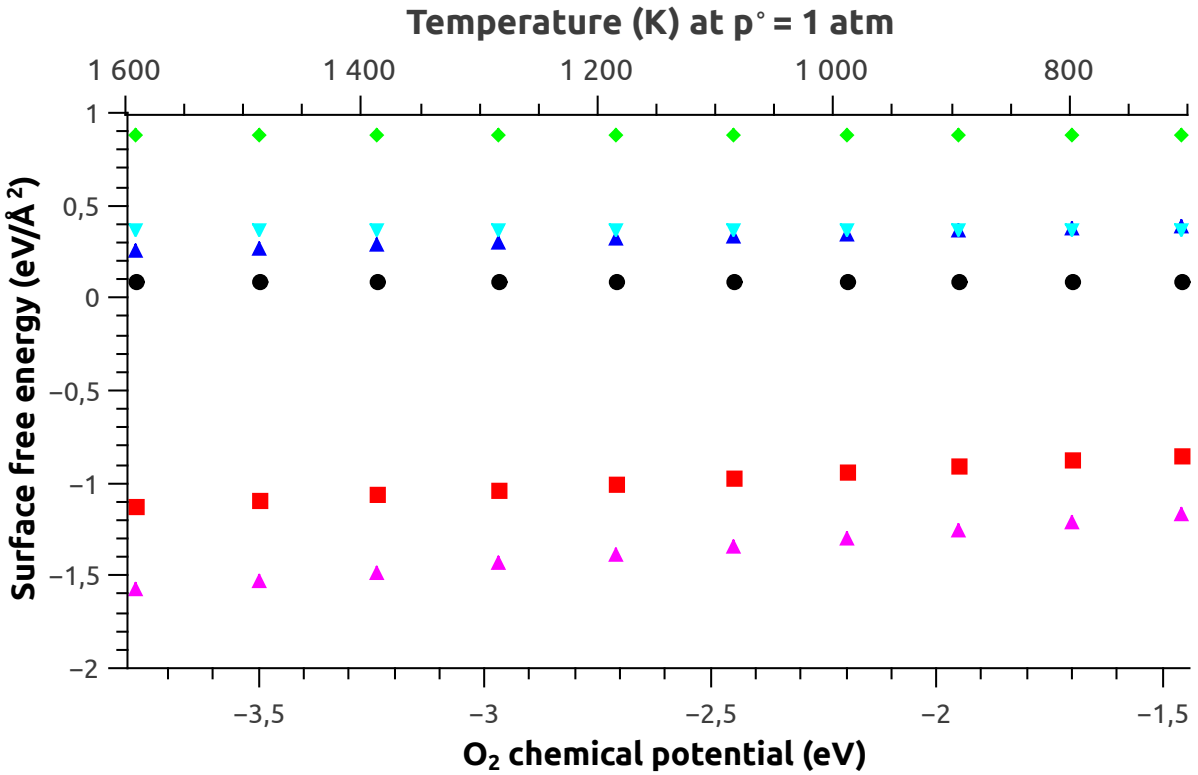

Figure 32: Surface free energy of $Cu_2O(111)$,$Mn_2O_3(110)$ and $Mn_3O_4(001)$ surfaces and surfaces with vacancy as a function of O_2 chemical potential and temperature at 1 atm. Temperature dependence has been obtained using atomistic thermodynamics. Black balls, red squares, green quadrangles, blue triangles, turquoise triangles and purple triangles represent pure Cu_2O surface, Cu_2O surface with a vacancy, pure Mn_2O_3 surface, Mn_2O_3 surface with a vacancy, pure Mn_3O_4 surface and Mn_3O_4 surface with a vacancy, respectively.

nano scale on the chemical looping combustion with oxygen uncoupling (CLOU). Based on the literature there are two things which enhance slow reaction kinetics. Owing to the increased volume per area ratio, the reactivity is improved. And another fact that makes reactivity faster is that porosity is distributed to the wider area. And this porosity enhances reactivity. Also better conversion efficiency and oxygen storage capacity have been obtained by using nano oxygen carriers.

Wider porosity has also a negative effect, weakening the mechanical strength of the structure. Due to their smaller size, melting points of nano carriers are lower than that of the conventional carriers. And because temperatures at the process are quite high, there is a risk that carriers melt or agglomerate. Mechanical strength and temperature resistance can be improved by using suitable support, like BHA. Increasing reactivity by reducing carriers size makes reactor design process more complex. The most recent articles have also shown that copper oxide CuO is toxic at the nanoscale and can cause DNA damage. So more information about toxicity of nano carriers is needed.

Literature on nano carriers is limited and more research is needed before nano carriers can be applied for commercial purposes. Especially computational studies and knowledge of the micro world and limited processes are required so that the full capacity off the nano carriers can be exploited.

Numerical part of this thesis is executed with the GPAW software, which utilizes density functional theory (DFT). Vacancy formation energies and activation energies for

diffusion are calculated both on the bulk and on the surface. Because nanostructures have more surface, it can be deduced from the result whether the nano carriers solve slow reaction kinetics or not, and is it useful to employ nano structures as oxygen carriers. Temperatures are high at CLC, so the temperature and pressure effects are investigated with the help of atomistic thermodynamics.

Vacancy formation is much easier on the surface than in the bulk. Especially Mn_2O_3 oxide has a large difference between formation energies on the bulk and on the surface. Exception to the result makes Mn_3O_4 wherein the vacancy formation is easiest on the bulk. However density of vacancies is different on the surface and on the bulk, and albeit this is taken into account, vacancies are formed easier on the surface than on the bulk. And when temperature rises high enough (in the temperature range under CLC) vacancy formation changes exothermic. As a whole, from this point of view, nano structures could have more potential to oxygen carriers for CLC. Vacancy formation energies and activation energies of diffusion are collected in the table 12.

Regardless of temperature, vacancy is formed easier to the Mn_3O_4 bulk, this reaction is exothermic. When temperature is high enough, all formation energies are exothermic. The second easiest vacancy is formed on the Mn_2O_3 surface and Cu_2O surface. The most difficult places for the vacancy formation are Cu_2O bulk and Mn_2O_3 bulk. Based on these results, nano sized, manganese based carrier should be the best alternative to the oxygen carrier.

Table 20: Calculated formation energies of vacancies (E_{form}) on the bulk and on the surface and under the surface are presented in the table. Also the activation energy for diffusion (E_A) on the bulk and on the surface is presented. All units are in eV. Temperature dependence has been obtained using atomistic thermodynamics

Metal oxide	$E_{form,\ bulk}$	$E_{A,\ bulk}$	$E_{form,on\ the\ surface}$	$E_{form,on\ the\ subsurface}$	$E_{A,surface}$
Cu_2O	1.98	3.24	2.87	1.89	1.69
Mn_2O_3	2.08	2.54	1.37	1.53	0.38
Mn_3O_4	0.98	0.81	3.60	4.00	0.55

One big hindrance towards commercial CLC is a slow reaction kinetic. One restrictive feature of the reaction kinetics is diffusion. Other factors which can affect to the kinetics are: vacancy concentration (affects right to the diffusion), interaction of oxygen carrier with fuel or support material, different catalyst (is it for example possible that some defect atom can catalyst the reaction?) and reaction conditions (temperature, pressure). Generally reaction kinetics can be healed by increasing reaction surface, this can be done for example using finer reactants (nano structures). Diffusion is clearly easier on the surface than on the bulk. Thus nanostructures are absolutely worth of further experiments and investigations. On the basis of this rough and preliminary study, nano oxygen carriers seem to have very much potential to solve slow reaction kinetics. Activation energy of diffusion is smallest on the Mn_2O_3 surface and the second smallest it is on the Mn_3O_4 surface. If this information is combined with the earlier results about vacancy formation energies, manganese based metal oxide in nano size seems to have most potential for the oxygen carrier.

Although the results are very promising further research is needed. First of all strange

behaviour of Mn_3O_4 is needed to find out. Why is more energy released when vacancy is formed on the bulk than on the surface? It could be possible that the calculation method is not suitable in this case. Or maybe the surface which is created with MaterialStudio is not the most stable surface. This have to be checked before making further conclusions. Due to a finite time, it is left for the future work. Furthermore the result for the energy barrier of diffusion can only be seen as a first estimate, and one should consider also alternative diffusion paths. More careful examination for Mn_2O_3 is needed, because energy barrier is so much larger on the bulk than energy barrier on the surface.

There are two ways to calculate activation energies of diffusion: NEB method and constraint plane/line method, both are discussed in the chapter 6.2. Because there were technical problems with the NEB, all diffusion calculations are carried out with the constraint line or constraint plane method. So the diffusion route (or at least line or plane where oxygen can move) is determined by a user. It could be possible that the NEB method gives physically more convenient diffusion route and a somewhat different activation energy. Though used calculation method should not affect to the results.

Calculations done in this thesis are rough and preliminary, and more information is needed. It has to be examined how the vacancy formation energy changes if the vacancy is made deeper under the surface. Further, diffusion deeper to the surface and diffusion deeper to the under surface must be researched. And overall diffusion with different vacancy locations must be examined. This method is suitable to investigate interaction between oxygen carrier and fuel. This is left for future work. Vacancy formation and activation energies of diffusion must be investigated with the different materials, different surfaces, different vacancy concentrations and surfaces with other defects than vacancies, for example some other, additional atom.

Lattice constant $a = 9.54$ Å of Mn_2O_3 applied in this study is slightly too small. It should be 9.647 Å. It needs to be examined how this affects to the vacancy formation and diffusion. Unit cell will be increase while the number of atoms remains same. So one could imagine that diffusion gets easier when oxygen has more space to move.

Although DFT is a zero temperature and zero pressure technique, it is possible to calculate how temperature and pressure affect to the vacancy formation and stability of the surfaces. Also some kind of approximations for the temperature effects to the diffusion are possible to made.

Many CLC properties and phenomena (for example vacancy formation, diffusion, interaction between the carrier and fuel) can be examined with DFT. Temperature resistance of the carriers is an important feature which can be studied experimentally but can not be examined using this method. So no information about the nano carriers temperature resistance, which is one disadvantage of the nanocarriers, is available this way.

References

[1] Adanez J., Abad A., Garcia-Labiano F., Gayan P.& de Diego L.F., *Progress in Chemical-Looping Combustion and Reforming technologies*, Progress in Energy and Combustion Science **38**, 2, (2012), p.215-282

[2] Sarshar Z., Kleitz F.& Kaliaguine S., *Novel oxygen carriers for chemical looping combustion: $La_{1-x}Ce_xBO_3$ (B=Co,Mn) perovskites syntesized by reactive grinding and nanocasting*, Energy & Environmental Science **4**, 10, (2011), p.4258-4269

[3] Global Greenhouse Gas Emission data: Trends in Global Emissions, United States Environmental Protection agency available `http://www.epa.gov/climatechange/ghgemissions/global.html`, cited 16.5.2013

[4] Thursfield a., Murugan A., Franca R.& Metcalfe I.S., *Chemical looping and oxygen permeable ceramic membranes for hydrogen production - a review*, Energy & Environmental Science **5**,6, (2012), p.7421-7459

[5] Mattisson T., Lyngfelt A.& Leion H., *Chemical-looping with oxygen uncoupling for combustion of solid fuels*, International Journal of Greenhouse Gas Control, **3**, 1, (2009), p.11-19

[6] Hossain M.M.& de Lasa H. *Chemical-looping combustion (CLC)for inherent CO_2 separations- a review*, Chemical Engineering Science **63**, 18, (2008), p. 4433-4451

[7] Markewitz P.,Kuckshinrichs W., Leitner W., Linssen J., Zapp P., Bongartz R., Schreiber A.& Müller T.E. *Worldwide innovations in development of carbon capture technologies and the utilization of CO_2*, Energy & Environmental Science **5**, 6, (2012), p.7281-7305

[8] Herzog H.J. *What future for the carbon capture and sequestration?*, Environmental Science & Technology **35**,7, (2001), p.148A-153A

[9] Zeng L., Luo S., Sridhar D.& Fan L-S., *Chemical looping processes- particle characterization, ionic diffusion-reaction mechanism and reactor engineering*, Reviews in chemical engineering **28**, 1, (2012), p.1-42

[10] Johansson M. *Screenin of oxygen-carrier particles based on iron-, manganese-, copper-, and nickel oxides fo use in chemical-looping technologies*, thesis for the degree of doctor of philosophy, Chalmers University of Technology, Göteborg, Sweden 2007

[11] Guo Q., Liu Y.& Tian H. *Recent advances on Preparation and Characteristics of Oxygen Carrier Particles*, International Review of Chemical Engineering **1**,4, (2009), p.357-368

[12] Garcia-Labiano F., De Diego L.F., Adanez J., Abad A.& Gayan P. *Temperature variations in the oxygen carrier particles during their reduction and oxidation in a chemical-looping combustion system*, Chemical Engineering Scince **60**, (2005), p.851-862

[13] Mattisson T., Lyngfelt A.& Cho P., *Possibility of using iron oxide as an oxygen carrier for combustion of methane with removal of CO_2-application of chemical-looping combustion* Greenhouse Gas Control Technologies: Proceedings of the fifth international conference, p.205-210

[14] Saha C., Zhang S., Hein K., Xiao R. & Bhattacharya S. *Chemical looping combustion (CLC) of two Victorian brown coals- Part 1: Assesment of interaction between CuO and minerals inherent in coals during single cycle experiment* Fuel article in press (2012)

[15] Song P., Wen D., Guo Z. & Korakianitis T. *Oxidation Investigation of nickel nanoparticles*, Physical Chemistry Chemical Physics **10**,33, (2008), pp.5057-5065

[16] Song P & Wen D. *Experimantal Investigation of the oxidation of Tin Nanoparticles* Journal Of Physical Chemistry C **113** (2009) pp. 13470-13476

[17] Jin H.& Ishida M. *A new type of coal gas fueled chemical-looping combustion*, Fuel **83**, (2004), p.2411-2417

[18] Xiang W.& Wang S. *Investigation of Gasification Chemical Looping Combustion Combined Cycle Performance*, Energy& Fuels **22**, (2008), p.961-966

[19] Adanez-Rubio I., Gayan P., Abad A., De Diego L.F., Garcia-Labiano f.& Adanez J. *Evalution of a Spray-Dried $CuO/MgAl_2O_4$ Oxygen Carrier for the Chemical Looping with Oxygen Uncoupling*, Energy& Fuels, **26**, (2012), p.3069-3081

[20] Tian H., Chaudhari K., Simonyi T., Poston J., Liu T., Sanders T., Veser G. & Siriwardande R. *Chemical-looping Combustion of Coal-derived Synthesis Gas Over Copper Oxide Oxygen Carriers*, Energy & Fuels, **22**, (2008), p. 3744-3755

[21] Fan Lian-Shih *Chemical looping systems for fossil energy conversions* A John Wiley & Sons, New Jersey, 2010

[22] Scott A., Dennis J., Hayhurst A.& Brown T. *In situ gasification of a solid fuel and CO_2 separations using chemical looping*, American Institute of Chemical Engineers **52**, 9, (2006), p.2325-2328

[23] Brown T.,Dennis J., Scott S., Davidson J. & Hayhurst A. *Gasification and chemical looping combustion of a lignite char in a fluidized bed of iron oxide*, Energy & Fuels **24**, (2010), p.3034-3048

[24] Adanez-Rubio I., Abad A.,Gayan P. De Diego L.F., Garcia-Labiano F.& Adanez J. *Identification of operational regions in the Chemical-Looping with Oxygen Uncoupling (CLOU) process with a Cu-based oxygen carrier*, Fuel, **102**, (2012), p.634-645

[25] Leion H., Mattisson T. & Lyngfelt A *Using chemical-looping with oxygen uncoupling (CLOU) for combustion of six different solid fuels*, Energy Procedia **1**, (2009), p.447-453

[26] Leion H., Mattisson T. & Lyngfelt A *Chemical Looping Combustion of Solid Fuels in a Laboratory Fluidized-bed Reactor* Oil & Gas Science and Technology- REV. IFP Energies nouvelles **66**, 2, (2011), p.201-208

[27] Shulman A., Cleverstam E., Mattisson T. & Lyngfelt A. *Manganese/Iron, Manganese/Nickel, and Manganese/Silicon Oxides Used in Chemical-Looping With Oxygen Uncoupling (CLOU) for Combustion of Methane*, Energy & Fuels **23**, (2009), p.5269-5275

[28] Shulman A., Cleverstam E., Mattisson Temperature dependence has been obtained using atomistic thermodynamicsT. & Lyngfelt A *Chemical- Looping with oxygen uncoupling using Mn/Mg-based oxygen carriers- Oxygen release and reactivity with methane*, Fuel **90**, (2011), p.941-950

[29] Solunke R.D. *Nanostructured oxygen carriers for chemical looping combustion and chemical looping hydrogen production*, thesis for the degree of doctor of Philosophy, University of Pittsburgh, Pittsburgh, Pennsylvia 2010

[30] Adanez J., de Diego L.F., Garcia-Labiano F., Gayan P. & Abad A. *Selection of Oxygen Carriers for Chemical-Looping Combustion*, Energy& Fuels **18**, (2004), p.371-377

[31] Ryden M., Lyngfelt A. & Mattisson T. *Combined manganese/iron oxides as oxygen carrier for chemical looping combustion with oxygen uncoupling (CLOU) in a circulating fluidized bed reactor system*, Energy Procedia **4**, (2011), p.341-348

[32] Chuang S.Y., Dennis J.S., Hayhurst A.N. & Scott S.A. *Development and performance of Cu-based oxygen carriers for chemical looping combustion*, Combustion and Flame **154**, (2008), p.109-121

[33] Zhang Y., Rubel A.M., Mehrez S., Neathery J.K. & Liu K *Influence of porosity on Performance of Freeze-grenulated Fe_2O_3/Al_2O_3 Oxygen Carriers Used for Chemical Looping Combustion*, Energy and Environment Research **2**,1, (2012), p.217-228

[34] Arjmand M., Azad A-M., Leion H., Lyngfelt A. & Mattisson T. *prospects of $Al_2O_3$and $MgAl_2O_4$-supported CuO Oxygen Carriers in Chemical-Looping Combustion (CLC) and Chemical Looping with Oxygen Uncoupling (CLOU)*, Energy& Fuels, **25**, (2011), p.5493-5502

[35] Lu C-H., Chang H-H & Yen C. *Reverse Microemulsion Synthesis and Electrochemical Properties of $LiNiO_2$ Powders* Tamkang Journal of Science and Engineering **7**,4, (2004), p.199-204

[36] Sakka S. *Handbook of sol-gel science and technology. 1. Sol-gel processing*, Springer, Kluwer Academic Publishers 2005, pp.680

[37] Demchenko A.P. *Advanced Fluorecence Reporters in Chemistry and Biology 2, Molecular constructions, Polymers and nanoparticles*, Springer 2010, pp.459

[38] Kirchhoff M., Specht U. & Veser G. *Engineering high-temperature stable nanocomposite materials*, Nanotechnology **16**, (2005), p.S401-S408

[39] Solunke R.D. & Veser G. *Hydrogen Production via Chemical Looping Steam Reforming in a Periodically Operated Fixed-Bed Reactor*, Industrial & Engineering Chemistry Research **49**, (2010), p.11037-11044

[40] Solunke R.D. & Veser G. *Integrating desulfurization with CO_2-capture in chemical looping combustion*, Fuel **90**, (2011), p.608-617

[41] Solunke R.D. & Veser G. *Nanocomposite oxygen carriers for Chemical-Looping Combustion of Sulfur-Contamined Synthesis Gas*, Energy Fuels **23**, (2009), p.4787-4796

[42] Najera M., Solunke R., Gardber T. & Veser G. *Carbon capture and utilization via chemical dry reforming*, chemical Engineering Research and Design **89**, (2011), p. 1533-1543

[43] Park J-N., Zhang P., Hu Y-S. & McFarland E. *Synthesis and characterization of sintering-resistant silica-encapsulated Fe_3O_4 magnetic nanoparticles active for oxidation and chemical looping combustion*, Nanotechnology **21**, (2010)

[44] Liu T., Simonyi T., Sanders T., Siriwardande R. & veser G. *Nanocomposite oxygen carriers for chemical looping combustion*, Preprint Papers- American Chemical Society, Division of fuel Chemistry **51**,2, (2006), pp.483-485

[45] Schalow T., Laurin M., Brant B., Schauermann S., Guimond S., Kuhlenbeck H., Star D., Shaikhutdinov S., Liduba J. & Freund H-J. *Oxygen storage at the Metal/Oxide Interface of Catalyst Nanoparticles*Angewandte Chemie International Edition **44**, (2005), pp.7601-7605

[46] Mattisson T., Johansson M. & Lyngfelt A. *The use of NiO as an oxygen carrier in chemical-looping combustion*, Fuel **85**, (2006), p.736-747

[47] Wen D., Song P., Zhang K. & Qian J. *Thermal oxidation of iron nanoparticles and its implication for chemical looping combustion*, Journal of Chemical Technology & Biotechnology **86**, (2011) p. 375-380

[48] Jerndal E., Mattisson T. & Lyngfelt A. *Thermal Analysis of Chemical-Looping Combustion*, Chemical Engineering Research & Design **84** A9, (2006), pp.795-806

[49] Kronberger B., Löffler G. & Hoffbauer H., *simulation of mass and energy balances of a chemical-looping combustion system* Proceedings of the International Conference in Energy for a Clean Environment,Lisbon, Portugal available in `http://www.chemical-looping.at/upload/Publikationen/36_Datei.pdf` cited 14.01.2013

[50] Song Q., Liu W., Bohn C., Harper R., Sivinahiah E., Scott S. & Dennis J.*A high performance oxygen storage material forTemperature dependence has been obtained using atomistic thermodynamics chemical looping processes with CO_2 capture*, Energy & Environmental Science **6**, 288 (2013) 288-298

[51] Zafar Q., Mattisson T. & Gevert B. *Redox investigation of some oxides of transition-state metals Ni, Cu, Fe and Mn supported on SiO_2 and $MgAl_2O_4$*, Energy & Fuels **20**, (2006), pp.34-44s

[52] Readman J., Olafsen A., Smith J. & Blom R. *Chemical looping combustion using $NiO/NiAl_2O_4$: mechanism and kinetics of reduction-oxidation (Red-Ox) reactions from in situ powder X-ray diffraction and thermogravimetry experiments*, Energy & Fuels **20**, (2006), pp. 1382-1387

[53] Peltola P., *Model-based study of a chemical-looping combustion process* Lappeeranta univeristy of Technology, Faculty of Technology, LUT Energy, Lappeenranta (2009), Masters thesis pp.68

[54] Mantipragada H. & Rubin E. *IECM Tehcnical Documentation: Chemical Looping combustion for Pre-combustion CO_2 Capture* Carnegie Mellon University, Pittsburgh (2012) [report] available `www.iecm-online.com`, cited 30.01.2013

[55] Schalow T., Laurin M., Brandt B., Schauermann S., Guimond S., Kuhlenbeck H., Starr D.E., Shaikhutdinov S.K., Libudada J. & Freund H-J. *Oxygen storage at the metal/oxide interface of catalyst nanoparticles* Surface Chemistry **44**, (2005), pp.7601-7605

[56] Mamontov E., Egami T., Brezny R., Korane M. & Tyagi S. *Lattice Defects and Oxygen Storage Capacity of Nanocrystalline Ceria and Ceria-Zirzonia* The Journal of Physical Chemistry B **104**, (2000), pp.11110-11116

[57] Sun C., Li H. & Chen L. *Nanostructured ceria-based mterials: synthesis, properties, and applications* Energy & Environmental Science **5**, (2012), pp.8475-8505

[58] Li P., Miser D.E., Rabueu S., Yadav R.T. & Hajaligol M. R. *The removal of carbon monoxide by iron oxide nanoparticles* Applied Catalysis B: Environmental **43** (2003), pp. 151-162

[59] Valverde J.A. & Castellanos A. *Fluidization, bubbling and jamming of nanoparticles agglomerates*, Chemical Engineering Science **62** (2007), pp.6947-6956

[60] Zhu C., Yu Q., Dave R.N. & Pfeffer R. *Gas Fluidization Characteristics of Nanoparticle Aggolmerates* American Institute of Chemical Engineers Journal **51**, 2, (2005), pp.426-439

[61] Hakim L.F., Portman J.L., Casper M.D. & Weimer A.W. *Aggregation behaviour of nanoparticles in fluidized beds*, Powder Technology **160**, (2005), pp.149-160

[62] Seipenbusch M., Rothenbacher S., Kirchhoff M., Schmid H.-J., Kasper G. & Weber A.P. *Interparticle forces in silica nanoparticle agglomerates* Journal of Nanoparticle Research **12**, (2010), pp.2037-204

[63] Joo SH., Park JY., Tsung CK., Yamada Y., Yang PD. & Somorjai GA. *Thermally stable Pt/mesoporous silica core-shell nanocatalyst for high-temperature reactions* Nature Materials **8**, 2, (2009), pp.126-131

[64] Pike J., Chan S-W., Zhang F., Wang X. & Hanson J. *Formation of stable Cu_2O from reduction of CuO nanoparticles* Applied Catalysis A: General **303**, (2006), pp. 273-277

[65] Mattisson T., Garci´a-Labiano F.,. Kronbeger B., Lyngfelt A., Adánez J.& Hofbauer H. *Chemical-looping using syngas as fuel* International Journal of Greenhouse Gas Control **1** (2007), pp. 158-169

[66] Cho P., Mattisson T. & Lyngfelt A. *Comparison of iron-, nickel-, copper-, and manganese-based oxygen carriers for chemical looping combustion* Fuel **8** (2004), pp.1251-1225

[67] Eyring E.M., Konya G., Lighty J.S., Sahir A.H., Sarofim A.F. & Whitty K. *Chemical Looping with Copper Oxide as Carrier and Coel as Fuel* **66**,2, (2011) pp.209-221

[68] Gayán P.,Adánez Rubio I., Abad A., de Diego L., García-Labiano F.& Adánez J. *Development of Cu-based oxygen carriers for Chemical-looping with Oxygen Uncoupling (CLOU) process* Fuel **96** (2012) pp.226-238

[69] Middander K., Cronholm P., Karlsson H., Elihn H., Möller L., Leygraf C.& Odnevall-Wallinder I. *Surface Characterícstic, Copper Release,and Toxicity of Nano- and Micrometer-Sized Copper (II) Oxide Particles: A Cross-Disciplinary Study* Small **5**, 3, (2009), pp.389-399

[70] Karlsson H., Cronholm P., Gustafsson J. & Möller L. *Copper Oxide Nanoparticles Are Highly Toxic: A Comparison between Metal Oxide Nanoparticles and Carbon nanotubes* Chemical Research in Toxicology (ACS) **21**, (2008) pp. 1726-1732

[71] Iablokov V. *Manganese and Cobalt Oxides as highly active catalyst for CO oxidation* Dissertation presented to obtain a PhD degree in science (2011), Université libre de Bruxelles

[72] Sholl D.S. & Sholl J.A. *Density Functional Theory: A Practical Introduction*, Wiley, Hoboken , NJ, USA (2009), 252 pp.

[73] Vanin M. *Projector augmented wave calculations with localized atomic orbitals* Master Thesis, Technical university of Denmark, Copenhagen (2008), pp.68

[74] Kohn W. & Sham L.J. *Self-consistent equations including exchange and correlation effects* Physical Review **140**, 4A (1965), pp. A1133-A1138

[75] Shewchuk J.C. *An Introduction to Conjugate Gradient Method Without the Agonizing Pain*, School of Computer Scince, Carnegie Mellon University, Pittsburgh (1994), pp.58

[76] Wang L., Maxisch T. & Ceder G. *Oxidation energies of transition metal oxides within the GGA+U framework*, Physical Review B **73**, 195107, (2006), pp.5

[77] Wu D. & Zhang Q. *LSDA+U study of cupric oxide: Electronic sturcture and native point defects*, Physical Review B **73**, 235206, (2006), pp.5

[78] Soon A., Todorova M., Delley B. & Stampfl C. *Thermodynamic stability and structure of copper oxide surfaces: A first-principles investigation* Physical Review B **75**, 125420 (2007), pp.9

[79] Ruiz E., Alvarez S., Alemany P. & Evarestov R.A. *Electronic structure and properties of Cu_2O* Physical Review B **56**, 12 (1997), pp.8

[80] Geller S. *Structures of alpha-Mn_2O_3, $(MnO \cdot 098\,Fe_0 \cdot 017)203$ and $(Mn_0 \cdot 37\,Fe_{063})2O3$ and relation to magnetic ordering* Acta Crystallographica B **27** (1971), pp.821-828

[81] Aminoff G. *Ueber die Kristallstruktur von Hausmannit (Mn Mn2 O4)* Zeitschrift fur Kristallographie **64** (1926), pp.475-490

[82] Jonsson H., Mills G. & Jacobsen K. *Nudged elastic band method for finding minimum energy paths of transitions* CHAPTER 16 pp.385-404

[83] Hu J., Li D., Lu J.G. & Wu R. *Effects on electronic properties of molecule adsroption on CuO surfaces and nanowires* Journal of physical chemistry C **114** (2010), pp.17120-17126

[84] Zheng Z., Huang B., Wang Z., Guo M., Qin X., Wang P. & Dai Y. *Crystal Faces of Cu_2O and their stabilities in photocatalytic reactions* The journal of physical chemistry C **113**, 32, (2009), pp.14448-14453

[85] Su H., Gorlin Y., Man I., Calle-Vallejo F., Norskov J., Jaramillo T. & Rossmeisl J. *Identifying active surface phases for metal oxide electrocatalysts: a study of manganese oxide bi-functional catalyst for oxygen reduction adn water oxidation catalysis* Physical Chemistry **14** (2012), pp.14010-14022

[86] Materials Research Institute, Materials Simulation Center, software, Materials Studio available `http://msc.psu.edu/software/materials-studio`, cited 7.5.2013

[87] Forsyth J., Brown P. & Wanklyn B. *Magnetism in cupric oxide* Journal of Physics C: Solid state physics **21** (1988), pp.2917-2929

[88] Yang B.X., Thurston T.R., Tranquada J.M. & Shirane G. *Magnetic neutron scattering study of single-crystal cubric oxide*Physical review B **39**, 7, (1989) pp.4343-4349

[89] Asbrink S. & Waskovska A. *CuO: X-ray single-crystal structure determination at 196 K and room temperature* Journal of physics: Condensed matter **3** (1991), pp. 8173-8180

[90] Werner H. & Hochheimer H.D. *High-pressure x-ray study of Cu_2O and Ag_2O* Physicaö Review B **25**, 9, (1982) pp.5929-5934

[91] Martínez-Ruiz A., Guadalupe Ma. & Takeuchi N. *First princibles calculations of electronic properties of bulk Cu_2O, clean and doped with ag, Ni and Zn* Solid State Science **5**, (2003), pp.291-295

[92] Bayer M., Podloucky., Franchini C., Allegretti A., Xu B., Parterder G., Ramsey M., Surnev S. & Netzer F.P. *Formation of Mn_3O_4(011) and MnO(001):surface and interface structural stability* Physical Review B **76**, (2007), pp.165428-165438

[93] Cockayne E., Levin I., Wu H. & Lobet A. *The magnetic srtucture of bixbyte α-Mn_2O_3: a combined density functional theory DFT+U and neutron diffraction study*, ArXiv:1211.6960v1[cond-mat.mtrl-sci] 29 Nov 2012

[94] Chiang N., Clokec M. & Chena G. *Nano-sized Mn_2O_3 prepared by a novel sololysis routes an electrochemical capacitor electrode material* Journal-the institution of Engineers **69**,3, (2008)

[95] Regulski M., Przenioslo R., Sosnokowa I., Hohlwein D. & Schneider *Neutron diffraction study of the magnetic structure of α-Mn_2O_3* Journal of Alloys and Compounds **36**, (2004), pp.236-240

[96] Soon A., Söhnel T. & Idriss H. *Plane-wave pseudopotential density functional theory periodic slab calculations of CO adsorption on $Cu_2O(111)$ surface* Surface Science **579**, (2005), pp.131-140

[97] Atomic simulations environments printable manual *ASE manual, RELEASE 3.8.0.3279*, July 01, 2013, available `https://wiki.fysik.dtu.dk/ase/`

[98] Reuter K., Stampfl C. & Scheffler M. *AB INITIO ATOMISTIC THERMODYNAMICS AND STATISTICAL MECHANICS OF SURFACE PROPERTIES AND FUNCTIONS*, H andbook of Materials Modeling, Springer 2005, Netherlands pp.149-194

[99] Reuter K. & Scheffler M. *Composition, structure, and stability of RuO_2 as a function of oxygen pressure* Physical Review B **65**, 035406

[100] Stull D.R. & Prophet H. *JANAF thermochemical Tables* 2nd edition, U.S. National Bureau of Standards, Washington, DC, (1971)

[101] Haynes W.M *CRC Handbook of chemistry and physics*, 91 st. edition, CRC press 2010 by Taylor and Francis Group USA, section 5

[102] Saidi W.A., Lee M., Li L., Zhou G. & McGaughey A.J.H *Ab initio atomistic thermodynamics study of the early stages of Cu(100) oxidation* Physical Review B **86**, 245429, (2012)

[103] Franchini C., Podloucky R., Paier J., Marsman M. & Kresse G. *Ground-state properties of multivalent manganese oxides: Density functional and hybrid density functional calculations* Physical Review B **75**, 195128, (2007)

[104] Hafner J. & Hobbs D. *Understanding the complex metallic element Mn. II. Geometric frustration in β-Mn, phase stability, and phase transition* Physical Review B **68**, 014408, (2003)

A Appendix: Surface free energies for Mn oxides

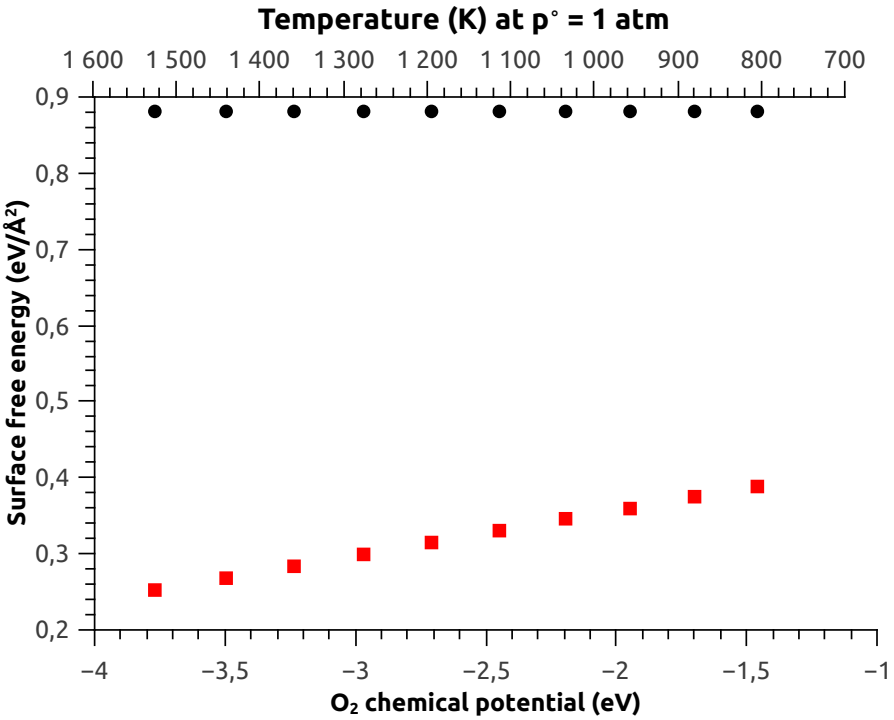

Figure 33: Surface free energy of $Mn_2O_3(110)$ surface and surface with vacancy as a function of O_2 chemical potential and temperature is presented in the figure. Temperature dependence has been obtained using atomistic thermodynamics. Black balls represent pure Mn_2O_3 surface and red squares represent Mn_2O_3 surface with a vacancy.

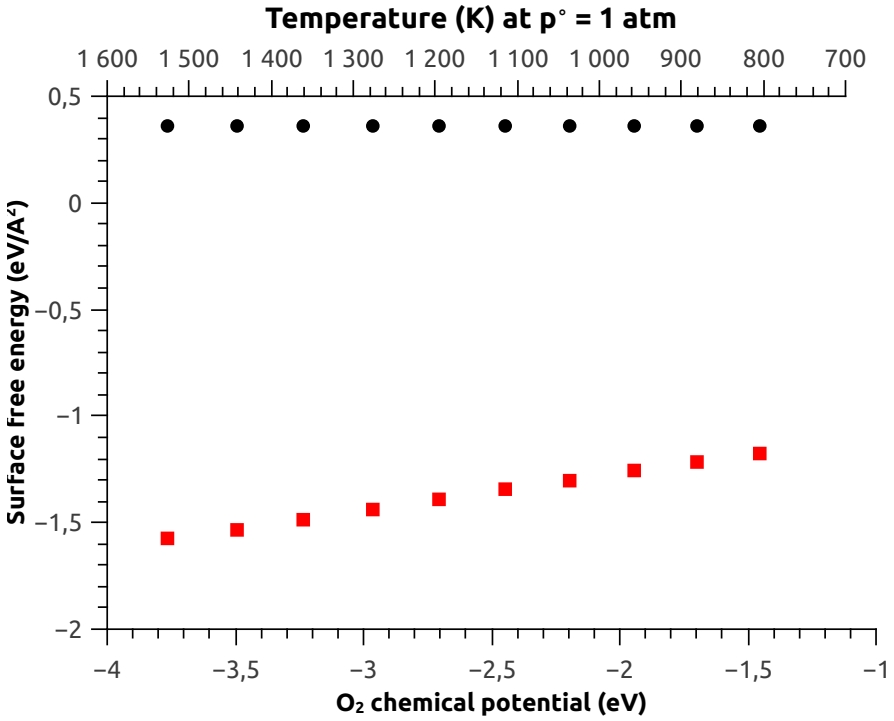

Figure 34: Surface free energy of $Mn_3O_4(001)$ surface and surface with vacancy as a function of O_2 chemical potential and temperature is presented in the figure. Temperature dependence has been obtained using atomistic thermodynamics. Black balls represent pure Mn_3O_4 surface and red squares represent Mn_3O_4 surface with a vacancy.